AD-A160 979 RELATIONSHIP OF IN-CYLINDER GASEOUS AND PARTICULATE 1/2
CONCENTRATION TO RADI..(U) RUTGERS - THE STATE UNIV NEW
BRUNSWICK N J DEPT OF MECHANICAL.. K T RHEE ET AL.
UNCLASSIFIED 15 APR 86 ARO-19869.13-EG DAAG29-83-K-0042 F/G 21/2 NL

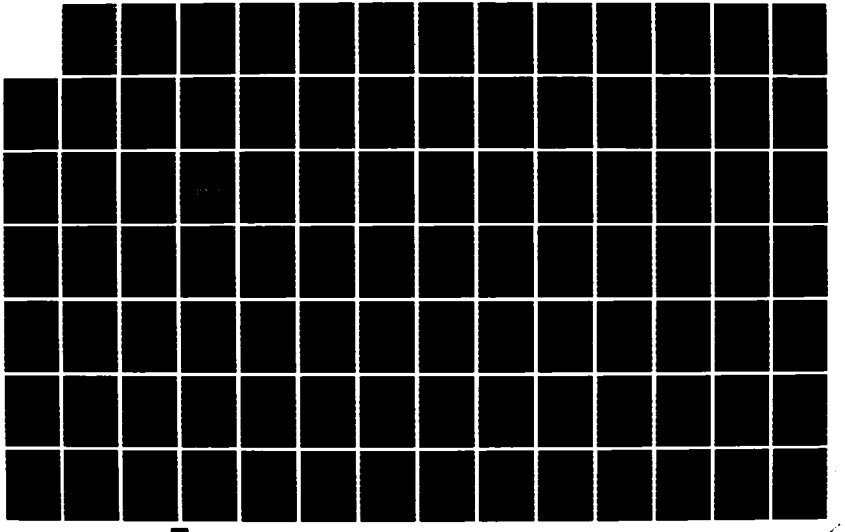

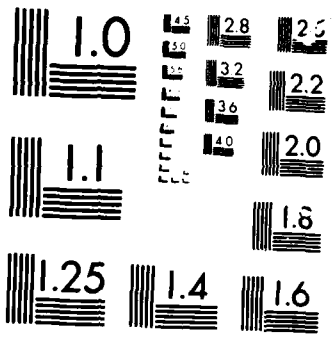

UNCLASSIFIED

SECURITY CLASSIFICATION OF THIS PAGE (When Data Entered)

REPORT DOCUMENTATION PAGE

READ INSTRUCTIONS BEFORE COMPLETING FORM

1. REPORT NUMBER	2. GOVT ACCESSION NO.	3. RECIPIENT'S CATALOG NUMBER
ARO 19869.13-EG	N/A	N/A

4. TITLE (and Subtitle)
Relationship of In-Cylinder Gaseous and Particulate Concentration to Radiative Heat Transfer in Direct Injection-Type Diesel Combustion

5. TYPE OF REPORT & PERIOD COVERED
Final Report
2/1/83 - 1/31/86

6. PERFORMING ORG. REPORT NUMBER

7. AUTHOR(s)
K.T. Rhee, S.L. Chang, J. Matonick and C. Sheft

8. CONTRACT OR GRANT NUMBER(s)
DAAG29-83-K-0042

9. PERFORMING ORGANIZATION NAME AND ADDRESS
Rutgers, The State University of New Jersey
Mechanical and Aerospace Engineering Department
P.O. Box 909, Piscataway, NJ 08854

10. PROGRAM ELEMENT, PROJECT, TASK AREA & WORK UNIT NUMBERS

11. CONTROLLING OFFICE NAME AND ADDRESS
U. S. Army Research Office
Post Office Box 12211
Research Triangle Park, NC 27709

12. REPORT DATE
April 15, 1986

13. NUMBER OF PAGES
146

14. MONITORING AGENCY NAME & ADDRESS (if different from Controlling Office)

15. SECURITY CLASS. (of this report)
Unclassified

15a. DECLASSIFICATION/DOWNGRADING SCHEDULE

16. DISTRIBUTION STATEMENT (of this Report)

Approved for public release; distribution unlimited.

17. DISTRIBUTION STATEMENT (of the abstract entered in Block 20, if different from Report)

NA

18. SUPPLEMENTARY NOTES

The view, opinions, and/or findings contained in this report are those of the author(s) and should not be construed as an official Department of the Army position, policy, or decision, unless so designated by other documentation.

19. KEY WORDS (Continue on reverse side if necessary and identify by block number)

Diesel Combustion, Radiation Heat Transfer, 3-D Radiation Model, Species Distribution, New Integration Function, Blackbody Function, Empirical Equation for Adiabatic Flame Temperature, Parametric Analysis of Diesel Radiation Heat Transfer

20. ABSTRACT (Continue on reverse side if necessary and identify by block number)

The objective of the reported research was to investigate the relationship of radiation heat transfer to the in-cylinder species distribution in direct injection-type diesel engine combustion.

In order to implement this objective, both the experimental and computational methods were employed during the course of the study. In the experiment, in order to obtain the in-cylinder species distribution at successive engine

(continued)

DD FORM 1 JAN 73 1473 EDITION OF 1 NOV 65 IS OBSOLETE

UNCLASSIFIED

SECURITY CLASSIFICATION OF THIS PAGE (When Data Entered)

(20. Abstract--continued)

crank angles, a rapid sampling valve has been used on a laboratory-built single cylinder direct injection-type diesel engine. Among the unique features of the new sampling system is dilution of the sampled gas immediately after sampling to minimize physical and chemical reactions which might take place in the sample train. The sampling system was tested in a bench apparatus before being directly used in the actual engine. At the same time, radiative heat transfer through the engine combustion chamber wall was measured by using thin-film thermocouple with quartz window in front. This was to measure portions of radiative and convective heat transfer, respectively. The engine for the data acquisition was constructed basically by combining a reciprocating system of an ASTM gasoline engine and a newly constructed engine cylinder head. Although, the development of the engine has offered a wide range of educational experiences, while some in-cylinder sampling and radiation heat transfer data were obtained, we encountered a series of problems in the engine requiring replacement of engine components, which were often difficult to obtain. At the end, the engine was regarded unable to meet the need of operating for an extended period of time for data gathering. Consequently, it was decided to use a new single cylinder engine that was made available through DOD-URIP. While the engine is being prepared for continuation of the experiment, more efforts were concentrated on the computational activities.

In the computational work, a radiation heat transfer model was developed to predict spectral radiation heat transfer through the engine combustion chamber wall for given in-cylinder species distributions. Several unique approaches were taken in the modeling. For reporting the results from this work eight separate manuscripts have been prepared under the present sponsorship: seven for publication in journals and one in an international symposium. They are for reporting our discovery of a new integral function, a new exact solution of blackbody functions, a new empirical equation of adiabatic flame temperature of fuel/air systems, an analytical solution of equation of radiation functions, a parametric analysis of diesel radiation heat transfer, etc.

RELATIONSHIP OF IN-CYLINDER GASEOUS AND PARTICULATE CONCENTRATION TO RADIATIVE HEAT TRANSFER IN DIRECT INJECTION-TYPE DIESEL COMBUSTION

Final Report

K. T. Rhee, S. L. Chang, J. Matonick and C. Sheft

April 15, 1986
(Reporting Period, 01 February, 1983 - 31 January, 1986)

U. S. Army Research Office

Contract Number, DAAG29-83-K-0042

Rutgers, the State University of New Jersey
College of Engineering
Mechanical and Aerospace Engineering Department
New Brunswick, New Jersey 08901

RELATIONSHIP OF IN-CYLINDER GASEOUS AND PARTICULATE CONCENTRATION TO RADIATIVE HEAT TRANSFER IN DIRECT INJECTION-TYPE DIESEL ENGINES

K. T. Rhee, S. L. Chang, J. Matonick and C. Sheft

Department of Mechanical and Aerospace Engineering
Rutgers, The State University of New Jersey
New Brunswick, New Jersey 08903

ABSTRACT

The objective of the reported research was to investigate the relationship of radiation heat transfer to the in-cylinder species distribution in direct injection-type diesel engine combustion.

In order to implement this objective, both the experimental and computational methods were employed during the course of the study. In the experiment, in order to obtain the in-cylinder species distribution at successive engine crank angles, a rapid sampling valve has been used on a laboratory-built single cylinder direct injection-type diesel engine. Among the unique features of the new sampling system is dilution of the sampled gas immediately after sampling to minimize physical and chemical reactions which might take place in the sample train. The sampling system was tested in a bench apparatus before being directly used in the actual engine. At the same time, radiative heat transfer through the engine combustion chamber wall was measured by using thin-film thermocouple with quartz window in front. This was to measure portions of radiative and convective heat transfer, respectively. The engine for the data acquisition was constructed basically by combining a reciprocating system of an ASTM gasoline engine and a newly constructed engine cylinder head. Although, the development of the engine has offered an wide range of educational experiences, while some in-cylinder sampling and radiation heat transfer data were obtained, we encountered a series of problems in the engine requiring replacement of engine components, which were often difficult to obtain. At the end, the engine was regarded unable to meet the need of operating for an extended period of time for data gathering. Consequently, it was decided to use a new single cylinder engine that was made available through DOD-URIP. While the engine is being prepared for continuation of the experiment, more efforts were concentrated on the computational activities.

In the computational work, a radiation heat transfer model was developed to predict spectral radiation heat transfer through the engine combustion chamber wall for given in-cylinder species distributions. Several unique approaches were taken in the modeling. For reporting the results from this work eight separate manuscripts have been prepared under the present sponsorship: seven for publication in journals and one in an international symposium. They are for reporting our discovery of a new integral function, a new exact solution of blackbody functions, a new empirical equation of adiabatic flame temperature of fuel air systems, an analytical solution of equation of radiation functions, a parametric analysis of diesel radiation heat transfer, etc.

TABLE OF CONTENTS

LIST OF FIGURES

STATEMENT OF PROBLEM

The proposed study was to conduct research to obtain a better understanding of the processes of particulate formation and heat transfer in direct injection-type diesel engines. Specifically, it was to obtain time- and space-resolved concentration of gaseous and particulate, to measure components of instantaneous heat transfer through convective and radiative processes, and to find the relationship of the in-cylinder species concentration distribution to radiative heat transfer data obtained in the combustion chamber.

The research objective was to be implemented by carrying out the following work tasks: (1) Construction of a new single-cylinder direct injection-type diesel engine; (2) Fabrication of an in-cylinder sampling valve and probes to measure heat transfer through convective and radiative processes; (3) Compilation of in-cylinder species data and heat transfer measurements; and (4) Development of a computational model to understand the relationship of the species concentrations to radiative heat transfer, consequently to compare results from both the computational and experimental approaches.

The research was to be conducted at the Department of Mechanical and Aerospace Engineering, Rutgers, the State University of New Jersey, by supporting two graduate students under the supervision of Dr. K. T. Rhee. One student was to be assigned to experimental part of the study, i.e., to set up an engine apparatus, measure in-cylinder species and radiative heat transfer from the engine combustion chamber. The other student was to develop a computational model of radiation heat transfer in diesel combustion to predict radiation heat transfer through the wall when the combustion product distribution is given.

1. BACKGROUND OF PROBLEM TO BE SOLVED

Although the current excess oil supply creating ecstatic pump prices of automobile fuels seems to have us forget the painful experiences undergone during the oil-shortage on the early 70s, no one expected such low pricing to occur when the present research was proposed, The global oil shortage has not gone away from us at all, but is a temporary disruption in the supply-demand structure. Actually, domestic petroleum resources are rapidly being depleted. Evidently, import of foreign oil will not be the solution for filling the increasing domestic-oil gap due to the rapid bottoming our oil-balance. Failure to implement solutions to the problem in a timely way may lead to serious economic, social and political disruption.

One viable approach to the oil-shortage is the efficient use of limited energy resources. As the transportation system, especially automobile, is the largest consumer of liquid fuels, advanced automobile technology is needed badly to help find the solution of the domestic energy shortage. Note that the severity associated with the shortage may be even stronger than before if it comes to reality again if not prepared for. For the future, improved technology for manufacture and operation should be identified to achieve better fuel economy or to use alternative fuels.

In spite of the current pause in development of synthetic fuels, sooner or later the United States will be making synthetic liquid fuels from coal and shale. One of the first problems to be solved is the determination of the composition of the new fuels. It is particularly important to know the compositions of the new fuels because existing highway transportation systems are highly sensitive to fuel grade. It is likely that new fuel compositions will not be much different from those of existing fuels. On the other hand, there is a consensus that the carbon/hydrogen ratio of the new fuels may be somewhat higher. The former consideration is based on the fact that there are millions of engines already in the field, and their owners expect many years of satisfactory service even by using new fuels in the future. The opinion on the C/H ratio is expressed because the price of new fuel will be very much dependent upon the cost of the hydrogen to be used in the process of new fuel production.

The diesel combustion engine produces a high power output per gallon of fuel, resulting in increased fuel economy in transportation. In spite of the advantage of high fuel economy, there are several main problems to be solved for becoming a better propulsion system. Among the problems associated with diesel engine powered vehicles is the emission of diesel smoke (or particulate). Such smoke emission is expected to be even worse if new fuels with high C/H ratios are used. The diesel smoke not only looks bad but also contains polynuclear aromatic hydrocarbons (PAH), some of which are known to cause mutagenic actions on living cells. In an attempt to reduce the smoke emission from diesel engines, the U.S. EPA has established an exhaust particulate regulation to apply to diesel-powered vehicles. Some studies (Lestz et al., 1982; Bradow, et al., 1982) suggested that pyrene, one of PAHs, might react with NOx in diesel engines to form nitropyrene which is considered to be one of the most active mutagenic reagents. It is highly desirable to know where, when and how this compound is formed in diesel engines. Ultimately,

one wants to minimize such harmful reagents contained in diesel exhaust. In addition, diesel exhaust produces unpleasant smells, which seem to be closely related to the composition and amount of smoke in the emission.

The direct injection-type diesel engine provides better fuel economy than the indirect injection-type diesel engine. This is due mainly to the smaller ratio of combustion chamber surface ratio to its volume, so that the heat loss to the chamber wall is less. And it is well known that the great portion of overall heat transfer in diesel combustion occurs through radiative heat transfer. As the radiative heat transfer is affected by the content of carbon particles appearing in the combustion flames, the heat loss may even be increased as the high C/H ratio fuels are used in diesel engines. The extent of smoke appearing in the exhaust during combustion is considered to relate closely to the heat loss in the combustion chamber. Without mentioning other complex processes affecting efficiency, the large amount of smoke appearing in the exhaust, therefore, may represent a red signal in diesel economy.

At the time the present research proposal was submitted, there had already been vigorous interest in eliminating the cooling system of the diesel engine, the adiabatic (or low-cooled) engine concept. Although the waste energy recovery by the approach may not be significant, the problems associated with the elimination of the cooling system of the engine remain as difficult tasks to be solved in the new engine development. Since the conventional diesel engine rejects as much as 35% of the total energy produced by the combustion processes to the cooling and lubrication systems, the elimination of the cooling devices poses considerable difficulty in various aspects of engine production: design modification, material, tribology, fuel system, etc. Specifically, greater concerns are those associated with thermal loading, processing/development of insulating materials and finding methods of long-term bonding of such materials to the combustion chamber, and lubrication/wear reduction between the cylinder liner and piston rings. Since those issues are closely dictated by the greater thermal loading than the engine components can withstand, it is highly desirable to have a better understanding of heat transfer in the engine. This is not only for the fundamental issue of better understanding the processes but also for helping to develop better low-cooled engines. For example, when the engine performance and endurance to survive of the newly designed engine concept (e.g., turbocompound) is analyzed, one of the first missing information for carrying out the task is suitable models predicting heat transfer in the engine.

In an attempt to obtain a better understanding of diesel combustion processes, Rutgers, University conducted diesel engine combustion research for some years before the award of the present research contract. The objective of the previous work was consistent with the proposed research goals in the present study enabling efficient continuation of the engine study in our engine laboratory. The construction of engine apparatus for the proposed study was in good progress and a preliminary radiative heat transfer model was almost complete when the proposal was submitted.

It was expected to obtain a better understanding of the relationship of radiation heat transfer to in-cylinder species distribution in diesel combustion upon the completion of the proposed research work.

2. OBJECTIVES OF THE STUDY

The objectives of the proposed work under the sponsorship were

(1) to obtain time- and space-resolved particulate data (and CO_2, CO, O_2, local fuel/air ratio) in a direct injection-type diesel engine combustion chamber,
(2) to measure the instantaneous heat transfer (convective and radiative, respectively) through the combustion chamber wall,
(3) to construct a computational model of radiation heat transfer to predict radiative heat transfer through the wall for given in-cylinder species distributions in diesel combustion, and
(4) to investigate the formation processes of nitropyrene in diesel combustion by determining its concentration during the reaction period.

3. RESEARCH METHODOLOGY

The following explains work tasks that were to be carried out for implementing the objectives.

(1) A new single-cylinder direct injection-type diesel engine which were being built under the previous research contract was to be completed for the study.
(2) A new sampling system having dilution for minimizing physical and chemical reactions that might take in the sample train was to be developed for determining in-cylinder species distributions.
(3) Heat transfer probes were to be fabricated for the measurement of instantaneous heat transfer through the combustion chamber wall.
(4) The preliminary 2-D radiation heat transfer model was to be improved for constructing an extensive 3-D non-gray radiation heat transfer model.

Upon the construction of the engine set-up and engine diagnostic tools, in-cylinder gaseous species and particulate concentrations were to be taken at different engine crank angles and different locations in the combustion chamber. At the same time, radiation heat transfer data were to be obtained at corresponding engine conditions.

Once the species distribution and radiation heat transfer data in the combustion chamber were obtained, predicted radiation heat transfer using the new computational radiation model based on the in-cylinder species distribution was to be compared with measured radiation heat transfer data.

The study of pyrene in diesel combustion was to be conducted in collaboration with a properly instrumented group for the analysis of samples, such as, EPA Mobile Source Emission Branch: Time-resolved in-cylinder samples taken from the engine using the new sampling system were sent to the analytical group for finding the history of pyrene formation in diesel combustion. This approach was expected to provide information as to when and where pyrene is formed in a diesel engine combustion chamber.

4. RESULTS FROM THE STUDY

The cumulative results achieved in the study are explained in two main parts, i.e., experimental and computational approaches. Included in the experimental side are the construction of engine apparatus, in-cylinder probes and a sample processing system. Extensive results from the computational work are reported.

4-1. EXPERIMENT

A. CONSTRUCTION OF APPARATUS

ENGINE SET-UP. The construction of the new engine was made by combining a reciprocating unit from an ASTM gasoline engine, a new cylinder head, a new cylinder block, and as many stock parts as possible to minimize the machining cost. For the construction of the system using various engine components from different sources, extensive modifications were needed in those components. Among the modifications made in the construction are balancing of the reciprocating system, machining of the cylinder block, special design of injection nozzle for the new engine, etc. Note the design details of individual engine components are explained in a separate report (DOT/RSPA/DMA-50/84-4). Although some of its content may seem somewhat repetitive because of various subsequent improvement and redesign made in the system during the present research contract, they are briefly explained in Appendix-I.

IN-CYLINDER SAMPLING PROBE. The probe for obtaining in-cylinder species determination was newly developed and tested using our laboratory built engine. Unlike the conventional intermittant flow-type sampling valve, the basic design idea of the new sampling system is based on a continuous sampling valve which was developed by Rhee, et al. (1978) for minimizing the potential effect of quenched boundary layer formed around the probe hole on the measurements. The new system constructed under the present support was to include an in-probe dilution method in order to eliminate or minimize the physical and chemical reaction which might take place in the sample train. The disturbance of the flow field by the presence of the probe in the cylinder may be greater with the present continuous flow-type system than the intermittent flow-type as some limited bench test exhibited. However, the disturbance, if noticeable at all, is not considered to significantly affect the sample because the volume of the sample being taken by the probe is from the uninterrupted part of the swirling in-cylinder charge: at most, the disturbance will affect the composition of the combustion products downstream of the probe. The details of the probe are explained in Appendix-II.

HEAT TRANSFER PROBES. In spite of strong interest by many auto engineers in measurement of heat transfer through the combustion chamber wall, the measurement in diesel engines has not been properly made due to the inherent nature of diesel combustion, namely, high soot formations. The high soot content in the cylinder combustion products rapidly fouls the windows installed for optical access and the thermocouple probe placed on the wall. Even neglecting the problems associated with the soot fouling formation on the probes, the separation of

the portions of heat transfer by convective and radiative processes remains as a difficult task to be solved in the diesel heat transfer analysis. Discussing the methodology for the goal, there are two basic approaches that one could choose for separating the individual effects: one is to isolate the portion of convection heat transfer in a measurement, which is basically a measurement of radiation heat transfer; the other is to exclude the radiation effect in a measurement, which is, then, a measurement of convective heat transfer. Although both approaches have carefully been studied in the present research, since the former method has been studies more intensively its details are only discussed here. (Presently, the latter method is at the evaluation stage and its discussion will be made upon conducting its bench test.) The surface thermocouple method (Overby et al., 1961) has been chosen to obtain the instantaneous heat transfer through the combustion chamber. Two probes were placed in a mounting plug, one installed flush with the wall for measurement of total (convection plus radiation) heat transfer and the other recessed with a quartz window in front for measurement of radiation heat transfer. More details of the probes are discussed in Appendix-III.

SAMPLE PROCESSING SYSTEM. In order to comply with the definition of soot by EPA in our measurement of in-cylinder combustion products, several sample processing methods are chosen in the present work: As mentioned previously, dilution of samples in the sampling probe is important for proper quantification of the in-cylinder soot distribution. Since soot is defined as "any material (excluding condensed water) collected by filtering a sample of diluted exhaust, and the sample train be maintained at 125^{o} F," the sample taken out of our probe was to be introduced into a filter unit at the recommended temperature. The measurement of soot was to be made by weighting a filter before and after a known volume of sample was passed through it. A new sample processing unit was constructed to stabilize the filter (before and after sampling) where the environment is controlled at a designated condition. Because of the relatively unstable nature of particulate samples, it was necessary to use a special caution in the collection and processing of data. The chamber built for this purpose exhibites a very satisfactory result by maintaining a typical condition of relative humidity of 55% and a constant temperature of 82^{o} F. In addition, in order to compare the in-cylinder soot formation to the exhaust soot emission, a new exhaust dilution tunnel was constructed in our laboratory by duplicating the GMR dilution tunnel (McDonald et al., 1980).

B. ENGINE DATA

ENGINE FAILURE. While we were conducting some preliminary engine tests by using the heat transfer probe and the sampling valve, there were a series of engine problems occurring in the laboratory built-engine: some were simple and others were seemingly serious. For example, we had to find three new sets of timing gear and oil pump driving gear (located in the same space in the engine) due to repeated chaotic failure of the components. This was considered to occur due to the greater load that the timing gear had undergone (by driving the fuel injection pump) than originally designed for use in an ASTM-CFR gasoline engine. Another persisting problem encountered in the set-up was the control of leakage in the newly constructed camshaft installed for driving the fuel injection pump. During the process of the engine construction and the preliminary measurements, we had to have a major overhaul of the entire engine many times. The engine upon its con

struction had more than fifty hours of compiled operation time before the most serious problem occurred lately. The problem in the engine found in the recent overhaul was that the crankshaft was noticeably deformed and needed proper repair or replacement. It was judged that the engine might not exhibit satisfactory functioning for the in-cylinder data acquisition and would take a considerably long period of operation. In the meantime, we were awarded a grant under the DOD-URIP to develop a new single cylinder direct injection-type diesel engine that can be used as both a conventional water-cooled mode and a new uncooled operation. Although the development of the new engine was not originally proposed for replacing our laboratory-built engine, it was concluded that use of the new engine would be the best solution for future data acquisition. Consequently, any systematic data acquisition has not yet been made for discussing meaningful engine data in this report.

Note that, in addition to the DOD-URIP sponsored engine, another new unit of Cummins 903-block base single cylinder direct injection-type diesel engine was made available to us (provided by Cummins) for fundamental studies of diesel combustion. This additional engine has been lined up for the measurement of instantaneous temperature variation on the engine combustion chamber walls. For this, a new grass-hopper linkage that was constructed in our laboratory is being placed in the engine.

4-2. COMPUTATIONAL WORK

While various difficult problems were encountered in the experimental work, which hampered the scheduled data acquisition, some very significant progress has been made in the computational approach. The main goal in the computational work was to develop a computer model to predict radiation heat transfer through the combustion chamber wall. The model is explained in the following and several new techniques employed in the modeling are separately explained.

A. RADIATION HEAT TRANSFER MODEL

In the construction of a radiation heat transfer model for combustion systems, several serious problems are faced, mainly due to the directionality and spectral nature of radiation heat transmission. Among the serious problems to be solved in modeling, as discussed next, may be

(1) A viable computation of spectral volume absorptance of a mixture of combustion products along with determination of emission characteristics of species,

(2) A more accurate computational method for solving the equation of radiation heat transfer along individual optical paths in the hemispherical volume faced by locations of the combustion chamber wall,

(3) A detailed description of in-reactor distribution of combustion products and temperature in terms of a suitable coordinate system centered at an

individual locations where heat transfer is computed and its coupling with the above mentioned equation of radiation heat transfer.

SPECTRAL VOLUME ABSORPTANCE OF SOOT/GAS MIXTURE. When a source of radiation heat transmission, particularly a mixture of combustion products including soot, is evaluated, it is necessary to find the volume absorptance and temperature of the mixture. The most widely accepted method of computing the spectral volume absorptance of such a mixture seems that the absorptance by soot cloud, $\kappa_{\lambda s}$ and that by gaseous components, $\kappa_{\lambda g}$ are found to find the summed absorptance, κ_{λ} . In the computation of soot radiation, since most of the practical combustion systems produce soot having much smaller thermal wavelength, the scattering effect on the radiation by soot cloud is minimal and its computation may be made by using the Rayleigh limit expression. The expression is independent of the soot size, inversely proportional to the wavelength, and proportional to the soot volume fraction, i.e.,

$$\kappa_{\lambda s} = \frac{36\, n^2\, k(\pi/\lambda)\, f_v}{[n^2(1-k^2)+2]^2 + 4\, n^4 k^2} \qquad (1)$$

The optical constant, n, k, the real and imaginary parts of the refractive indices, were measured from the intensity of polarizing light reflected from the soot particles and the measurements were fitted to the dispersion equation (Dalzell and Sarofim, 1969; Lee and Tien, 1981). More details of the computation are shown in Appendix-IV, where results from our preliminary radiation heat transfer analysis in diesel combustion are reported.

For computation of emission from gaseous mixture, the empirical wide band model proposed by Edwards and Balarkrishnan (1973) has often been used by others in the past, and the same techniques were employed in the present modeling. The details of this method for our modeling is extensively explained in Appendix-IV.

The remaining question for the computation of spectral radiation of a soot laden mixture may be the summation of both the soot radiation and gas radiation. In view of a previous method of summation of gas emittance, ϵ_g and soot emittance, ϵ_s in order to find the total radiation, ϵ for gray body analysis, i.e., $\epsilon = 1-(1-\epsilon_g)(1-\epsilon_s)$ (Siegel and Howell, 1981), the following similar approach to the method was employed in the computation of spectral volume absorptance: The spectral volume absorptances for gas, $\kappa_{\lambda g}$ and soot cloud, $\kappa_{\lambda s}$ were computed as

$$\kappa_{\lambda\, g} = C/\lambda \qquad (2\text{-a})$$

where, C is found from

$$A_{\lambda} = \int_{\Delta\lambda} 1-\mathrm{Exp}(-C\ell/\lambda)\, d\lambda$$

and in Eq. (1), one finds

$$\kappa_{\lambda,s} = C'/\lambda. \qquad (2\text{-b})$$

The summation, then, was found by the following:

$$\kappa_\lambda = (C+C')/\lambda \qquad (3).$$

The validity of the new method for the spectral property, Eq. (3), although similar to that widely used for gray body computations, remains to be studied.

EQUATION OF RADIATION HEAT TRANSFER. Although the equation of radiation heat transfer in radiatively participating fluid is well known, its solution for practical combustions is not readily solvable, due to complexities of the equation. Elaborating further on the abovementioned problem, Fig. 1 is shown for writing the governing equation of the process as

$$I_\lambda(r) = \int_r^{r_o} \frac{\kappa_\lambda(r')}{\pi} e_{b\lambda}(r') \, \mathrm{Exp}\left(-\int_r^{r'} \kappa_\lambda(r'')dr''\right)dr' \qquad (4)$$

where,

$$e_{b\lambda} = \frac{2\pi hc^2}{\lambda^5 \left[\mathrm{Exp}(hc/\lambda KT)-1\right]}$$

is the spectral volume absorptance at (r,θ,ζ), $c = 2.998 \times 10^{10}$ cm/sec, $h = 6.625 \times 10^{-27}$ erg-sec, and $k = 1.380 \times 10^{-16}$ erg/K. The heat flux along an optical path of a solid angle in the radiation range may be computed from,

$$q_{\theta\zeta} = \int_0^{\infty} I_\lambda(0) \cos\theta \, d\lambda \qquad (5).$$

Among the main difficulties in finding a solution of Eq. (4) are that is a function of both species concentrations and temperature, that both variables are a function of the location along the individual optical path, r, and that the mathematical complexity of the equation is severe so as to employ simplified methods (as in previous studies). Since the species distribution along the individual optical paths is discussed in the following section, the new mathematical approaches taken for Eq. (4) are mentioned here.

The equation of radiation heat transfer, Eq. (4), due to its mathematical complexity, has been solved by using various simplified methods in the past, e.g., the Monte-Carlo method (Steward and Cannon, 1971), the zonal method (Hotel and Sarofim, 1967; Menguc et al., 1985) and the use of geometric factors (Chang and Rhee, 1983). Since we reported the abovementioned results obtained from using the geometric factors in 2-D model, a new analytical method of non-gray 3-D radiation heat transfer has been developed. Equation (4) has been processed by using several unique analytical methods for finding analytical solutions for both optically thin and thick media and for using a relatively simple numerical method for optically medially thin medium. The details of the solution are explained in Appendix-VI.

SPECIES DISTRIBUTION ALONG INDIVIDUAL OPTICAL PATHS. In conducting radiation heat transfer computation for a container having soot-laden combustion products, one of the most important pieces of information needed for it is to

find the species distribution along individual optical paths in the hemispherical volume faced by the location where heat transmission is considered. Two tasks have to be carried out for the objective (refer to Fig. 1): The combustion product distribution has to be given with respect to a reference location in the combustion chamber, most probably the injection nozzle (C in Fig. 1); a convenient method of finding the species distribution along optical paths with respect to D. In conducting these tasks, it is necessary to find distribution functions that can be coupled with Eq. (4) for attempting to find its solution.

When Eq. (4) was studied, with reference to experimental data and computational results as to in-cylinder combustion product distribution reported by others, it was found that several needs for the goal would be met, if the distribution with respect to the nozzle is expressed in the following form of new equation,

$$F = f \exp\left(-a\rho - b\phi^2 - cz^2\right) \tag{6}$$

where F represents either fuel/air ratio, or soot concentration, or CO_2 of H_2O concentrations; f, a, b and c are constants to be determined by using experimental method or computational means. This new form of equation is considered to reasonably well describe the species distribution of nonaxisymmetric plumes and offer various advantages, e.g., that the expression can be used for describing the spray plume in swirl motions by including its effect in -direction, and again, that it facilitate solutions of Eq. (4) as mentioned in the previous section. For this, however, with a given species distribution with respect to the nozzle, Eq. (6), it was necessary to find the distribution along individual optical paths (refer to Fig. 1).

In order to meet this need, a new coordinate transformation method was developed in the present study. Since the details of derivation are shown in Appendix-VII, our new results are only shown in the following.

$$F_o = f_d \exp\left(-[(r-r_o)/r_w]^2\right) \tag{7}$$

where, f_d, r_o and r_w are functionally related to θ, ξ, p_d, Φ_d, z_d, f, a, b, c and c. Basically, when the distribution of combustion products in a chamber with respect to a reference location, the distribution can be calculated along any chosen optical path in the chamber so that the the distribution of volume absorptance along an optical path is computed, according to Eq. (3), as

$$\kappa_o = \kappa_1 \exp\left(-c_1 (r-r_1)^2\right) \tag{8}$$

This relation is used for implementing Eq. (4) for predicting radiation heat transfer through a combustion chamber by integrating Eq. (5) over the entire hemispherical volume faced by the location of heat transmission.

B. NEW TECHNIQUES FOR EQUATION OF RADIATION HEAT TRANSFER

Several new techniques have been developed during the process of developing a new model of radiative heat transfer, Eq. (4). Among those worthy of mention are a new integral function, a new blackbody function, and a new empirical equation for adiabatic flame temperature of fuel/air systems.

A NEW INTEGRAL FUNCTION FOR RADIATION CALCULATIONS.

During the process of finding a solution of Eq. (4), we encountered a new integral function in the following form.

$$\varepsilon_s = 1 - \frac{15}{\pi^4} \int_0^{\infty} e^{-ax} \frac{x^3}{e^x - 1} \, dx \qquad (9).$$

Since an analytical solution for the equation in not known, it was considered to be very difficult to solve Eq. (4). Fortunately, an exact solution of Eq. (9) was discovered in a more general form as,

$$\int_{x_1}^{x_2} \frac{e^{-ax} x^m}{e^x - 1} \, dx = F(m,a,x_1) - F(m,a,x_2). \qquad (10)$$

where, $F(m,a,x) = \sum_{n=1}^{\infty} \left\{ e^{-(n+a)x} \sum_{i=0}^{m} \left[\frac{\Gamma(m+1)}{\Gamma(m-i+1)} (n+a)^{-i-1} x^{m-i} \right] \right\}$

Note that a special form of Eq. (9) is Debye functions of which values are included in most of the mathematics tables. That is, we can find a solution in closed form of Debye function as follows.

$$\varepsilon_{g,i} = \frac{15}{\pi^4} \left[F(3, 0, x_{u,i}) - F(3, 0, x_{l,i}) \right] \qquad (11).$$

Details of the derivation of this new integral function are explained in Appendix-VIII.

BLACKBODY RADIATION FUNCTIONS. Among the more significant of our new integral functions was another new discovery of blackbody radiation functions by using Eq. (10), as defined in the following.

$$F_{o-\lambda T} \equiv \frac{\int_o^{\lambda} E_{b\lambda} \, d\lambda}{\int_o^{\infty} E_{b\lambda} \, d\lambda} = \int_o^{\lambda} \frac{E_{b\lambda}}{\sigma T^5} \, d(\lambda T) = f(\lambda T) \qquad (12)$$

Note that the functions are tabulated in most basic heat transfer textbooks. In addition, for the computer solution of various types of radiation problems, previous researchers employed polynomial curves fitted to the function (Pivovonsky and Nagel (1961). With the new exact solution of the abovementioned integral equation, it was found that the blackbody fuctions can be solved in a closed form as shown below.

$$F_{o-\lambda T} = \int_o^{\lambda T} \frac{E_{b\lambda}(T)}{\sigma T^5} \, d(\lambda T) = \frac{15}{\pi^4} \sum_{n=1}^{\infty} \left[\frac{e^{-nx}}{n} \left(x^3 + \frac{3x^2}{n} + \frac{6x}{n^2} + \frac{6}{n^3} \right) \right] \qquad (13)$$

The further details of the solution derivation are shown in Appendix-X.

EMPIRICAL EQUATIONS FOR ADIABATIC FLAME TEMPERATURES.

One of the most time-consuming processes in computation of the new model was to compute the adiabatic flame temperature (AFT), which was made based on fuel/air ratios. Primarily, in an attempt to reduce the computer time in the beginning, a careful study of the relationship of AFT to its main variables was carried out.

In the analysis, a new equation was developed to estimate the AFT for fuel-air systems of several families of fuel under varied reaction pressures as shown in the following.

$$T_a = a[1 + b \cdot \ln\phi + c \cdot (\ln\phi)^2]\ (^\circ K) \qquad (14)$$

where $a = a_1 + a_2 \cdot \ln(P/P_0)$

$b = b_1 + b_2 \cdot \ln(P/P_0)$

$c = c_1 + c_2 \cdot \ln(P/P_0)$

$\phi = \dfrac{\text{Fuel volume fraction}}{(\text{Fuel volume fraction})_{\text{stoich}}}$

$P_0 = 1$ atm

and a_1, b_1, ... are coefficients of each family of fuels separately given as shown in Appendix-XI.

This formula, however, does not include the variation of initial temperature of fuel/air mixture. Upon extensive study of the AFT of fuel/air systems, a better formula for computing AFTs was developed by including all the major fuels and variables as shown below.

$$T_a = A_1[1 + A_2 \ln\phi + A_3(\ln\phi)^2],$$

$$A_i = A_{i1} + A_{i2} \ln P + A_{i3}(\ln P)^2 \quad (i = 1, 2, 3) \qquad (15)$$

$$A_{ij} = A_{ij1} + A_{ij2} \ln T + A_{ij3}(\ln T)^2 \quad (j = 1, 2, 3)$$

$$A_{ijk} = A_{ijk1} + A_{ijk2} \ln N_c + A_{ijk3}(\ln N_c)^2 \quad (k = 1, 2, 3)$$

where, A_{ijkl} were found for individual fuel families and also fuels. Considerations given in its development and the abovementioned constants for fuels are given in Appendix-XII.

When the AFT is computed for a mixture of the initial temperature of 298° C, use of Eq. (12) may be more convenient; and for mixtures at temperature other than 298° C, use of Eq. (13) is recommended.

C. RELATIONSHIP OF GASEOUS AND PARTICULATE CONCENTRATIONS TO RADIATION HEAT TRANSFER IN DIESEL COMBUSTION

The objective of the proposed study has been implemented by conducting parametric analysis of radiative heat transfer in diesel combustion using our new computational model. Granted that the new model remains to be verified, some results from the present analysis appear to be very reasonable.

Several major variables were considered for the analysis as listed in the following (An in-depth discussion is found in Appendix-XII). They are.

(1) The location in the combustion chamber,
(2) The surface emissivity,

(3) The soot concentration,
(4) The soot and gas radiation,
(5) The reaction pressure,
(6) The combustion chamber wall temperature, etc.

Some of the more significant conclusions drawn from the analysis are listed in the following:

- o. The most portion of radiation heat flux incident on a location in the chamber wall comes from the radiation source right near the location.
- o. The effect of surface emissivity on diesel radiation may not be negligible, in particular, when the surface temperature is high as in a new uncooled diesel engine.
- o. The diesel radiation heat transfer is highly dependent on the soot concentration and weakly sensitive to the gaseous species concentration.
- o. The pressure effect on the radiation is almost negligible in diesel combustion.
- o. The surface temperature of the chamber wall is not a sensitive parameter on the diesel radiation heat transfer.

5. SUMMARY AND RECOMMENDATION

The relationship of radiation heat transfer to gaseous and particulate concentrations in diesel combustion has been studied by using both experimental and computational methods.

In the experimental work, because of unfortunate and serious engine failure the in-cylinder measurement was deferred until a new engine that is being set up becomes fully functional. Among the work tasks which have been carried out in the experiment are (1) construction of a single-cylinder direct injection-type diesel engine, (2) development of an in-cylinder sampling probe, (3) fabrication of heat transfer probes, and (4) construction of sample processing systems, including an exhaust dilution unit and a sample stabilization chamber. These engine diagnostic tools are being prepared using data acquired from the new engine.

The computational work modeling radiation heat transfer in diesel combustion has been greatly successful, to the present researchers' view, who have prepared seven separate refereed publications on the subject, as listed in section-7 and included in the appendices.

Due to the engine problem encountered in the experimental approach, the objective of verifying our new computational model has not accomplished before the contract period was over. It is highly desirable to continue the present work for achieving this remaining objective and a continuation would make it possible to achieve the objective in the most economical way in time and cost because we have trained ourselves and acquired tools needed for the study.

6. ACKNOWLEDGMENT

The entire course of the study was closely monitored by Dr. David M. Mann. Mr. J. Konczyk in Engineering Machine Shop, Rutgers University greatly participated in construction of the engine and diagnostic tools. Their interest and help are greatly appreciated.

7. LIST OF PUBLICATIONS AND TECHNICAL REPORTS

Eight separate papers have been prepared under the present sponsorship during the three-year contract period. They are included in the Appendices. The title of the papers are listed in the following.

1. "Computation of Radiation Heat Transfer in Diesel Combustion", SAE Transactions, 1984, pp. 3.1002-3.1016.

2. "Adiabatic Flame Temperature Estimates of Lean Fuel/Air Mixtures", Combustion Science and Technology, 1983, vol. 35, pp. 203-206.

3. "A Useful Integral Function and Its Application in Thermal Radiation Computations," Int. Comm. Heat and Mass Transfer, 1983, vol. 10, pp. 329-333.

4. "Blackbody Radiation Functions," Int. Comm. Heat and Mass Transfer, 1984, vol. 11, pp. 451-455..

5. "Empirical Equations for Adiabatic Flame Temperatures for Some Fuel-Air Combustion Systems," Combustion Science and Technology, 1985, vol. 44, pp. 75-88.

6. "Coordinate Transformation Method for Radiation Heat Transfer Prediction in Soot Laden Combustion Products," being reviewed for publication.

7. "An Analytical Method of Non-Gray Three-dimensional Radiation Heat Transfer in Spray Combustion," being reviewed for publication.

8. "A Parametric Analysis of Radiation Heat Transfer in Diesel Injection Diesel Combustion," Proceedings of Int'l Symposium on Diagnostics and Modeling of Combustion in Reciprocating Engines, Sept. 4-6, 1985, Tokyo, pp. 167-174.

8. PARTICIPATING SCIENTIFIC PERSONNEL

The following individuals have contributed in carrying out the present project during the period of contract. Note that the personnel support was available to provide two research assistantships under the sponsorship.

Professor K. T. Rhee, Principal Investigator,

Student Participation:

Dr. S. L. Chang,

Mr. Jeff Matonick,

Mr. Chirs Sheft, and

Mr. X. L. Yang.

The degrees awarded on the present support are two M.S. for S. L. Chang and X. Yang; and one Ph.D for S. L. Chang.

9. REFERENCES

Aaman, C. A., "Why Not a New Engine?" SAE Paper-801428, 1980

Bradow, R. L., Zweidinger, R. B., Black, F. M. and Dietzman, H. M., "Sampling Diesel Engine Particule and Gaseous Emission Artifacts from Nitrogen Dioxide Interactions," SAE Paper-820182, 1982.

Edwards, D. K. and Balakrishnan, A., "Thermal Radiation by Combustion Gases," Int'l J. Heat Transfer, vol 16, 1973, pp. 25-40.

Dalzell, W. H. and Sarofim, A. F., "Optical Constants of Soot and Their Application to Heat Flux Calculation," ASME Transactions, vol 9, 1969, pp. 100-104.

Ebersole, G. D., Myers, P. S. and Uyehara, O. A., "The Radiation and Convective Components of Diesel Engine Heat Tranfer,: SAE Paper-701C, 1963.

Hottel, H. C.. and Sarofim, A. F., Radiative Transfer, McGraw-Hill Book Co., New York, 1967

Lee, S. C. and Tien, C. L., "Optical Constants of Soot in Hydrocarbon Flame," 18th Symposium (Int'l) on Combustion, The Combustion Institute, 1980, pp. 1159-1165.

Lestz, S. S., Herr, J. D., Dukovich, M., Yergey, J. A., Risby, T. H. and Tejada, S. B., "The Role of Nitrogen in the Observed Direct Microbial Mutagenic Activity for Diesel Engine Combustion in a Single Cylinder DI Engine," SAE Paper-820467.

MacDonald, J. S., Plee, S., D'Arcy, J. B. and Schreck, R. M., "Experimental Measurements of the Independent Effects of Dilution Ratio and Filter Temperature on Diesel Exhaust Particulate Sampling," SAE Paper-800185, 1980.

Menguc, M. P., Viskanta, R. and Ferguson, C. R., "Multidimensional Modeling of Radiative Heat Transfer in Diesel Engines," SAE Paper-850503, 1985

Obert, E. F., Internal Combustion Engines and Air Pollution, Harper and Row Publication, New York, 1973.

Overbye, V. D., Bennethum, J. E., Uyehara, O. A. and Myers, P. S., "Unsteady Heat Transfer in Engines," SAE Transactions, vol 69, 1961, pp 461-494.

Primus, R. J., Hoag, K. L., Flynn, P. F., and Brands, M. C., "An Appraisal of Advanced Engine Concepts Using Second Law Analysis Techniques," SAE Paper-841287, 1984

Rhee, K. T., Myers, P. S. and Uyehara, O. A., "Time- and Space-Resolved Species Determination in Diesel Combustion Using Continuous Flow Type Gas Sampling," SAE Transactions (Paper-780226), 1979.

Siegel, R. and Howell, J. R., The Radiation Heat Transfer, 2nd Edition, McGraw-Hill Book Co., 1981.

Steward, F. R. and Cannon, P., "The Calculation of Radiative Heat Flux in a Cylindrical Furnace Using the Monte Carlo Method," Int'l J. Heat Mass Transfer, vol. 14, No. 2, 1971, pp. 245-262.

Whitehouse, N. D., Clough, E. and Roberts, P. S., "Investigating Diesel Combustion by Means of a Timed Sampling Valve," SAE Paper-77409, 1977

Zvonow, V. A., Stewart, H. E. and Starkman, E. S., "Hydraulically Actuated Combustion Gas Sampling Valve," Review of Scientific Instruments, 33, No. 12, 1968.

APPENDIX-I

CONSTRUCTION OF A SINGLE CYLINDER LABORATORY DIESEL ENGINE

Construction of the system was a continuing endeavor for our engine research. Several main engine components were newly designed/constructed for the construction of the system. Details of the components are explained in the following.

RECIPROCATING UNIT AND CRANKCASE. Among the main design and modification details are,

-a large hole (6 in. diameter) bored at the top of the crankcase,
-a new camshaft for replacing the existing one in the ASTM engine to connect a fuel injection pump and an encoder,
-balancing of the reciprocating system by installing two balancing weights (1,109 grams each), etc.

The sealing at both ends of the camshaft was constructed a few times for eliminating excessive leakage found during engine operation. The installation of balancing weights at the end of the connecting rod and balancing piston was rather involved due to the space limitation in the crank case: a new oil strainer was fabricated at a new location for reserving space for their installation. Of greater concern in the reciprocating unit was the endurance of the timing gear because the gear took a heavier load to the drive injection pump unlike the simple load undergone when operated as a ASTM gasoline engine: the gear was repeatedly broken three times requiring replacement of both the timing gear and the oil-pump driving gear. It was found that the original crank shaft might not been suitable for being used in the new diesel engine as we discovered that the unit was bent to one direction creating excessive vibrations of the engine.

CYLINDER BLOCK. A new cylinder block was constructed where the cylinder liner was installed and a water jacket was attached for cooling the liner (the cooling of the cylinder head was made through a separate coolant flow). The construction details are,

-a cylinder block that houses a cylinder liner from GM-53 series,
-accommodation of corresponding engine components including liner, piston, piston-ring, con-rod, bearings with proper modifications where needed,
-a newly fabricated water jacket package installed on two cavities of the new cylinder block,
-new intake and exhaust manifolds connected to the engine block, etc.

The construction of the cylinder block was a difficult task since the proper scavenging of the engine was required in the system. An approach taken for this goal was to install several different newly fabricated vane blocks before the intake ports in order to identify the most suitable one for the engine: this was basically to minimize the soot emission from the engine. In this experience, a swirl meter was installed in the cylinder under steady flow conditions to find the highest swirl motion of the intake air, since the swirl of the engine configuration

was very low due to the simple design of the engine components. An aluminum block carved for air flow seemed the most suitable of all we tried. Upon extensive engine operation periods, we found, however, a severe deposit of wet soot on the intake port indicating significant back flow of air during the early part of the exhaust period. Since the fuel was injected every two cycles providing an extra scavenging, the construction of vane blocks was not further pursued. However, this approach might have been responsible for the deposit of wet soot due to overcooling of the engine components.

CYLINDER HEAD. The construction of the engine cylinder head was another unique experience. The main head was constructed out of a cold-roll block including the following machinings:

-a cylindrical cavity for the combustion chamber by matching with the cylinder liner and head gasket (Fig A-1),
-a water jacket around the cavity connecting the coolant flow separate from that in the cylinder block (Fig A-2),
-a mounting plug and its cavity in the cylinder head for in-cylinder probes enabling selection of measurement locations during the engine operation,
-installation of the injection nozzle with minimum use of space in the head for reserving maximum room for the in-cylinder probe mounting as mentioned above,
-three injection nozzles with different sac volumes which were specially manufactured for the new engine experiment (Fig A-3), and
-brackets for mounting thermostat and coolant connections.

Two of the main concerns in its construction were the cooling of the cylinder head and selection of the injection nozzle suitable to the engine. It was found that the cylinder head was excessively cooled in the early tests. A new thermostat was installed for eliminating the problem. The selection of the injection nozzle still remains as an unresolved experience due to the insufficient detailed measurements and relatively short period of experiment with the engine; we have been using one type of nozzle of three selections for eliminating various immediate engine design issues.

ENGINE ACCESSORIES. Several new engine accessories were required in the engine apparatus for facilitating the engine operation and control.

-a mounting plate (24-24-0.5 inches) installed in the front side of the engine for mounting various engine components: a fuel injection pump (American Bosch, APE 1B50P5625B); a water pump; a fuel filter and water separator assembly; a phase shifter (for the timing control of in-cylinder sampling); installation of an encorder; etc.,
-a new phase shifter which is to vary the relative phase angle between the engine camshaft and the sampling system enabling the shift of timing during the engine operation,
-an air induction unit for controlling the inlet air pressure and flow rate,
-a closed-loop coolant unit including devices for control of its flow rate and temperature: control thermostat; magnetic valve; water pump; electric heater, etc., and

-an exhaust gas system including a surge tank where exhaust samples were taken.

The new coolant system needs more explanation. It was required to operate the engine for an extensive period before achieving its warm-up condition. It seemed undesirable to operate the laboratory-built engine for such repeated periods of time particularly when the system had some unresolved design problems including various stock items from various sources of which mutual compatibility was not established. In order to minimize the warm-up period, a separate heating unit was employed to heat the coolant and to circulate it through the engine so that the entire engine block attained an elevated temperature before the firing of the engine.

APPENDIX-II

DEVELOPMENT OF SAMPLING PROBE

When the research proposal for the present work was submitted, the principal investigator found more than thirty major technical papers prepared (as early as the 1920s) reporting results obtained by using in-cylinder sampling probes for engine studies. Some more papers appeared since then to add to the archives of the sampling method. The sampling valves used in those studies were mostly of the intermittent flow-type where the sampling hole is kept normally closed and rapidly opened for a short period of time to take a small amount of in-cylinder gas volume at the desired time of sampling. This type of valves were considered to have some problems in obtaining reliable sample compositions (Zvonov et al., 1968; Whitehouse et al., 1977) due to the quenched layer which might exist in the close vicinity of the sampling hole. In an attempt to minimize such a potentially severe problem, Rhee et al. (1978) developed a new continuous sampling system.

The new system employs a continuous stream of in-cylinder gas flow through the sampling hole (Fig A-4). The flow is rapidly diverted for a short period of time to sample volume for the subsequent analysis. Briefly mentioning the operation of the new system, a flow passing through the orifice in the probe (Fig A-4 (A)) is normally connected to a large (waste gas) section of the oscillation tube (Fig A-4 (C)) which is placed in the probe under spring load. When the sample is to be obtained, the sampling tube is rapidly rotated through a sectoral range as indicated by the broken lines in the figure. During this period the sampling hole is briefly swept by the sample tube by taking a small amount of gas out of the continuous flow stream. The sampling in the next cycle is made by moving the oscillation tube in the opposite direction for a new sampling. This actuation motion of the tube was made by using a hydraulic piston-cylinder unit controlled by a four-gate valve that was operated in phase of the phase shifter connected to the engine (Fig A-5). The hydraulic force was provided from a separate high-pressure accumulator.

Of more significance, the new system constructed in the current study was to include the dilution tube in the sample tube so that a dilution gas having a non-combustion product trace-gas is injected into the sample tube for quenching any physical and chemical reactions that potentially take place in the

system. Due to the limited resources, only one student was assigned to the experimental work (further, there were unexpectedly large amounts of work needed in the engine construction) so that the usefulness of the new sampling system has not yet been evaluated. It will be very interesting to systematically evaluate the new system in an engine in our continuing study.

APPENDIX-III

HEAT TRANSFER PROBES

There have been two views of heat transfer, in particular radiation heat transfer, that potentially determines diesel economy: "Since the combustion flame in the diesel engine is luminous (but not in the SI engine), it has been speculated for many years that radiation heat loss may be an important factor of diesel economy" (Obert, 1973). This view has the same emphasis of the portion of radiation out of the total in-cylinder heat radiation as that by Ebersole et al. (1963) who reported that the portion by radiative process was as high as 40% of the total measured. On the other hand, Amann (1980) reported his computation suggesting that the improvement in thermal efficiency might be only a few percent with up to 85% of recovery in heat loss through the water jacket and lubricating system of diesel engines. This view is supported by a second law analysis of an engine by Primus, et al. (1984). Although more data on radiation heat transfer is neededfor a better evaluation of its impact on engine economy since the loss through the radiative process when the compression ratio is very high, the importance of the heat transfer clearly resides in the thermal loading of engine components of the combustion chamber. Particularly since the radiative heat transfer is highly direction-dependent and since the fate of critical components of the advanced engines, are affected by the thermal load, the further study of heat transfer analysis is warranted.

The basic details of the present probes are the same as the original design as shown in Fig A-6. The Figure shows the probes mounted in the cylinder head: one is to measure the total (convective plus radiative) heat transfer and the other is to measure the portion of radiative heat transfer through the combustion chamber wall. The measurement of the radiative portion of heat transfer was to be obtained by eliminating the convective portion out of the total heat transfer. The detector is ASEA double thermocouples which enable measurement of unsteady heat flow with rising time of up to 2 microseconds. The main weakness of this method are that there are soot fouling formation on the window and that the recessed mount of the probe needs a proper evaluation of its geometric factor. The evaluation of the geometric factor was attempted by using the flash bulb technique. The method is to employ flash bulbs used in photography that produces a relatively strong radiation with designated intensities by the manufacturers. After several trials by using a bench rig, this method was found unsuitable due to the excessive variation of radiation intensity of the flash bulbs overtaking the effect of the recessed mount.

Consequently, we decided to directly evaluate the effects in the engine as Ebersole et al. (1963). Some engine measurements were made by using

the probe in the engine, which need further processing prior to analysis. This task has not been made because of the following reason. While the construction of the engine setup and the sampling probe was carried out by a graduate student (J. Matonick) (note that the remaining graduate assistantship was given to S.L. Chang for the computational work), the investigation of heat transfer was conducted by another student (C. Sheft) on a Departmental support. At the time of writing the thesis, C. Sheft accepted a job offer from industry and decided to complete the work, which is being carried out.

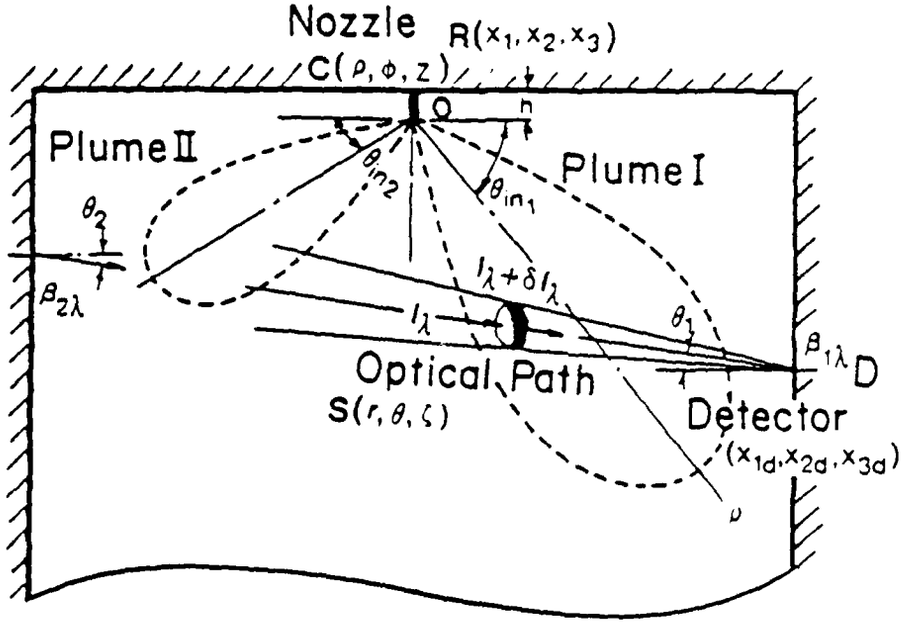

Fig. 1 A Schematics of Flame Plumes in a Combustion Chamber

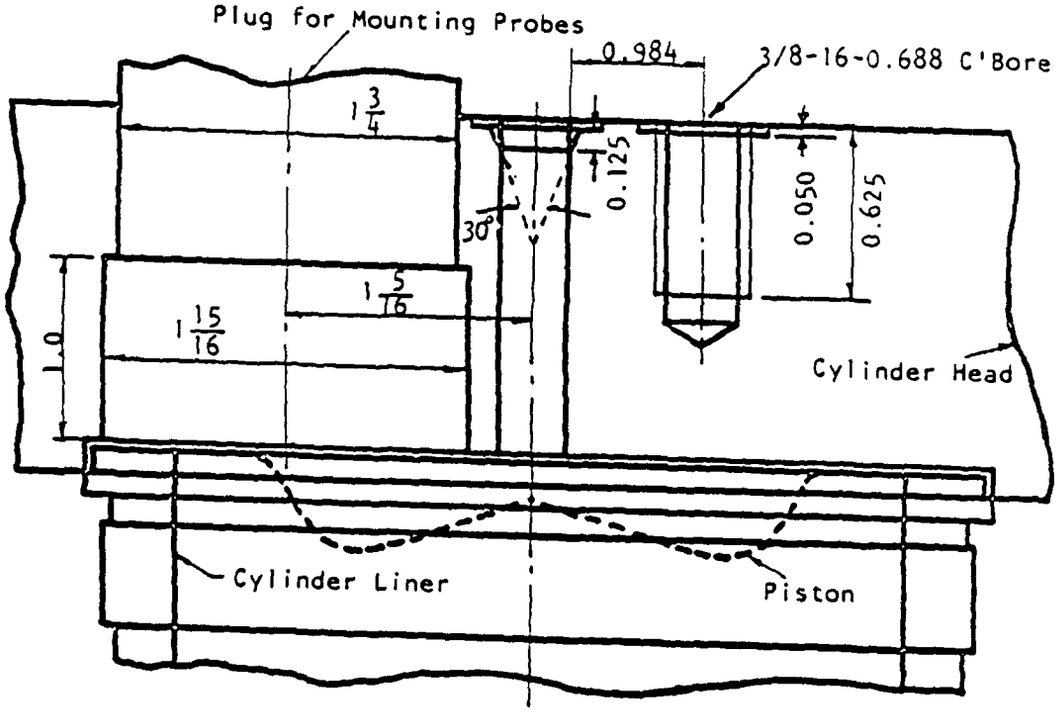

Fig. A-1 The Laboratory-Built Cylinder Head

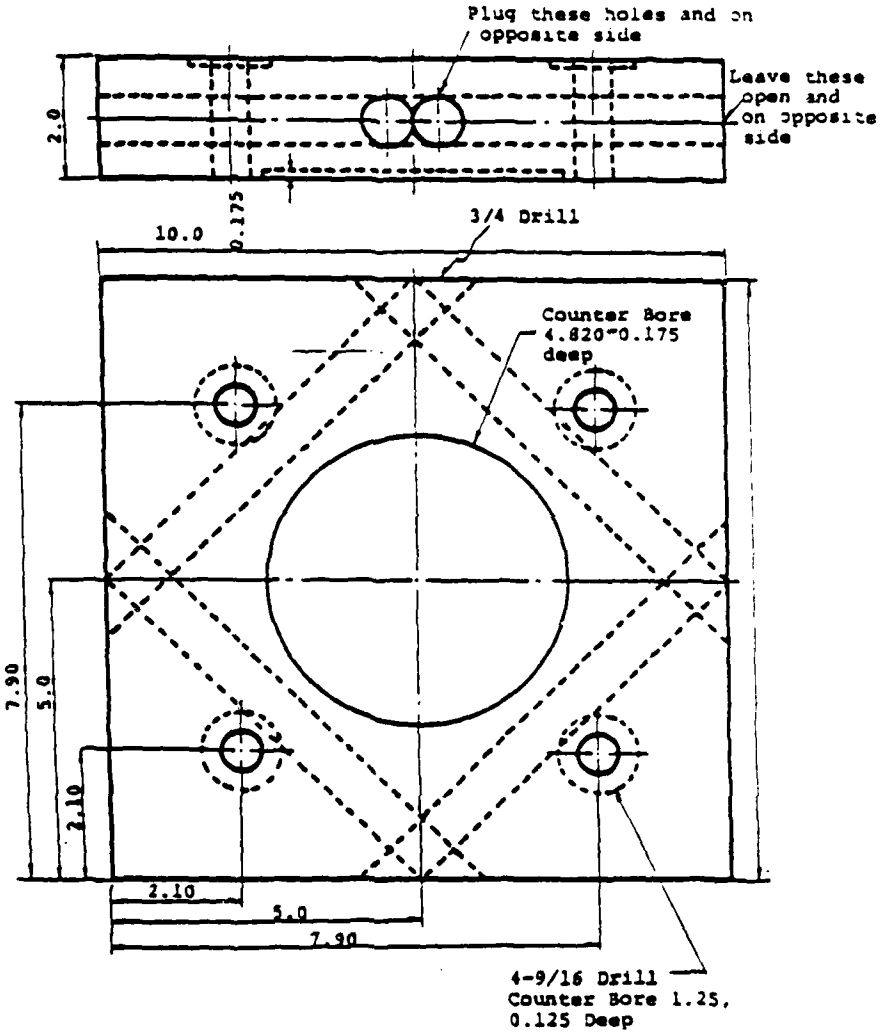

Fig. A-2 The Water Jacket in the Cylinder Head

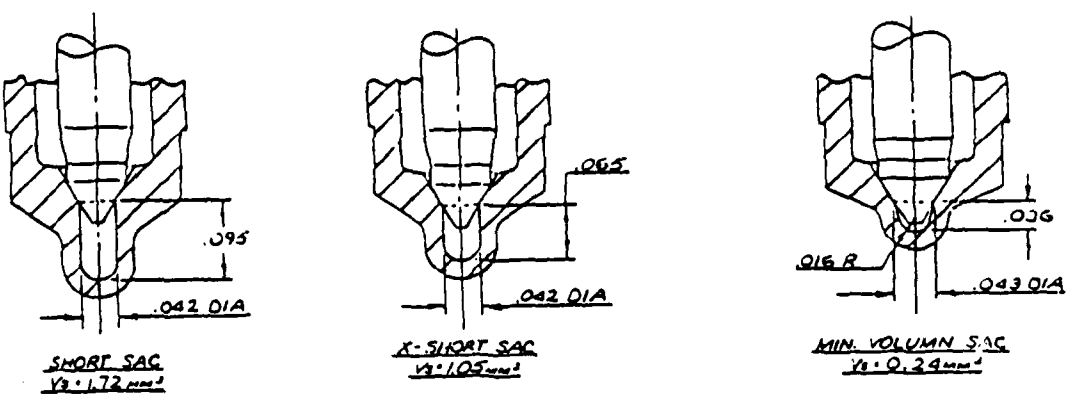

Fig. A-3 The injection Nozzle for the New Engine

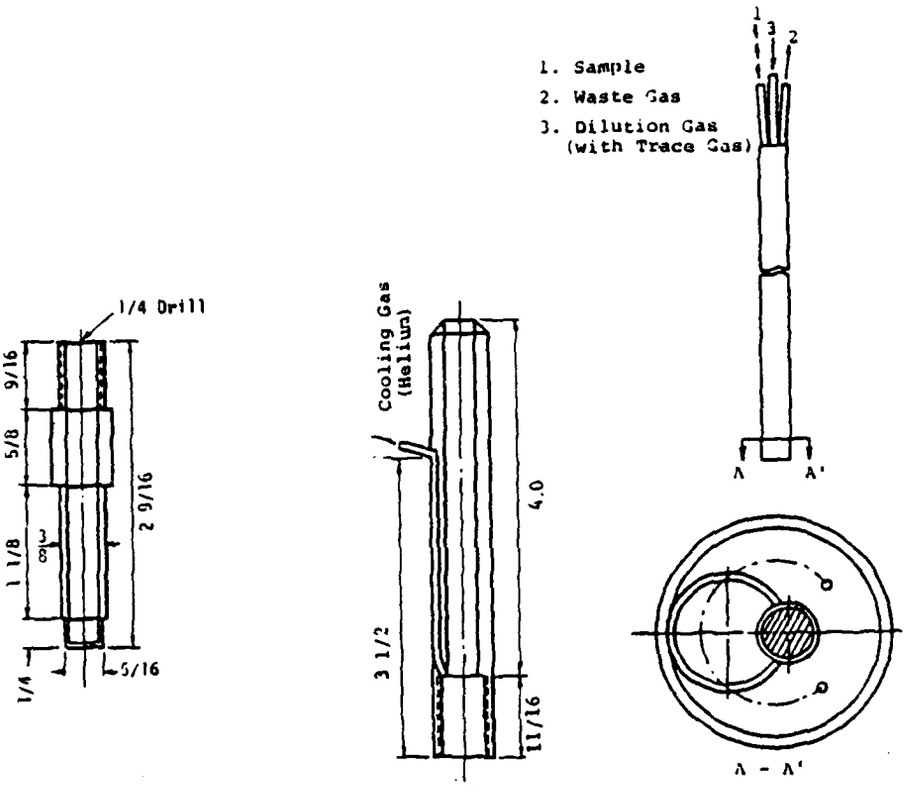

Fig. A-4 The Continuous Flow-Type Sampling System with Dilution

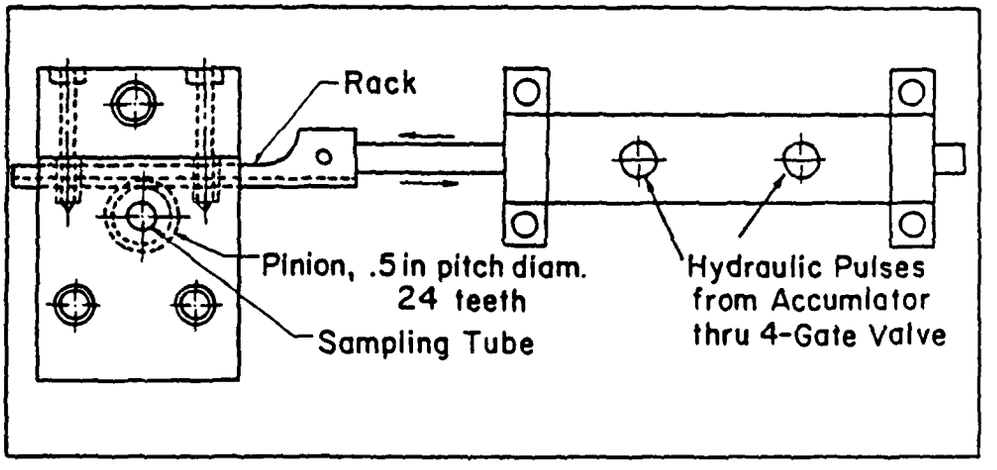

Fig. A-5 The Sampling Valve Actuation System

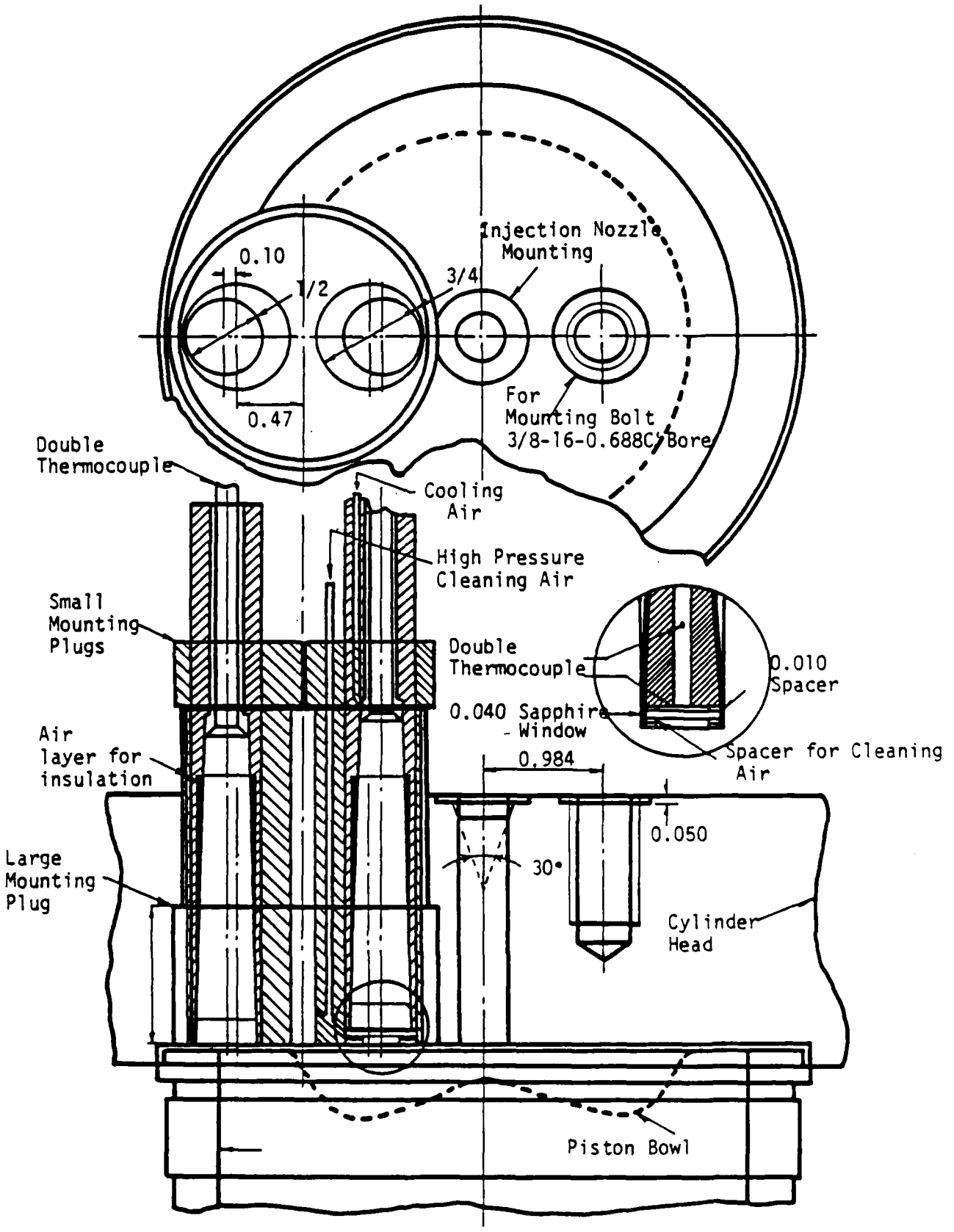

Fig. A-6 The Heat Transfer Probes Mounted in the Cylinder Head

831332

Computation of Radiation Heat Transfer in Diesel Combustion

S. L. Chang and K. T. Rhee
Dept. of Mechanical and Aerospace Engrg.
Rutgers Univ.

ABSTRACT

A theoretical model of radiation heat transfer has been developed. A computation of radiation heat flux at a particular location in the combustion chamber by using the present model requires in-cylinder time- and space-resolved species data and cylinder pressure. From the species data, the burned fuel/air ratio distribution is inferred to compute space-resolved adiabatic flame temperature. For the computation of the spectral emissivity of an isothermal volume of adiabatic temperature containing soot, the Rayleigh-limit expression is used. The refraction indices in the expression are obtained by using the dispersion equations based on the electronic theory encompassing both free and bound electrons. For the spectral emissivity from the gaseous component in the volume, the semi-empirical band model is used. A parametric analysis of radiation heat transfer in diesel combustion is made by using the present model; a prediction by the model qualitatively compares with some of the reported experimental data.

INTRODUCTION

The diesel combustion engine produces high power output per unit volume of fuel. Because of the ever growing shortage of petroleum, the diesel engine has been recognized to be a more important means for transportation, which is well reflected in the recent increased number of diesel engine-powered vehicles.

One of the concerns in the wide use of diesel engines is the emission of diesel smoke (or particulate). The diesel smoke not only looks bad, but also contains polynuclear aromatic hydrocarbon, some of which are known to cause mutagenic actions on living cells (1)*. In addition, in spite of the high fuel economy of diesel powered vehicles, there is a consensus that it can be further improved. Since the conventional diesel engines reject as much as 40% of the total energy produced by the combustion reaction to the cooling and lubrication system, one is interested in reducing the heat loss for improving the engine system. Unlike the premixed spark-ignition engines, the flames in diesel combustion are highly luminous. Although it varies from engine to engine, the portion of radiation heat loss out of the total heat transfer in diesel engines has been reported to range up to 30% or more (2-5). Owing to the fact that the concentration of the particulates appearing in the combustion flame is closely related to its radiation heat emission, without mentioning other complex processes affecting the efficiency, the large amount of smoke appearing in the exhaust, therefore, may suggest a negative sign in diesel economy.

Regarding the engine improvement, it was suggested (6) the thermal efficiency of diesel engines would gain a mere few percent with up to 85% of recovery in heat loss through the water jacket and lubrication system of diesel engines by insulating the combustion chamber. The insulation was proposed to achieve, by using ceramic components in the engine, an adiabatic engine concept (7). A successful development of an adiabatic diesel engine will eliminate the cumbersome engine cooling system, e.g., the water jacket and the radiator making the system more compact and tidy, an additional factor in improving fuel economy (8). A prototype engine of the adiabatic concept has exhibited a specific fuel consumption rate of 0.28 lb/hp-hr (8). Furthermore, when a turbocharger is combined with the adiabatic engine (as a "compound engine"), the overall efficiency of the engine will be increased (6,9).

It appears to be clear that the detailed understanding of heat transfer in diesel combustion, a precondition in the improvement of diesel engines in various aspects, requires extensive information as to the in-cylinder species distribution during the reaction period. In order to

*Numbers in parenthesis designate references at end of paper.

0096-736X/84/9203-1002$02.50

help meet such needs, research of diesel combustion has been conducted at Rutgers, The State University of New Jersey. The study is to investigate the processes of diesel particulate formation and radiation heat transfer in direct injection-type diesel engines by achieving the following objectives: (1) to obtain time- and space-resolved gaseous and particulate concentration in direct injection-type diesel engine combustion, (2) to measure instantaneous heat transfer (convective and radiative, respectively) through the combustion chamber wall, and (3) to identify the relationship of the in-cylinder species concentrations to the radiative heat transfer by constructing a theoretical radiation heat transfer model. The present paper reports the theoretical model of radiation heat transfer developed during the course of the above mentioned diesel combustion research. A computation of radiation heat transfer in diesel combustion by using the present model requires the in-cylinder species distribution and cylinder pressure.

APPROACH OF THEORETICAL MODEL

Among in-cylinder information needed in the computation of the radiative energy incident over a particular location of the diesel combustion chamber wall are the distribution of species and temperature, pressure, and geometric factor. In the computation, it is necessary to find the time-resolved spectral absorption coefficient of each volume of combustion products throughout the chamber, since the reaction process is highly nonuniform in nature with both location and time.

Since Kunitomo et al. (10) reported a model to predict radiation heat flux in diesel combustion that employed a gray body of gaseous and particulate mixtures with a uniform concentration so as to exclude the geometric factor, much research has been carried out on radiation heat transfer of flames enabling a more extensive computation: the in-cylinder sampling of diesel combustion shed a light to offer in-depth species information in the combustion chamber (11,12); a comprehensive technique was proposed to compute thermal radiation by gaseous mixture (13); the method of computing the optical constants of soot mixture has greatly been improved (14,15); the computation of chemical equilibrium properties of combustion becomes feasible (16,17,18).

The present model is an attempt to combine those improved techniques for the computation of radiation energy incident over individual locations of the combustion chamber wall. In the computation, the radiation from a small isothermal volume of combustion products is assumed to be the superimposed result of the emissions from soot and gaseous mixtures without mutual interference. The emissivity of soot, ε_s, may be expressed in terms of the volumetric absorptance of soot, κ_s, and the optical length, L, determined by the size of the volume, as follows,

$$\varepsilon_s = 1 - e^{-\kappa_s L}$$

Similarly, the emissivity of gases, ε_g, can be shown by using the volumetric absorptance of gases, κ_g,

$$\varepsilon_g = 1 - e^{-\kappa_g L}$$

Since it is assumed that the total absorption coefficient, κ, is the sum of κ_s and κ_g, one may write the emissivity of the combined radiation, ε, as,

$$\varepsilon = 1 - (1-\varepsilon_s)(1-\varepsilon_g) \qquad (1)$$

Therefore, the radiation energy streaming away from the volume, B, by knowing its temperature, T, can be found as,

$$B = \varepsilon\sigma T^4 \qquad (2)$$

where, σ is the Stefan-Boltzman constant.

The incident radiation flux, H, on a particular detecting area, A_d, originated from the emitting source area, A_e, can be expressed as,

$$H_{A_e \to A_d} = F_{A_e \to A_d}\, \varepsilon\sigma T^4 \qquad (3)$$

where, $F_{A_e \to A_d}$ is the geometric factor from A_e to A_d.

Integrating over the entire emitting source, one can find the total radiation energy incident on the detecting area, that is,

$$H_{A_d} = \int_{A_e} F_{A_e \to A_d}\, \varepsilon\sigma T^4\, dA \qquad (4)$$

The result of the present computation is reported by using the "apparent emissivity" defined as,

$$\varepsilon_a = H_{A_d} / \sigma T_r^4 \qquad (5)$$

where, T_r is arbitrarily chosen to be 2400°K.

COMPUTATIONAL DETAILS

The details of the computational steps and assumptions of the methodology outlined above are explained for the following items: (1) the temperature of each mixture volume, (2) the soot radiation, (3) the gas radiation and (4) a computation of radiation heat transfer in diesel combustion.

Adiabatic Flame Temperature —— The temperature of a designated volume of in-cylinder mixture was assumed to attain the adiabatic flame temperature which can be computed by using the species distribution which may be obtained either theoretically or experimentally. In addition, the entity in the volume is assumed to be at an equilibrium of the temperature and pressure.

Besides fuels, eleven gaseous species were included in the computations of the adiabatic flame temperature and the equilibrium composition by using the burned fuel/air ratio inferred from the species distribution. Although such computations have been widely employed by others for flame studies in the past (16,17), the present paper offers a new technique of their computations that greatly reduce the computer time. The details of the computation and the new iteration technique are shown in Appendix I.

Soot Radiation —— The thermal radiation of soot in diesel combustion is the combined result of the emission, absorption, and scattering of soot particles. Since, according to Planck's function, the main portion of the thermal emission from the soot is infrared, i.e., in the range of wavelength, λ = 1~10μm, the present computation considers the corresponding range of wavelength. Regarding the absorption, if the designated volume of mixture attains a thermal equilibrium, the absorption of the radiation can be determined by the Kirchhoff principle which states that the spectral volume absorption coefficient is exactly equal to the spectral volume emissivity for a system in a thermal equilibrium with its surroundings. In the present paper, for convenience, the absorption coefficient is used instead of the volume emissivity or absorptivity. Discussing the scattering, Kunitomo (19) reported that the great majority of diesel exhaust particulate was so small that their scattering affected less than 1% at a photon wavelength of 1μm and considerably less at a larger wavelength. Assuming that the in-cylinder soot size distribution is in the similar range of that in the exhaust, which was supported by a recent experimental study (20), the scattering of soot is neglected in the thermal radiation of diesel combustion.

With the above assumptions, the soot radiation is computed in the following sequence: (1) to formulate the spectral emissivity of the soot $\varepsilon_{s\lambda}$, (2) to find the spectral absorption coefficient, $\kappa_{s\lambda}$, which is related to the refraction index of the soot, and (3) to compute the soot emissivity.

As explained earlier, the spectral absorption coefficients can be found from the following relationship,

$$\varepsilon_{s\lambda} = 1 - e^{-\kappa_{s\lambda} L} \qquad (6)$$

Since the median size of soot is in the range of 0.1μm (21,22), which is approximately one tenth of infrared wavelength, $\kappa_{s\lambda}$ may be found using the following Rayleigh-limit expression (21).

$$\kappa_{s\lambda} = \frac{36n^2k(\pi/\lambda)f_v}{[n^2(1-k^2)+2]^2+4n^2k^2} \qquad (7)$$

where, n and nk are the complex refraction indices of the soot, and f_v is the soot volume fraction.

The above expression to employ dispersion equations based on the classical electronic theory (14,15) was used in the present computation. According to the experimental results, the complex optical constants (n-ink) in Eq. (7) vary with the wavelength as shown in Table I.

Table I: Optical Constants of Soot (14)

	Acetylene Soot (H/C=1/14.7)		Propane Soot (H/C=1/4.6)	
λ(μm)	n	nk	n	nk
0.4358	1.56	0.46	1.57	0.46
0.45	1.56	0.48	1.56	0.50
0.55	1.56	0.46	1.57	0.53
0.65	1.57	0.44	1.56	0.52
0.8065	1.57	0.46	1.57	0.49
2.5	2.31	1.26	2.04	1.15
3.0	2.62	1.62	2.21	1.23
4.0	2.74	1.64	2.38	1.44
6.0	3.22	1.84	2.62	1.67
10.0	4.80	3.82	3.48	2.46

Dalzell and Sarafim (14) suggested that the optical constants of different soot may depend, to a small extent, on difference in molecular structure and, to a large extent, on the differences in the ratio of hydrogen to carbon molecules (H/C). Note that the H/C of the soot in most combustion systems is found to fall between the two extremes as shown in the table. As for the temperature dependency, it was found that the optical constants were insensitive to temperature (14,15). In providing a basis for interpolating the results of the table, a dispersion model was found to fit the data by choosing the appropriate parametric constants (14). More details of the use of the dispersion equation for finding the optical constants are shown in Appendix II.

Upon the given values of fuel/air ratio and f_v, the spectral emissivity of soot, $\varepsilon_{s\lambda}$, of a volume can be determined by using the above mentioned optical constants of the soot. From the definition, the soot emissivity, ε_s, is expressed as,

$$\varepsilon_s = \int_0^\infty \varepsilon_{s\lambda} E_{b\lambda}(T) d\lambda / \sigma T^4 \qquad (8)$$

where, $E_{b\lambda}(T)$ is the Planck's radiation function

$$E_{b\lambda}(T) = \frac{2\pi hc^2}{\lambda^5[\exp(hc/\lambda KT)-1]}$$

$c = 2.998 \times 10^{10}$ cm/sec,

$K = 1.380 \times 10^{-16}$ erg/°K, and

$h = 6.625 \times 10^{-27}$ erg-sec.

Substituting Eq. (6) into Eq. (8), one obtains,

$$\varepsilon_s = 1 - \int_o^\infty e^{-\kappa_\lambda L} E_{b\lambda}(T)d\lambda/\sigma T^4 \qquad (9)$$

Many researchers (23-26) attempted to find the solution to Eq. (9) by assuming a simple expression of the spectral absorption coefficient as,

$$\kappa_\lambda = \kappa_o f_v/\lambda^d \qquad (10)$$

where, κ_o is a constant independent of temperature and d is chosen to be close to 1.

Although this enabled one to further simplify Eq. (9) to obtain an integral equation containing the hexagamma function (24,27), the final result was calculated by numerical means.

Even though their method was relatively simple and widely used, a better technique to find an exact solution of Eq. (9) has been developed in the present work. Since the refraction indices are almost constant in each subinterval of the entire integration range, the solution to Eq. (9) can be found as a closed-form by using the following variable transformation method. In order to replace the temperature and wavelength variables in Eq. (9), a new dimensionless variable x is defined as follows.

$$x = hc/\lambda KT \qquad (11)$$

To obtain a tidy expression, another parameter, a, is given as,

$$a = \frac{36\pi n^2 k}{[n^2-n^2k^2+2]+4n^4k^2} f_v L \frac{KT}{ch} \qquad (12)$$

Equation (9), then, can be expressed in terms of x and a as,

$$\varepsilon_s = 1 - \frac{15}{\pi^4} \int_o^\infty e^{-ax} \frac{x^3}{e^x-1} dx \qquad (13)$$

or in the following numerical integration form,

$$\varepsilon_s = 1 - \frac{15}{\pi^4} \sum_{i=1}^{M} \int_{x_i}^{x_{i+1}} e^{-a_i x} \frac{x^3}{e^x-1} dx \qquad (14)$$

where, M is the number of the intervals in the whole integral range and a_i is the parameter a of the ith interval.

The solution of the integral in Eq. (14) has been found by using a unique method developed by the authors (28). Without showing the procedure, the exact solution is given as follows.

$$\int_{x_i}^{x_{i+1}} e^{-a_i x} \frac{x^3}{e^x-1} dx = S(3,a_i,x_i) - S(3,a_i,x_{i+1}) \qquad (15)$$

where,

$$S(3,a,x) = \sum_{n=1}^{\infty} e^{-(n+a)x} \sum_{i=0}^{3} \left[\frac{\Gamma(3+1)}{\Gamma(3-i+1)}(n+a)^{-i-1} x^{3-i}\right] \ldots \qquad (16)$$

and Γ is the gamma function defined as $\Gamma(m+1) = m \cdot \Gamma(m)$ and $\Gamma(1) = 1$.

By using the above solution, the soot emissivity of an isothermal volume at a given temperature can be found as,

$$\varepsilon_s = 1 - \frac{15}{\pi^4} \sum_{i=1}^{M} [S(3,a_i,x_i) - S(3,a_i,x_{i+1})] \qquad (17)$$

Gas Radiation —— Although there are many gaseous species in flames, carbon dioxide and water vapor are reported to be mainly responsible for the thermal radiation (10,24,29). Therefore, these two species were only considered in the present model. The gas radiation, depending upon the molecular structure, has several blocks of the lines in the spectra of soot. By averaging over the wave number of each block, a continuous distribution of the emission (or absorption) coefficient, which is also called a band, can be computed by assuming that waves outside these bands neither emitted or absorbed.

The major bands of both gases occur, for water vapor, of the principal vibration-rotational bands at 1.38μm, 1.87μm, 2.7μm, and 6.3μm and of a weak rotational band at 20μm; for carbon dioxide, of the principal bands at 1.9μm, 2.7μm, 4.3μm, and 15μm, and of the two minor bands at 9.4μm, 10.4μm. There are two overlapping bands at 2.7μm; one is from water vapor and the other from carbon dioxide.

By definition, the spectral band absorptance, α_ν, of an isothermal volume is written in a similar form of Eq. (6) as,

$$\alpha_\nu = 1 - \exp(-\kappa_\nu L) \qquad (18)$$

where, ν is the wave number, L is the optical length, and κ_ν is the volume absorption coefficient of the gas.

The experimental results (30-33) exhibited the distribution of the spectral absorption coefficient to be rather irregular so that a general expression of the radiation bands is unavailable. For practical applications, several models have been proposed to fit the experimental data. Of those, the wide band model proposed by Edwards and Balakrishnan (13) was employed in the present work. The model assumes a block approximation that calls for black-body in the bands and is transparent otherwise. The total band absorbence, A_i, which is band width of the ith band, is defined as,

$$A_i = \int_{\text{band } i} d(\alpha_\nu) \qquad (19)$$

where, ν_i is the wave number at the center of the ith band.

The model provides, for each band of the gas radiation, a semiempirical correlation of the integrated band intensity, α, the band width parameter, A_{oo}, the line width parameter, β, and the effective pressure, P_e. The use of these parameters for finding A is shown later in Table II, and computation of each parameter is shown in the following.

The effective pressure, P_e, which is responsible for the pressure broadening effect, is written as,

$$P_e = [P/P_o + (p_i/P_o)(b-1)]^N \qquad (20)$$

where, P_o is one atmosphere, P is the cylinder pressure of the engine, P_i is the partial pressure of the absorbing gas, and b,N are the self-broadening coefficients given in Appendix III.

The computation of several band parameters (e.g., integrated band intensity and band width parameters) needed in the computation of the band absorptance is explained in Appendix III.

By knowing the gas density, ρ, optical length, L, and the above mentioned band parameters, a set of universal band absorption correlations can be found for the computation of the total absorptance, A_i, of the ith gas radiation band. Table II shows the correlations, which relate the dimensionless integrated band absorptance, $A^* = A/A_o$, to the optical depth parameter, $\tau = \alpha\rho L/A_o$, and the effective pressure parameter, $\eta = \beta P_e$.

Table II: Band Absorption Correlations (13)

η	τ_{min}	τ_{max}	A^*
< 1	0	η	τ
	η	$1/\eta$	$(4\eta\tau)^{1/2} - \eta$
	$1/\eta$	∞	$\ln(\eta\tau) + 2 - \eta$
≥ 1	0	1	τ
	1	∞	$1 + \ln\tau$

where, $\tau = \alpha\rho L/A_o$, $\eta = \beta P_e$, and $A^* = A/A_o$. Note that the line width parameter, β, and the band width parameter, A_o, are found as explained in Appendix A-III.

Since the gas emissivity in the bands is assumed to be unity while outside the band is zero, the gas emissivity of the ith band may be expressed in a dimensionless variable, x,

$$\varepsilon_{g,i} = \frac{15}{\pi^4} \int_{\text{band } i} \frac{x^3}{e^x - 1}\, dx \qquad (21)$$

where, $x = hc\nu/KT$.

The exact solution of Eq. (21) can be found by using a similar method employed for Eq. (13).

Table III:
Ranges of H_2O amd CO_2 Emission Band

	Bands (μ)	ν_l (cm^{-1})	ν_c (cm^{-1})	ν_u (cm^{-1})
H_2O	20	0		
	6.3		1600	
	2.7		3760	
	1.87		5350	
	1.38		7250	
CO_2				
	15		667	
	10.4		960	
	9.4		1060	
	4.3			2410
	2.7		3660	
	2.0		5200	

The range of integration for each band is shown in Table III. For the case of a nonoverlapped band, if the lower or upper bound of the band is given, the other bound can be found by

$$\nu_{u,i} - \nu_{l,i} = A_i \qquad (22)$$

If the center of the band, $\nu_{c,i}$, is given (Table III), both upper and lower bound wave number can be calculated by

$$\nu_{u,i} = \nu_{c,i} + A_i/2 \qquad (23)$$

$$\nu_{l,i} = \nu_{c,i} - A_i/2 \qquad (24)$$

After all, the gas emissivity of ith band whose range is $x_{l,i} < x < x_{u,i}$ can be expressed as follows.

$$\varepsilon_{g,i} = \frac{15}{\pi^4} [S(3,0,x_{l,i}) - S(3,0,x_{u,i})] \qquad (25)$$

where,

$$S(3,0,x) = \sum_{n=1}^{\infty} \left\{ e^{-nx} \sum_{i=0}^{3} \frac{x^{3-i}\,\Gamma(3+1)}{n^{i+1}\,\Gamma(3-i+1)} \right\}.$$

The gas emissivity of an isothermal gas volume at a flame temperature, T, and pressure, P, can be determined by summing the radiation of all bands of water vapor and carbon dioxide, i.e.,

$$\varepsilon_g = \sum \varepsilon_{g,i} \qquad (26)$$

The emissivity of the combined radiation is obtained by introducing Eqs. (17) and (26) in Eq. (1).

Computation of Radiation Heat Transfer in Diesel Combustion —— For a parametric computation

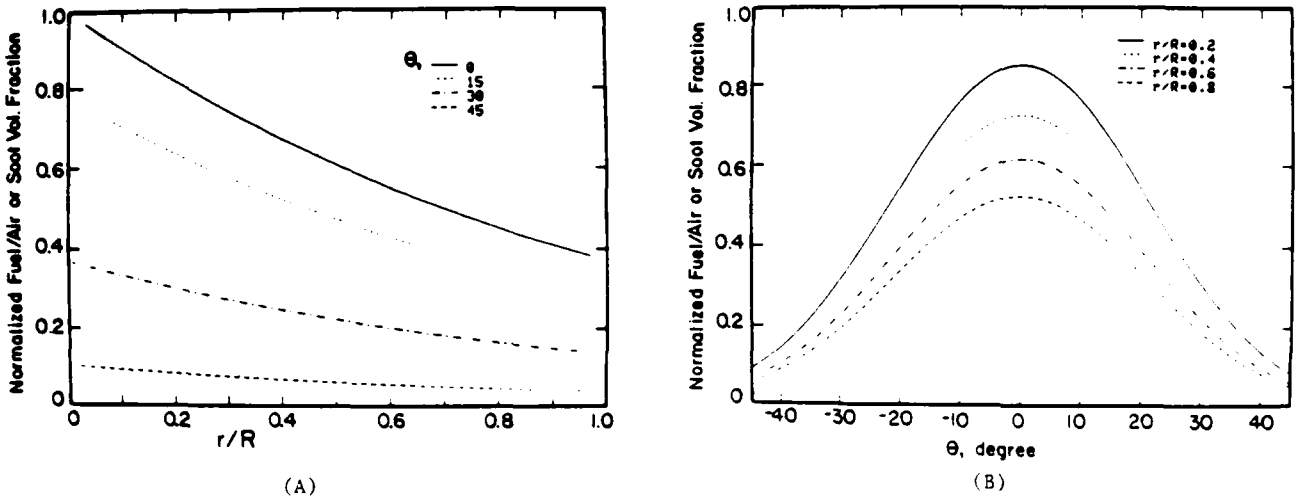

Figure 1. Normalized Distribution of Burned Fuel/Air Ratio and Soot Volume Fraction in (A) Radial Direction and (B) Angular Direction.

of radiation heat transfer in diesel combustion, several assumptions were taken as listed below.

(1) The system of which size is small but large enough to represent the local volume of mixture is isolated allowing no heat and work flow across the boundaries.
(2) The gaseous species in the system attain an equilibrium state of the adiabatic flame temperature determined by the local burned fuel/air ratio and cylinder pressure.
(3) The radiation source is a 2-dimensional surface with prescribed optical length.
(4) The fuel/air ratio, soot volume fraction, and gas species concentration are available enabling construction of the 2-dimensional radiation source.

As to the assumption of isolated system, the system receives the piston work while it loses energy through radiation; this mutual compensation may partially justify the assumption. Although the processes in diesel combustion occur at highly non-equilibrium states, the system volume was chosen to be small and to attain an equilibrium for simplicity of computation. Since the optical length is varied over the source, the 2-dimensional emission source was considered to represent the emission characteristics of the in-cylinder mixture volume. Note a study to construct a 3-dimensional model to eliminate this assumption is under way. Although in-cylinder species information will be obtained either experimentally or theoretically, the present computation was carried out for assumed distributions of species. The distributions of the burned fuel air ratio and soot concentration assumed for the present parametric study showed that they decreased exponentially along the radial direction and held a normal distribution in the angular direction [Fig. 1]. The non-dimensional form of the distribution, f, may be expressed as follows.

$$f = f_o \, e^{-a\theta^2} \, e^{-br} \qquad (27)$$

where, r, θ are the radius and angular coordinates, f_o, a, and b are to be determined from experimental data.

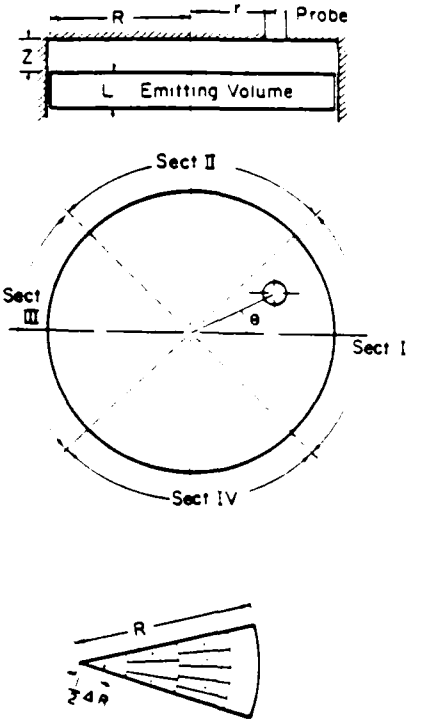

Figure 2. Two-Dimensional Radiation Emitting Source

In order to complete the computation, a numerical scheme was employed. Figure 2 shows the 2-dimensional emission surface divided into

sectors according to the fuel plume position. Each sector is divided into n rings with a uniform width, and each ring is again cut into equisize cells. By setting a nodal point at the center of each cell, one obtains n^2 nodals with the same area in a sector. In each nodal point, the fuel/air ratio, gas species concentration, soot volume fraction, and optical length were specified according to Eq. (27).

Upon the implementation of the above numerical scheme, a computer program became available for computation of radiation heat flux incident on any location in the cylinder head. Table IV shows nineteen subroutines included in the program in addition to the main program.

Table IV. Subroutines for Various Computations

Subroutines	Subject of Computation
AFT	Adiabatic flame temperature
HEAT	Enthalpies of species
EQSTAT	Equilibrium state composition
EQCON	Gibbs free energy
ROOT	Positive real root of 2nd or 3rd order algebraic eq. in EQSTAT
FACT	Gamma function values
RA	Combined radiation heat flux
SFACT	Geometric factor
POINTER	Interpolation procedure in EQCON
POINTER1	Interpolation procedure in HEAT
SOOT	Soot emissivity
OPTI	Optical constants of soot by Eq. (A15)
SERIES	Integration of Eq. (16)
GAS	Gas emissivity
CHIWHI	χ and ψ defined in Eqs. (A17) & (A20)
BANDA	Integrated band absorptance-Table III
A1	Integrated band absorptance-Table III
AH2O	Evaluate the emission band positions of H_2O
ACO	Evaluate the emission band positions of CO_2

PARAMETRIC STUDY OF RADIATION HEAT TRANSFER

The construction of the present model of radiation heat transfer has enabled a parametric analysis of its processes in diesel combustion. Several assumptions were employed in the analysis.

(1) The detection surface of which incident radiation heat flux is computed is parallel with the emitting surface so that the shape factor can be explicitly expressed.
(2) There are four plumes of pie shape with a uniform optical length of 10 mm over the emitting surface.
(3) The fuel volume fraction of stoichiometric, ϕ, and soot volume fraction, f_v, have profiles in the plume as expressed in the following equations.

$$\phi = 2.933\,\phi_o \exp[-1.5(\theta/\theta_o)^2] \exp(-0.8r/R) \quad (28)$$

$$f_v = 2.933\,f_{v0} \exp[-1.5(\theta/\theta_o)^2] \exp(-0.8r/R) \quad (29)$$

where, θ_o is $\pi/4$, R is the cylinder radius, and ϕ_o, f_{v0} are the mean values of the fuel volume fraction of stoichiometric and soot volume fraction in the combustion chamber, respectively.

Among the parameters varied in the computation were the position of detection surface on the cylinder head, the mean burned equivalence ratio, the mean soot volume fraction, and the clearance between the emitting surface and the cylinder head, and the cylinder pressure. Some of the results from the computation are shown in the following. Note that, for comparison purposes, the results are expressed in apparent emissivity (this will be represented by AE hereafter) defined in Eq. (5) instead of the heat flux.

Location of Detector —— The radiation heat flux incident on different locations of the cylinder head was computed. The AE at different locations along r-direction and over θ-direction are shown in Figs. 3 and 4, respectively. The AE monotonously decreases in the positive r-direction, and holds a bell-shaped profile over the θ-direction. Although expected, it is interesting to find such non-uniformity of AE over the cylinder head. The variation is much greater over the θ-direction than the r-direction. The distribution of AE is quite similar to those of burned fuel/air ratio, species concentration projected on the cylinder head, which is not a surprising result since the radiation heat flux is strongly dependent on those distributions. This suggests that the present model may help evaluate the thermal load of a new engine head once the engine fuel injector and combustion characteristics are predicted or given. The bell-shaped distribution of AE over the θ-direction indicates that the AE at a particular location is almost entirely dictated by the fuel plume right underneath. This is mainly due to the small clearance, z, between the cylinder head and the emitting source and its further analysis is followed in the next.

Location of Emitting Plain —— Since the diesel combustion products move away from the cylinder head as the piston descends, it is important to evaluate the AE for different clearances between the cylinder head and the emitting plain, z. Figure 5 exhibits some interesting results. For smaller z, the AE of locations close to the axis of the plume is greater and more rapidly decreases in the θ-direction; the AE therefore attains greater values for greater z at the locations far from the axis. This is explained by the larger value of the shape factor for greater z.

Position of plumes —— In the above analyses, it was found that the radiation heat flux incident on a location is strongly affected by the plume right below. Figure 6 shows the evaluation of the contribution by the spray plumes on the AE at locations along r/R = 1/2 and z/R = 3/40 over the θ-direction. The AE due to the plume right under the detector at $\theta = 0$ is 0.147 while the AE due to all other plumes is only 0.0026. This reaffirms that the AE of a particular location is almost entirely controlled by the nearest spray plume.

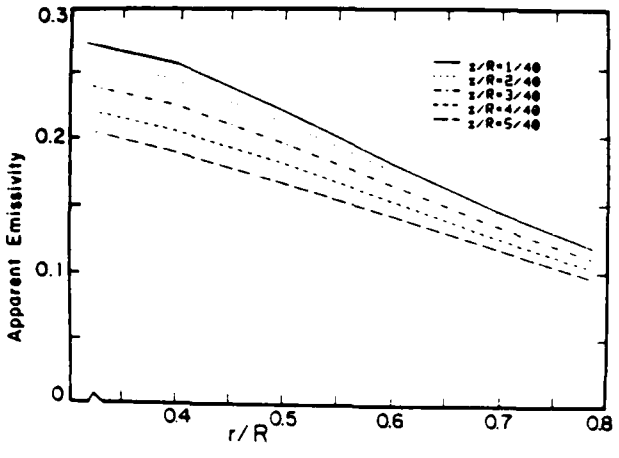

Figure 3. Apparent Emissivity at Different Locations Along the r-direction

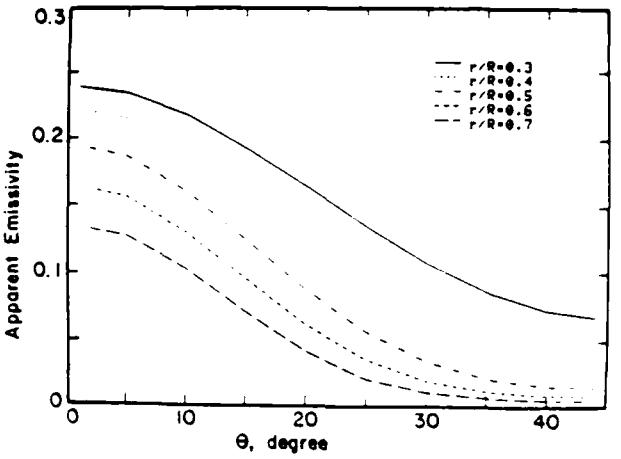

Figure 4. Apparent Emissivity at Different Locations over the θ-direction with z/R = 3/40

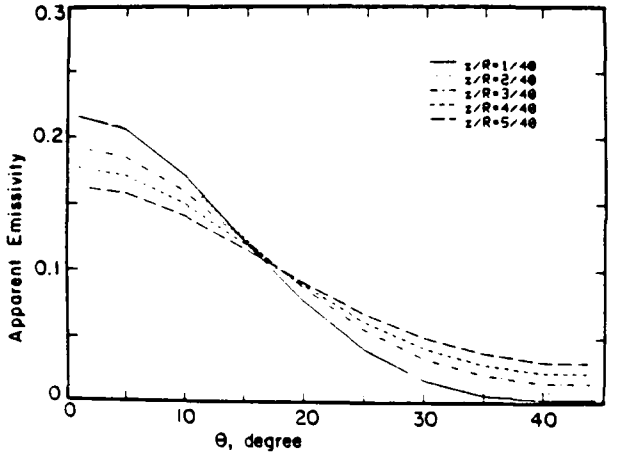

Figure 5. Apparent Emissivity due to the Emitting Plain Located at Different Clearances with r/R = 1/2

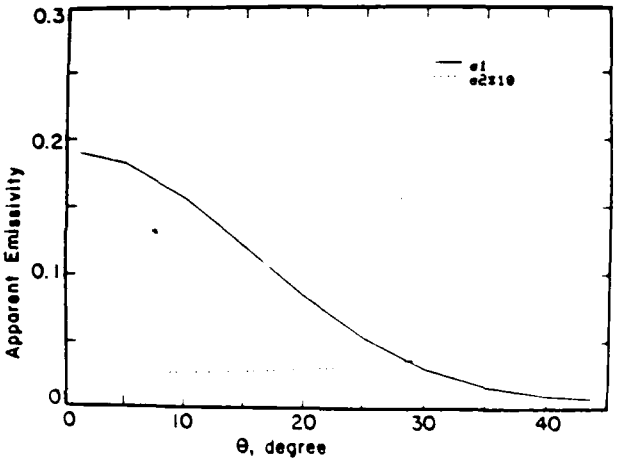

Figure 6. Effect of Plume Locations on Apparent Emissivity

Soot Concentration —— Since the representative in-cylinder soot data are not presently available, the effect of soot volume fraction, f_v, on the AE was analyzed by using various values of f_v arbitrarily chosen but within 5 to 100 times greater than the reported exhaust f_v. This is consistent with reports by Aoyagi et al. (12) who suggested that the amount of soot per exhaust gas volume is approximately 1/40 of the amount of soot per cylinder volume and by Kittleson and Du (20) who measured to find that the amount of soot in the exhaust is approximately 1/3 of the total soot appearing in the cylinder. The mutual consistency stands since the volume of the soot at TDC is expected to be approximately 1/11 of that in the exhaust. Figure 7 shows the AE of a detecting area over the θ-direction with r/R = 1/2, z/R = 3/40. The AE increases with soot concentration as expected. However, it is interesting to find that the emissivity does not proportionally increase with the soot concentration. The increment of the AE is larger at lower concentration range of f_v and vice versa. The partial reason for the convergence of AE at high soot concentration is due to the exponential function in the relationship of the emissivity and the absorption coefficient as shown in Eq. (6).

Soot and Gass Radiation —— Although it has often been mentioned in literature (37) that the high luminosity of soot flames in diesel combustion is responsible for the diesel radiation heat loss, only a limited evaluation has been separately made on the contribution on AE by soot and gas of combustion products in diesel combustion. Figure 8 shows the AEs by soot and its mixture

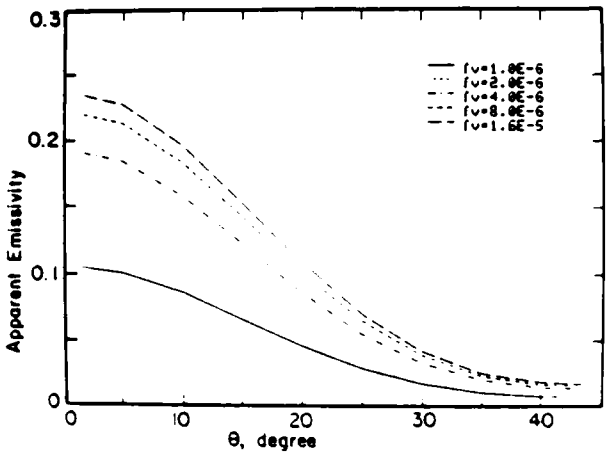

Figure 7. Soot Volume Fraction Effect on Apparent Emissivity

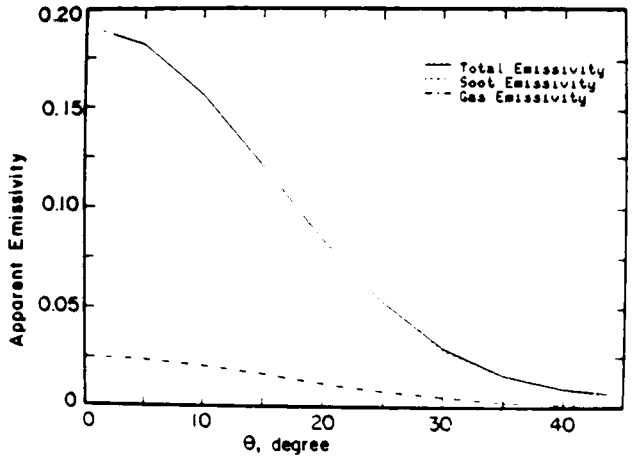

Figure 8. Apparent Emissivities by Soots and Gases in Diesel Combustion

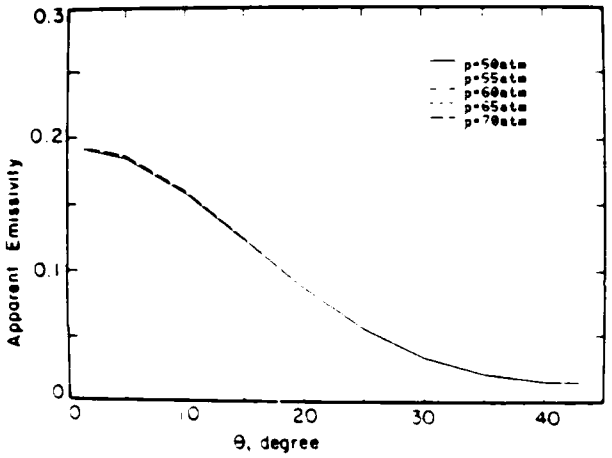

Figure 9. Pressure Effect on Apparent Emissivity for a High Soot Concentration Combustion

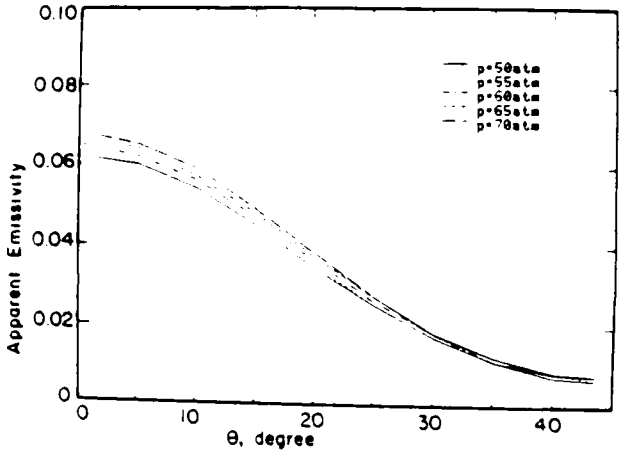

Figure 10. Pressure Effect on Apparent Emissivity for a Low Soot Concentration Combustion

computed for seemingly a typical diesel combustion condition. The total AE which results from both soot and gas is found almost entirely caused by the soot in flames, i.e., the gas radiation in diesel combustion is extremely small compared to the soot radiation. This may suggest that the radiation heat loss from premixed gasoline-fueled engine combustion is negligible. Note that the present result suggesting the gas radiation to be a mere fractional contribution on the total radiation is considerably different from those computed by Kunitomo et al. (10). Their results predicted that the gas radiation ranged between 20% to 50% of the combined radiation. The discrepancy between the present results and their results may be caused by the differences in the computation.

Pressure Effect —— Because of the inherently high pressure reaction condition of diesel combustion, it may be important to look into the pressure effect on the thermal radiation in the combustion chamber. The analysis was made without including the modification of fuel spray and atomization affected by pressure. The computation was made for plumes with a high soot concentration ($f_v = 4.0*10^{-6}$) and with low concentration ($f_v = 4.0*10^{-7}$) as shown in Figs. 9 and 10, respectively. The results suggest that for high soot concentration flames the pressure effect on the AE is almost negligible. Since the flame temperature is very insensitive to the pressure variation, the results indicate no effect on the soot radiation. In Fig. 10 plotting for a low soot radiation, the pressure effect on the AE is remarkable, which suggests that there exists the pressure broadening effect of the gas radiation in diesel combustion. Note, however, that the impact of the pressure broadening in a typical diesel combustion condition is found negligible.

Radiation Heat Loss in Diesel Combustion — Due to the lack of in-cylinder particulate and gaseous species data, the present parametric study was limited for an engine crank angle, although the new model can be employed for the evaluation of the entire period of combustion. A computation was made, however, for a limited portion of the combustion period by using a set of in-cylinder data arbitrarily chosen but close to real based on the following assumptions. (1) The cylinder pressure increases with engine crank angle until 8°CA after top dead center (TDC) and decreases thereafter. (2) The soot volume fraction increases with crank angle but starts to decrease 16°CA after TDC. The relationship of f_v to CA was chosen to be identical to that of heat release rate to CA based on the experimental findings reported by Kittleson and Du (20). They found that the amount of in-cylinder soot almost exactly followed the heat release rate to CA history. (3) The burned fuel/air ratio continuously increases during the period of combustion. (4) The optical length is assumed to be 10mm over the entire emitting surface with varying species concentration. The combined AE (due to soot and gases), ε_c, and gas AE, ε_g, computed by using the above input for a detecting area at r/R = 1/2 and θ = 0 are shown in Fig. 11. It is interesting to find the AE is very low prior to 180°CA while f_v is relatively high and vice versa after 190°CA. This may be explained in terms of temperature that is dictated by the burned fuel/air ratio. Again, it is predicted that the gas AE is a negligible portion of the combined AE in diesel combustion.

Comparison with Other Reports — The present model will not be compared with other models (3,10) since they did not report the in-cylinder species data and the computation of space-resolved heat flux in diesel combustion. However, a comparison with some experimental results is attempted to a limited extent. The main difficulty encountered in the selection of compatible experimental data for the comparison was the variety in measurement techniques, measurement locations in the cylinder, engine operating condition, types of engine chosen for the previous data acquisition, etc. (2,36,38,39). The "potential" radiation heat transfer data reported by Flynn et al. (1972) were chosen for the present discussion since their data did not include the emissivity of the detector. The same data shown in Fig. 11 were used to compute the optical thickness, KL, to compare with Flynn's data. Note that since the apparent optical thickness reported by them were computed based on the measured apparent radiation temperature, an adjustment was made on two sets of data of different injection timing to achieve a more consistent comparison with the present results. Fig. 12. Even with the above mentioned difficulties, some interesting notes may be drawn from the comparison. The prediction is lower than the measurements by a factor of 2-4. Among probable reasons for the prediction of low optical thickness may be the substantially greater optical length, L, in their measurement than the present one. However, it is encouraging to find that the trend of predicted KL relationship to CA compares well with that from the experiment. When the in-cylinder radiation heat flux data become available from the present ongoing study, the model will be further analyzed for the verification.

SUMMARY

A new radiation heat transfer model of diesel combustion has been developed. Use of the present model requires in-cylinder information as to time- and space-resolved particulate and gaseous species and pressure-time data.

The model employs, for the emissivity of a volume gases containing soot, Rayleigh-limit expression to compute the spectral absorption coefficient of soot, the dispersion equations to compute the refraction indices included in the

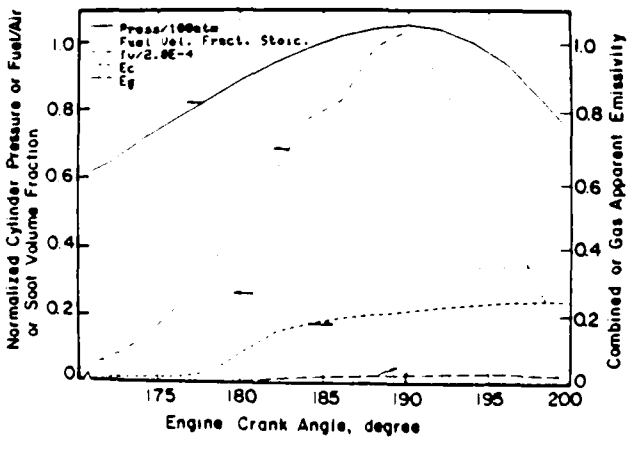

Figure 11. A Set of In-cylinder Data Chosen for a Computation Radiation Heat Transfer and Computed Apparent Emissivity

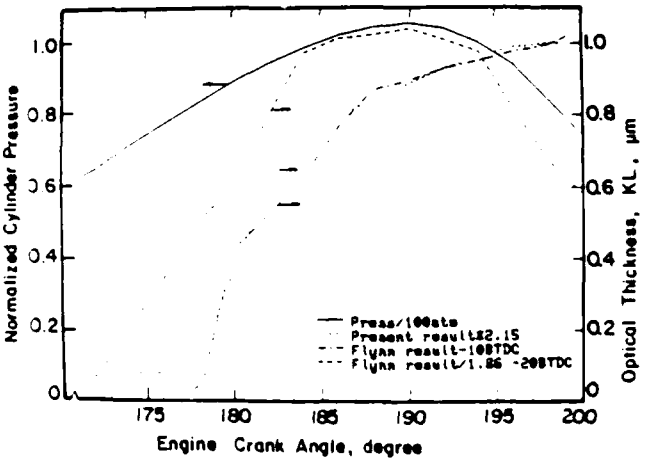

Figure 12. A Comparison of Present Computation with Other Investigator's Reports.

Rayleigh-limit expression, the band model to obtain the spectral band absorptance of gaseous mixture, the adiabatic flame temperature obtained based on the burned fuel/air ratio, and for the computation including the geometric consideration of the combustion system, a numerical scheme including the shape factor to integrate over the entire non-uniform emitting source.

A parametric analysis of the diesel radiation heat transfer was carried out by using the present model. Among the findings from the analysis are:

(1) The thermal radiation flux incident on a particular location of the cylinder is mainly originated from the nearest fuel plume and very little from other plumes;
(2) The radiation flux greatly decreases as the clearance between the detecting location and the plain of emitting source increases;
(3) The radiation flux is generated mostly due to the presence of soot and negligibly due to the presence of gaseous combustion products;
(4) The soot radiation increases with the soot concentration greatly when the average soot concentration is low and vice versa;
(5) There is an obvious pressure broadening effect on the gas radiation in diesel combustion. However, its impact on the combined radiation in diesel combustion is negligible;
(6) The thermal radiation in the very beginning of the combustion period may be low due to the low temperature even though the soot concentration is potentially high at the time; and,
(7) A prediction by the present model qualitatively compares with some of the reported experimental data.

ACKNOWLEDGEMENT

This research has been supported by the U.S. Department of Transportation, contract no. DTRS 5680-C-00029 and the U.S. Army Research Office, contract no. DAAG 29-83-K-0042 (Scientific program officer, Dr. David M. Mann). Messrs. Christopher Sheft, Jeffrey Matonick, and Xiaolong Yang have greatly contributed to the present work.

REFERENCES

1. Barth, D.S. and Blacker, S.M., "The EPA Program to Assess the Public Health Significance of Diesel Emissions", JAPCA, Vol. 28, No. 8, pp. 769-771, 1978.

2. Ebersole, G.D., Myers, P.S., and Uyehara, O.A., "The Radiant and Convective Components of Diesel Engine Heat Transfer", SAE Paper-701C, 1963.

3. Sitkei, G. and Ramanaiah, G.V., "A Rational Approach for calculation of Heat Transfer in Diesel Engines", SAE Paper 720027, 1972.

4. Kamel, M. and Watson, N., "Heat Transfer in the Indirect Injection Diesel Engine", SAE Paper 790826, 1979.

5. Murphy, M.J., Hillenbrand, L.J., Trayser, D.A., and Wasser, J.H., "Assessment of Diesel Particulate Control - Direct and Catalytic Oxidation", SAE Paper 810112, 1981.

6. Amann, C.A., "Why not a New Engine?", SAE Paper 801428, 1980.

7. Woods, M.E. and Oda, I., "PSZ Ceramics for Adiabatic Engine Components", SAE Paper 820429, 1982.

8. Bryzik, W. and Kamo, R., "Cummins/TACOM Adiabatic Engine", SAE Paper 830314, 1983.

9. Wallas, F.J., Kao, W.D., Alexander, A. C., and Cole, M.T., "Thermal Darrier Pistons and Their Effects on the Performance of Compound Diesel Engine Cycles", SAE Paper 830312, 1983.

10. Kunimoto, T., Matsuoka, K., and Oguri, T., "Prediction of Radiative Heat Flux in a Diesel Engine", SAE Paper 750786, 1975.

11. Rhee, K.T., Myers, P.S., and Uyehara, O.A., "Time- and Space-Resolved Species Determination in Diesel Combustion Using Continuous Flow Gas Sampling", SAE Paper 780226, 1978.

12. Aoyagi, Y., Kamimoto, T., Matsui, Y., and Matsuoka, S., "A Gas Sampling Study on the Formation Processes of Soot and NO in a DI Diesel Engine", SAE Paper 800254, 1980.

13. Edward, D.K. and Balakrishnan, A., "Thermal Radiation by Combustion Gases", J. of Heat Mass Transfer, Vol. 16, pp. 525, 1973.

14. Dalzell, W.H. and Sarofim, A.F., "Optical Constants of soot and their application to Heat Flux Calculation", Trans. of ASME, Vol. 9, pp. 100, 1969.

15. Lee, S.C. and Tien, C.L., "Optical Constants of soot in Hydrocarbon Flame", 18th Symposium of Combustion, The Combustion Institute, pp. 1159-1165, 1981.

16. Gordon, S. and McBride, B.J., "Complex Chemical equilibrium Calculation", NASA, SP-273, 1971.

17. Olikara, C. and Borman, G.L., "A Computer Program for Calculating Properties of Equilibrium Combustion Products with some Application to I.C. Engines", SAE Paper 750468, 1975.

18. Kestin, J., A Course in Thermodynamics. Vol. (II), McGraw Hill Book Company, 1979.

19. Kumitomo, T., and Sato, T., "Experimental and Theoretical Study on the Infrared Emission of Soot Particles in Luminous Flame", Heat Transfer, Vol. III, Elsovier Publishing Co., Amsterdam, pp. R1.6, 1970.

20. Kittleson, D.B., Du, C.J., and Pipho, M., "Total Cylinder Sampling from a Diesel Engine: Part II - Particulate Measurement", SAE Paper 830243, 1983.

21. Bard, S. and Pagni, P.J., "Carbon Particles in Small Pool Fire Flame", ASME Trans., J. of Heat Transfer, Vol. 103, pp. 357-362, 1981.

22. Khatri, N.J. and Johnson, J.H., "Physical Size Distribution Characterization of Diesel Particulate Matter and the Study of the Coagulation Process", SAE Paper 780788, 1978.

23. Balakrishnan, A. and Edwards, D.K., "Radiative Flame Cooling for Reduction of Nitric Oxide Emission", ASME Trans., J. of Heat Transfer, Vol. 96, pp. 37-42, 1974.

24. Buckius, R.O. and Tien, C.L., "Infrared Flame Radiation", Int. J. of Heat Mass Transfer, Vol. 20, pp. 93-106, 1977.

25. Liu, C.N. and Shih, T.M., "Laminar, Mixed-Convection Boundary-layer, Nongray-Radiative, Diffusion Flames", ASME Trans., J. of Heat Transfer, Vol. 102, pp. 724-730, 1980.

26. Felske, J.D. and Lee, K.M., "Nongray Particulate Radiation in an isothermal Cylindrical Medium", J. of Heat Transfer, Vol. 103, pp. 121-126, 1981.

27. Grosshaudler, W.L. and Modak, A.T., "Radiation from Non-homogeneous Combustion Products", 18 Symposium (International) on Combustion, The Combustion Institute, pp. 601-609, 1981.

28. Chang, S.L. and Rhee, K.T., "A Useful Integral Function and Its Application in Thermal Radiation Calculations", to appear in International Communications in Heat and Mass Transfer.

29. Cess, R.D., Mighdoll, P., and Tiwari, S.N., "Infrared Radiative Heat Transfer in Nongray Gases", Int. J. of Heat Mass Transfer, Vol. 20, pp. 1521-1532, 1967.

30. Edwards, D.K. and Menard, W.A., "Correlations for Absorption by Methane and Carbon Dioxide Gases", Applied Optics, Vol. 3, No. 7, pp. 847-852, 1964.

31. Edwards, D.K. and Sun, W., "Correlations for Absorption by the 9.4 μ and 10.4 μ CO_2 Bands", Applied Optics, Vol. 3, No. 12, pp. 1501-1502, 1964.

32. Ferrisco, C.C. and Ludwig, C.B., "Spectral Emissivities and Integral Intensities of the 1.87-, 1.38-, and 1.14-μ H_2O Bands Between 1000°K and 2200°K", J. of Chemical Physics, Vol. 41, No. 6, pp. 1668-1674, 1964.

33. Edwards, D.K., Flornes, B.J., Glassen, L.K., and Sun, W., "Correlation of Absorption by water vapor at temperature from 300 K to 1100 K", Applied Optics, Vol. 4, No. 6, 1965.

34. Breeze, J.C., Ferriso, C.C., Ludwig, C.B., and Malkmus, W., "Temperature Dependence of the Total Integrated Intensity of Vibration-Rotational Band Systems", J. of Chemical Physics, Vol. 42, No. 1, pp. 402-406, 1965.

35. Weiner, M.W. and Edwards, D.K., "Theoretical Expression of water vapor spectral Emissivity with Allowance for Line Structure", Int. J. of Heat Mass Transfer, Vol. 11, pp. 55-65, 1968.

36. Flynn, P., Mizusawa, M., Uyehara, O.A., and Myers, P.S., "An Experimental Determination of the Instantaneous Potential Radiation Heat Transfer Within an Operating Diesel Engine", SAE Paper-720022, 1972.

37. Obert, E.F., Internal Combustion Engines and Air Pollution, p. 578, Intex, Harper and Row Publishers, 3rd Edition, 1973.

38. Le Feuvre, T., Myers, P.S., and Uyehara, O.A., "Experimental Instantaneous Heat Fluxes in a Diesel Engine and their Correlation", SAE Paper 690464, 1969.

39. Dent, J.C. and Suliaman, S.J., "Convective and Radiative Heat Transfer in a High Swirl Direct Injection Diesel Engine", SAE Paper 770407, 1977.

APPENDIX I
Adiabatic Flame Temperature Computation

In the computation of adiabatic flame temperature, eleven gaseous species were considered besides the fuel, including seven dissociation reactions with known individual equilibrium constants, a stoichiometric equation and an energy equation.

The stoichiometric equation for the reaction is

$$C_I H_J + w(I+J/4)\ O_2 + 3.764w(I+J/4)\ N_2 \longrightarrow (w-1)(I+J/4)\ O_2 + 3.764w(I+J/4)\ N_2 + I\ CO_2 + J/2\ H_2O \qquad (A1)$$

In addition, the equations showing the dissociation reactions involving eleven species are,

$$CO_2 \longrightarrow CO + 1/2\ O_2 \qquad (e_1) \qquad (A2\text{-}1)$$

$$H_2O \longrightarrow H_2 + 1/2\ O_2 \qquad (e_2) \qquad (A2\text{-}2)$$

$$1/2\ H_2 + 1/2\ O_2 \longrightarrow OH \qquad (e_3) \qquad (A2\text{-}3)$$

$$1/2\ N_2 + 1/2\ O_2 \longrightarrow NO \qquad (e_4) \qquad (A2\text{-}4)$$

$$1/2\ H_2 \longrightarrow H \qquad (e_5) \qquad (A2\text{-}5)$$

$$1/2\ O_2 \longrightarrow O \qquad (e_6) \qquad (A2\text{-}6)$$

$$1/2\ N_2 \longrightarrow N \qquad (e_7) \qquad (A2\text{-}7)$$

where

$$w = (F/A)_s/(F/A) = 1/\phi, \qquad (A3)$$

F/A is the molar fuel-air ratio, $(F/A)_s$ is the stoichiometric molar fuel-air ratio, ϕ is, therefore, the fuel volume fraction of stoichiometric, and e_i is the extent of the corresponding reaction (A2-i) which is defined as the ratio of the change of each species to its stoichiometric coefficient (18).

In the computation, seven extents of reaction (e_i, i = 1, ..., 7) were used instead of the eleven species mass-terms in the equations by identifying the number of moles of each species, namely, ZO_2, ZN_2, ..., etc., and the total number of moles in the product, Z_{all}.

$$Z_{O_2} = (w-1)(I+J/4) + (e_1+e_2-e_3-e_4-e_6)/2 \qquad (A4\text{-}1)$$

$$Z_{N_2} = 3.764w(I+J/4) - (e_4+e_7)/2 \qquad (A4\text{-}2)$$

$$Z_{CO_2} = I - e_1 \quad \text{(A4-3)}$$

$$Z_{H_2O} = J/2 - e_2 \quad \text{(A4-4)}$$

$$Z_{CO} = e_1 \quad \text{(A4-5)}$$

$$Z_{H_2} = e_2 - (e_3+e_5)/2 \quad \text{(A4-6)}$$

$$Z_{OH} = e_3 \quad \text{(A4-7)}$$

$$Z_{NO} = e_4 \quad \text{(A4-8)}$$

$$Z_{H} = e_5 \quad \text{(A4-9)}$$

$$Z_{O} = e_6 \quad \text{(A4-10)}$$

$$Z_{N} = e_7 \quad \text{(A4-11)}$$

and

$$Z_{all} = 4.764w(I+J/4) + J/4 + (e_1+e_2+e_5+e_6+e_7)/2 \quad \text{(A5)}$$

Seven equilibrium constant equations for Eqs. (A2) can be written in those terms defined in Eqs. (A4) as follows

$$Kp_1 = \frac{Z_{CO}\, Z_{O_2}^{1/2}}{Z_{CO_2}} (P/Z_{all})^{1/2} \quad \text{(A6-1)}$$

$$Kp_2 = \frac{Z_{H_2}\, Z_{O_2}^{1/2}}{Z_{H_2O}} (P/Z_{all})^{1/2} \quad \text{(A6-2)}$$

$$Kp_3 = \frac{Z_{OH}}{Z_{H_2}^{1/2}\, Z_{O_2}^{1/2}} \quad \text{(A6-3)}$$

$$Kp_4 = \frac{Z_{OH}}{Z_{N_2}^{1/2}\, Z_{O_2}^{1/2}} \quad \text{(A6-4)}$$

$$Kp_5 = \frac{Z_{H}}{Z_{H_2}^{1/2}} (P/Z_{all})^{1/2} \quad \text{(A6-5)}$$

$$Kp_6 = \frac{Z_{O}}{Z_{O_2}^{1/2}} (P/Z_{all})^{1/2} \quad \text{(A6-6)}$$

$$Kp_7 = \frac{Z_{N}}{Z^{1/2}} (P/Z_{all})^{1/2} \quad \text{(A6-7)}$$

where, P is the cylinder pressure.

Substituting Eqs. (A4) and (A5) into the above equilibrium constant equations, one obtains seven simultaneous algebraic equations. In addition, the energy equation of the adiabatic system is written as follows.

$$\sum_{prod.} Z_i \left[(H_{T_2} - H_{T_f}) + (\Delta H_f)_{T_f}\right]_i = \sum_{reac.} Z_j \left[(H_{T_1} - H_{T_f}) + (\Delta H_f)_{T_f}\right]_j \quad \text{(A7)}$$

where H_{T_1} is enthalpy at initial temperature, H_{T_2} is the enthalpy at flame temperature, ΔH_f is the heat of formation at reference temperature T_f, and T_f is 273°K.

A new iteration scheme was developed to find the adiabatic flame temperature and the equilibrium composition by using the above equations and reported Kp's and ΔH_f's.

The key of the method is the simplified forms of equation after introducing Eqs. (A4) into Eqs. (A6). They are

$$0.5(P-Kp_1^2)e_1^3 + (C_1-C_2+IKp_1^2)e_1^2 + (2IC_2-0.5I^2Kp_1^2)e_1 - I^2C_2 = 0 \quad \text{(A8)}$$

$$[Kp_2e_1+(I-e_1)Kp_1]e_2 - 0.5[Je_1Kp_2 + (e_3+e_5)(I-e_1)Kp_1] = 0 \quad \text{(A9)}$$

$$(1-1/4Kp_3^2)e_3^2 + [C_3/2-e_5/4+e_2/2]Kp_3^2e_3 + (e_5/2-e_2)C_3Kp_3^2 = 0 \quad \text{(A10)}$$

$$(1-Kp_4^2/4)e_4^2 + 0.5(C_4+C_5Kp_4^2)e_4 - C_4C_5 = 0 \quad \text{(A11)}$$

$$(Z_{CO_2}^2Kp_1^2)e_5^2 + 0.5e_1^2Z_{O_2}Kp_5^2e_5 - e_1^2Z_{O_2}(e_2-0.5e_3)Kp_5^2 = 0 \quad \text{(A12)}$$

$$[(I-e_1)Kp_1+e_1Kp_6/2]e_6 - [(w-1)(I+J/4) + 0.5(e_1+e_2-e_3-e_4)]e_1Kp_6 = 0 \quad \text{(A13)}$$

$$(Z_{CO_2}^2Kp_1^2)e_7^2 + 0.5Z_{CO}^2Z_{O_2}Kp_7^2e_7 + Z_{CO}^2Z_{O_2}e_4e_7 - 3.764w(I+J/4)]Kp_7^2 = 0 \quad \text{(A14)}$$

where

$$C_1 = [(w-1)(I+J/4) + (e_2-e_3-e_4-e_5)/2]P$$

$$C_2 = [(4.764w-1)(I+J/4)+I+J/2 + (e_2+e_5+e_6+e_7)/2]Kp_1^2$$

$$C_3 = [(w-1)(I+J/4) + (e_1+e_2-e_4-e_6)/2]$$

$$C_4 = [(w-1)(I+J/4) + (e_1+e_2-e_3-e_6)/2]Kp_4^2$$

and

$$C_5 = 3.764w(I+J/4) - e_7/2.$$

A brief inspection of the above equations suggests that if the values of e_2, e_3, ..., e_7 are fixed, the value of e_1 can be easily found as an exact solution of a simple third order algebraic equation. Similarly, others can be found in sequence. This is repeated to find a set of converged values of e_i, which are used to find the equilibrium composition in Eqs. (A2). The above process is iterated to find a convergence of the adiabatic flame temperature of the compositions.

APPENDIX II
Optical Constants of Soot By Using Dispersion Equations

The complex refraction indices of the soot are calculated by using the dispersions equations. The dispersion equations that are known to include the contributions of both free and bound electrons are shown as

$$n^2(1-k^2) = 1 - \frac{F_c e^2/m\varepsilon_0}{h_c^2+\omega^2} + \sum_j \frac{F_j(\omega_j^2-\omega^2)e^2/m\varepsilon_0}{(\omega_j^2-\omega^2)^2+\omega_j^2 h_j^2} \qquad \text{(A15-1)}$$

and

$$2n^2k = \frac{F_c h_c e^2/m\varepsilon_0}{\omega(h_c^2+\omega^2)} + \sum_j \frac{F_j \omega h_j e^2/m\varepsilon_0}{(\omega_j^2-\omega^2)^2+\omega_j^2 h_j^2} \qquad \text{(A15-2)}$$

where, F_j is the number of effective electrons per unit volume; h_j is the electron damping constant; ω is the frequency of the radiation; ω_j is the natural frequency of the jth electron; e is the electron charge, $1.602*10^{-19}$C, m is the mass of the electron, $9.1*10^{-31}$Kg; and ε_0 is the electric permittivity, $8.854*10^{-12}C^2sec^2/Kg\text{-}m^3$. Note that the numerical value of each constant is shown in Table AI.

APPENDIX III
Computation of Band Parameters of Gases

The integrated band intensity of each band is approximated by (34,35),

$$\alpha(T) = \alpha_0 \frac{[1-\exp(-\sum_{k=1}^{m} \pm x_k \delta_k)]\ \Psi(T)}{[1-\exp(-\sum_{k=1}^{m} \pm x_{0,k} \delta_k)]\ \Psi(T_0)} \qquad \text{(A16)}$$

where,

$$x_k = hc\nu_k/KT$$

$$x_{0,k} = hc\nu_k/KT_0$$

$$T_0 = 100°K$$

and

$$\Psi(T) = \frac{\sum_{k=1}^{m} \sum_{v_k=v_{0,k}}^{\infty} \frac{\Gamma(v_k+g_k+\delta_k)}{\Gamma(g_k)\Gamma(v_k+1)} e^{-x_k v_k}}{\sum_{k=1}^{m} \sum_{v_k=v_{0,k}}^{\infty} \frac{\Gamma(v_k+g_k)}{\Gamma(g_k)\Gamma(v_k+1)} e^{-x_k v_k}} \qquad \text{(A17)}$$

In the above equations, the statistical weight g_k is unity for the degenerate vibration and the $v_{0,k}$ is zero if a plus sign is associated with δ_k in the upper state $(v_k+\delta_1, \ldots, v_k+\delta_k, \ldots)$ and is δ_k when a minus sign appears. The quantity α_0 had to be determined experimentally (30, 31,33) for each species of the combustion products.

The band width parameter, A_0, is approximated by (13),

$$A_0 = A_{00}(T/T_0)^{1/2} \qquad \text{(A18)}$$

where, A_{00} is experimentally determined for each band.

The line width parameter, β, is calculated by (35),

$$\beta(T) = \beta_0(T_0/T)^{1/2} \frac{\Phi(T)}{\Phi(T_0)} \qquad \text{(A19)}$$

where,

$$\Phi(T) = \frac{\sum_{k=1}^{m} \left(\sum_{v_k=v_{0,k}}^{\infty} [\frac{\Gamma(v_k+g_k+\delta_k)}{\Gamma(g_k)\Gamma(v_k+1)} e^{-x_k v_k}, \right)^{1/2}}{\sum_{k=1}^{m} \sum_{v_k=v_{0,k}}^{\infty} \frac{\Gamma(v_k+g_k+\delta_k)}{\Gamma(g_k)\Gamma(v_k+1)} e^{-x_k v_k}} \qquad \text{(A20)}$$

Two weak bands of H_2O require a special method of computation as explained in the following.

For the inclusion of two weak bands of H_2O, the following method was taken in the present computation. In the computation of α and β, for the pure rotational band ($v_k = 0$, $k = 1,2,3$), the following equations were used.

$$\alpha(T) = \alpha_0 \qquad \text{(A21)}$$

and

$$\beta(T) = \beta_0 (T/T_0)^{-1/2} \qquad \text{(A22)}$$

For the 2.7μm H_2O band where three overlapping bands occur, α was found by summing $\alpha_j (j = 1,2,3)$ by using Eqs. (A16) and (A17). Values of β_j were computed by using Eqs. (A19) and (A20) and averaged by

$$\beta = \frac{\left\{\sum_{j=1}^{3} (\alpha_j \beta_j)^{1/2}\right\}^2}{\sum_{j=1}^{3} \alpha_j} \qquad \text{(A23)}$$

Table AIII shows the recommended values of α_0, β_0, and A_{00} for the major absorption bands of H_2O and CO_2 (13).

Table AI. The Constants of the Dispersion Equations (14)

Electron	F_j(electrons/m^3)	h_j(rad./sec.)	ω_j(rad./sec.)
free c	4.06×10^{27}	6.00×10^{15}	---
bound 1	2.69×10^{27}	6.00×10^{15}	1.25×10^{15}
bound 2	2.86×10^{26}	7.25×10^{15}	7.25×10^{15}

Table AII. Exponential Wide Band Model Parameters

Gas	Vibrations ν_k (cm^{-1})	Bands δ_k	Pressure Parameters N	b	Band Absorption Parameters α_0 (cm^{-1}/gm m^{-2})	β_0	A_{00} (cm^{-1})
H_2O							
	m =3	1. 20u	1	+*	5200.0	0.14311	28.4
	ν_1=3652	0,0,0					
	ν_2=1595	2. 6.3u	1	+	41.2	0.09427	56.4
	ν_3=3756	0,1,0					
	g_1=1	3. 2.7u	1	+			
	g_2=1	0,2,0			0.19		
	g_3=1	1,0,0			2.3	0.13219	60.0
		0,0,1			22.4		
		4. 1.87u	1	+	3.0	0.08169	43.1
		0,1,1					
		5. 1.38u	1	+	2.5	0.11628	32.0
		1,0,1					
CO_2							
	m =3	1. 15u	0.7	1.3	19.0	0.06157	12.7
	ν_1=1351	0,1,0					
	ν_2=667	2. 10.4u	0.8	1.3	2.47×10^{-9}	0.04017	13.4
	ν_3=2396	-1,0,1					
	g_1=1	3. 9.4u	0.8	1.3	2.48×10^{-9}	0.11888	10.1
	g_2=2	0,-2,1					
	g_3=1	4. 4.3u	0.8	1.3	110.0	0.24723	11.2
		0,0,1					
		5. 2.7u	0.65	1.3	4.0	0.13341	23.5
		1,0,1					
		6. 2.0u	0.65	1.3	0.066	0.39305	34.5
		2,0,1					

*+: $8.6(T_0/T)^{1/2} + 0.5$

Appendix-V. An Analytical Method of None-Gray 3-D Radiation Model

An Analytical Method of None-gray Three-dimensional Radiation Heat Transfer in Spray Combustion

by

S.L. Chang and K.T. Rhee

Department of Mechanical and Aerospace Engineering
Rutgers, The State University of New Jersey
New Brunswick, New Jersey 08903

Subjects

(12) Heat Transfer (Radiation Heat Transfer)
(13) Heterogeneous Combustion
(18) Modeling and Scaling

Forward correspondence to K.T. Rhee

ABSTRACT

A computational study of radiation heat transfer in a combustor having fuel spray combustion is reported in the present paper. When the distribution of radiatively participating species is known in either a normal distribution or an exponential distribution in any direction of a cylindrical coordinate with respect to a referenced location, e.g., in a form, $F = f \exp(-a\rho - b\phi^2 - cz^2)$, where f, a, b, and c are distribution constants for individual species, the governing equation of radiation heat transfer without scattering in such a system can readily be solved by using the herein reported method. Several results from the present authors' work are explained that are employed for implementing the solution: a new coordinate transformation method to find the species distribution along individual optical paths centered at any chosen location in the combustor; a new formula for the adiabatic flame temperature in a logarithmic function expressed in terms of relevant variables; a new integral function facilitating solutions for various radiation equations; a new inverse error function enabling some exact solution of the governing equation of radiation heat transfer, etc.

An exact solution is found for both optically thin and thick media. And a numerical solution is offered for optically medially thin medium. The present analytical method is applied to radiation heat transfer in a direct injection-type diesel engine combustion chamber. Some representative results are discussed that have been obtained from a parametric analysis of its radiation heat transfer.

INTRODUCTION

When an equation of radiative heat transfer is solved for predicting the heat flux incident upon various locations over the surface of a combustor having flame plumes, several difficult problems are encountered. In order to briefly review the difficulties, a combustor having a jet flame is considered as shown in Fig. 1. The heat flux through an optical path (r,θ,τ) centered at location, D may be calculated by solving the governing equation of radiation neglecting scattering effect,

$$q_{\theta\xi} = \int_0^\infty I_\lambda(0) \cos\theta \, d\lambda \tag{1}$$

when the spectral radiation intensity, $I_\lambda(r)$ is represented as

$$I_\lambda(r) = \int_r^{r_o} \frac{\kappa_\lambda(r')}{\pi} e_{b\lambda}(r')\exp\left(-\int_r^{r'} \kappa_\lambda(r'')dr''\right)dr' \tag{2}$$

where κ_λ is the spectral volume apsorptance at (r,θ,τ) and $e_{b\lambda}$ is the spectral blackbody radiation. The total radiation flux on location D, then, is calculated by integrating $q_{\theta\xi}$ over the entire hemispherical volume faced by the location. Among the main difficulties in implementing the above computation are that κ_λ can be determined only when the distributions of radiatively participating species and temperature are known along the individual optical paths and that I_λ is spectrum-dependent.

In order to obtain a better solution of Eq. (1), some new methods were proposed for overcoming the abovementioned difficulties when the authors computed radiation heat transfer in a direct injection-type diesel engine: a coordinate transformation technique to find the species distribution along individual optical paths when the distribution is given with respect to a chosen location, e.g., the injection nozzle hole [1]; a computation method of

finding the spectral volume absorptances of soot and gas for their mixtures [1,2] by using reported results [3,4,5] and new analytical and numerical methods of solving Eq. (1), which is considered in the present paper. This paper, therefore, may serve as a summary report of the authors' modeling study of radiation heat transfer in a combustor having flame jets.

Elaborating the species distribution in the combustion chamber, it was found to conveniently be described by the following equation in a cylindrical coordinate with respect to the injection nozzle [1] when distribution is known in either a normal (or a skewed normal) distribution or an exponential distribution in any direction of a cylindrical coordinate, e.g., in a form:

$$F = f \exp(-a\rho - b\phi^2 - cz^2) \tag{3}$$

where F represents either fuel/air ratio or soot concentration or CO_2 or H_2O concentration; f, a, b and c are constants to be separately determined for each medium by either experimental or theoretical means. The expression is considered to reasonably well describe the species distribution of non-axisymmetric plumes in view of some reported results from both theoretical and experimental studies [6,7], and the new expression offers various advantages, e.g., that the expression can be used to describe the spray plume in swirl motions by including its effect in ϕ-direction and that it facilitates the sought solution of Eq. (1) [1]. When the species distribution with respect to a referenced position in the combustor is known, the species distribution along the optical path, r, of any chosen direction (r,θ,ξ) and location, D (ρ_d,ϕ_d,z_d) may be found as [1],

$$F_o = f_d \exp(-[(r-r_o)/r_w]^2 \tag{4}$$

where f_d, r_o and r_w are functionally related to θ, ξ, ρ_d, ϕ_d, z_d, f, a, b, and c. This distribution equation, then, may be used for determining the volume absorptance according to the reported methods [3,4,5] as

$$\kappa_o = \kappa_1 \exp(-c_1(r-r_1)^2) \qquad (5).$$

The temperature distribution, T, needed in the above equation and $e_{b\lambda}$ for Eq. (1) may be determined by using the distribution of burned fuel/air ratio, ω, from Eq. (3). This can be achieved by using our new formula for the adiabatic flame temperature [8];

$$T = T_o + T_1 \ln\omega + T_2 (\ln\omega)^2 \qquad (6)$$

where T_1, T_2 and T_3 are functionally related to the reaction pressure, the initial mixture temperature and the number of carbon atoms of the fuel molecule. Even with the above rearrangement and simplification of terms in Eq. (1), its solution was not readily found until some new mathematical techniques were employed as explained in the following.

ANALYTICAL AND NUMERICAL SOLUTIONS

The solution of Eq. (1) may be considered for the following three cases: (1) the optically thin medium; (2) optically thick medium and (3) optically medially thick medium: the solution for each case will be explained upon further simplifying the governing equation as follows. Introducing new terms,

$$\kappa_o = \kappa_\lambda . \lambda \text{ [3,9]}, \quad x = hc/k\lambda T \text{ and } a = \frac{kT}{hc}\int_0^r \kappa_o \, dr,$$

where h is Planck's constant; c the speed of light and κ the Boltzmann constant, Eq. (1) can be rewritten for directional radiation intensity as,

$$I_{\theta\xi} = q_{\theta\xi}/\cos\theta,$$

$$I_{\theta\xi} = \int_0^{r_o} \kappa_o \int_0^\infty \frac{1}{\lambda} e_{b\lambda} e^{-\frac{1}{\lambda}\int_0^r \kappa_o dr} d\lambda dr$$

$$= \frac{15\, ak}{\pi^5 hc} \int_0^{r_o} \kappa_o T^5 \int_0^\infty \frac{x^4 e^{-ax}}{e^x - 1} dx\, dr.$$

During the process of simplifying the above equation, the authors discovered a new useful integration function [10], i.e.,

$$\int_{x_1}^{x_2} \frac{e^{-ax} x^m}{e^x - 1}\, dx = F(m,a,x_1) - F(m,a,x_2), \qquad (7)$$

$$F(m,a,x) = \sum_{n=1}^{\infty} \{e^{-(n+a)x} \sum_{i=0}^{m} [\frac{\Gamma(m+1)}{\Gamma(m-i+1)} (n+a)^{-i-1} x^{m-i}]\}, \text{ where } \Gamma(m+1) = 1,2,\ldots m.$$

Note that Eq. (7) can also be used for determining a solution in closed form of the black body radiation function, $F_{0-\lambda T}$ [11],

$$F_{0-\lambda T} = \int_0^{\lambda T} \frac{E_{b\lambda}(T)}{\sigma T^4}\, d(\lambda T)$$

$$= \frac{15}{\pi^4} \sum_{n=1}^{\infty} [\frac{e^{-nx}}{n} (x^3 + \frac{3x^2}{n} + \frac{6x}{n^2} + \frac{6}{n^3})] .$$

From Eq. (7), since one can find

$$\int_0^{\infty} \frac{x^4 e^{-ax}}{e^x - 1}\, dx = \sum_{n=1}^{\infty} \frac{4!}{(n+a)^5},$$

the governing equation is simplified as

$$I_{\theta\xi} = \frac{360\ \sigma k}{\pi^5\ hc} \sum_{n=1}^{\infty} \frac{1}{n^5} \int_0^{r_o} \frac{\kappa_o T^5}{(1+a/n)^5}\, dr .$$

With the definition of the optical depth, $\tau = \int_0^r \kappa_o\, dr$, the equation may be rewritten in a tidier form,

$$I_{\theta\xi} = \frac{360\ \sigma k}{\pi^5\ hc} \sum_{n=1}^{\infty} \frac{1}{n^5} \int_0^{\tau_o} \frac{T^5}{(1+\frac{kt\tau}{nhc})^5}\, d\tau \qquad (8)$$

The solution of this equation is considered for the previously mentioned three cases as follows.

OPTICALLY THIN MEDIUM: When τ approaches zero, i.e., an optically thin limit, an exact solution for Eq. (8) was found. In this case, Eq. (8) becomes

$$I_{\theta\xi} \simeq \frac{360\ \sigma k}{\pi^5 hc} \sum_{n=1}^{\infty} \frac{1}{n^5} \int_0^{\tau_o} T^5 (1 - \frac{5kT\tau}{nhc})\, d\tau \qquad (9$$

For finding the solution of the above equation, since T is functionally related to the optical depth, τ and the burned fuel/air ratio, ω, and since ω may be found as $\omega = \omega_1 e^{\bar{r}^2}$ from Eq. (4), Eq. (6) may be written as

$$T = T_o + T_1 (\ln \omega_1 - \bar{r}^2) + T_2 (\ln \omega_1 - \bar{r}^2)^2 = T_3 - T_4 \bar{r}^2 + T_2 \bar{r}^4 \qquad (10)$$

where, $T_3 = T_o + T_1 \ln \omega_1 + T_2 (\ln \omega_1)^2$ and

$T_4 = T_1 + 2T_2 \ln(\omega_1)$.

In addition, for obtaining the solution of Eq. (8), it was necessary to find the relationship between τ and r. From definition and Eq. (5), the optical depth, τ is rewritten as,

$$\tau = \kappa_1 \int_0^r e^{-c_1(r-r_1)^2} dr$$

$$= \frac{\kappa_1}{2} \sqrt{\frac{\pi}{c_1}} \{\text{erf } [\sqrt{c_1}(r-r_1)] + \text{erf } (\sqrt{c_1}\, r_1)\}$$

$$\text{or, erf } [\sqrt{c_1}(r-r_1)] = \frac{2\pi}{\kappa_1} \sqrt{\frac{c_1}{\pi}} - \text{erf } (\sqrt{c_1}\, r_1). \qquad (11)$$

In view of Eq. (10) and for further simplifying Eq. (11), a variable transformation was employed to obtain

$$\bar{r} = \sqrt{c_1}\, (r-r_1),$$

$$\bar{\tau} = \frac{2}{\kappa_1} \sqrt{\frac{c_1}{\pi}} [\tau - \frac{\kappa_1}{2} \sqrt{\frac{\pi}{c_1}} \text{erf } (\sqrt{c_1}\, r_1)]$$

$$= d_1 [\tau - \tau_1] \qquad (12)$$

Then Eq. (11) may be written as

$$\text{erf } (\bar{r}) = \bar{\tau}$$

$$\text{or,} \qquad \bar{r} = \text{erf}^{-1}(\bar{\tau}) \qquad (13)$$

where, erf^{-1} represents the inverse error function, whose exact solution is found as (note the details of its derivation are explained in Appendix)

$$\bar{r} = \text{erf}^{-1}(\bar{\tau})$$

$$= \frac{\sqrt{\pi}}{2}\left(\bar{\tau} + \frac{\pi}{2.3!}\bar{\tau}^3 + \frac{7\pi^2}{4.5!}\bar{\tau}^5 + \ldots.\right) \tag{14}$$

Next, the above equation is introduced into Eq. (10) to find

$$T = T_3 - \frac{T_4\pi}{4}\left(\bar{\tau} + \frac{\pi}{2.3!}\bar{\tau}^3 + \frac{7\pi^2}{4.5!}\bar{\tau}^5 + \ldots.\right)^2$$

$$+ \frac{T_2\pi^2}{16}\left(\bar{\tau} + \frac{\pi}{2.3!}\bar{\tau}^3 + \frac{7\pi^2}{4.5}\bar{\tau}^5 + \ldots.\right)^4$$

$$\equiv T_3 - \frac{\pi}{4}T_4\bar{\tau}^2 + \left(-\frac{\pi^2 T_4}{4.3!} + \frac{\pi^2}{16}T_2\right)\bar{\tau}^4$$

$$= T_3 - T_5\bar{\tau}^2 + T_6\bar{\tau}^4 \tag{15}$$

where, $T_5 = \frac{\pi}{4}T_4$ and $T_6 = \left(-\frac{\pi^2 T_4}{4.3!} + \frac{\pi^2}{16}T_2\right)$.

From Eq. (15), one also may find the following in order to use them in Eq. (9):

$$T^5 = T_3^5 - 5T_3^4T_5\bar{\tau}^2 + 5T_3^4T_6\bar{\tau}^4,$$

$$T^6 = T_3^6 - 6T_3^5\bar{\tau}^2 + 6T_3^5T_6\bar{\tau}^4.$$

Finally, the above equations and Eq. (12) are introduced into Eq. (9) to obtain

$$I_{\theta\xi} = \frac{360\,\sigma k}{\pi^5 hc}\sum_{n=1}^{\infty}\frac{1}{n^5}\int_{-d_1\tau_1}^{d_1(\tau_0-\tau_1)}\left[T^5 - \frac{5k\tau_1}{nhc}T^6 - \frac{5k}{nkc}\bar{\tau}T^6\right]d\bar{\tau}$$

$$= \frac{360\,\sigma k}{\pi^5 hc}\sum_{n=1}^{\infty}\frac{1}{n^5}\int_{-d_1\tau_1}^{d_1(\tau_0-\tau_1)}\left\{\left[T_3^5 - 5T_3^4T_5\bar{\tau}^2 + 5T_3^4T_6\bar{\tau}^4\right]\right.$$

$$- \frac{5k\tau_1}{nhc}\left[T_3^6 - 6T_3^5\bar{\tau}^2 + 6T_3^5T_6\bar{\tau}^4\right]$$

$$\left. - \frac{5k}{nhc}\left[T_3^6\bar{\tau} - 6T_3^5T_5\bar{\tau}^3 + 6T_3^5\bar{\tau}^5\right]\right\}d\bar{\tau}$$

$$= \frac{360\ \sigma k}{\pi^5\ hc} \sum_{n=1}^{\infty} \frac{1}{n^5} \int_{-d_1\tau_1}^{d_1(\tau_0-\tau_1)} \{(T_3^5 - \frac{5k\tau_1}{nhc} T_3^6 - \frac{5kT_3^6}{nhc} \bar{\tau} - (5T_3^4 T_5 - \frac{3k\tau_1 T_3^5 T_5}{nhc})\bar{\tau}^2$$

$$+ \frac{30\ kT_3^5 T_5}{nhc} \bar{\tau}^3 + (5T_3^4 T_6 - \frac{30\ k\tau_1 T_3^5 T_6}{nhc})\bar{\tau}^4$$

$$- \frac{30\ kT_3^5 T_6}{nhc} \bar{\tau}^5\} d\bar{\tau} \qquad (16)$$

Consequently, Eq. (16) can be used for finding an exact solution of the equation of radiation for an optically thin medium in a combustor with flame plumes as,

$$I_{b\xi} = \frac{360\ \sigma k}{\pi^5\ hc} \sum_{n=1}^{\infty} \frac{1}{n^5} \{(T_3^5 - \frac{5k\tau_1}{nhc} T_3^6)\ d_1\tau_0 - \frac{5kT_3^6}{2nhc} [d_1^2(\tau_0-\tau_1)^2 - d_1^2\tau_1^2]$$

$$- (\frac{5}{3} T_3^4 T_5 - \frac{10\ k\tau_1 T_3^5 T_5}{nhc})[d_1^3(\tau_0-\tau_1)^3 - d_1^3\tau_1^3]$$

$$+ \frac{15kT_3^5 T_5}{2nhc} [d_1^4(\tau_0-\tau_1)^4 - d_1^4\tau_1^4]$$

$$+ (T_3^4 T_6 - \frac{6k\tau_1 T_3^5 T_6}{nhc})\ (d_1^5(\tau_0-\tau_1)^5 - d_1^5\ \tau_1^5)$$

$$- \frac{2k\tau_3^5 T_6}{nhc} [d_1^6(\tau_0-\tau_1)^6 - d_1^6\tau_1^6)\}.$$

Optically thick medium: An exact solution can also be found in an optically thick medium: assuming the volume absorptance κ is 0 for $r < r_o$, and κ_o for $r_o < r < r_o+\varepsilon$, one can rewrite Eq. (2) as

$$I_{\theta\xi} = \int_0^{r_o+\varepsilon} \frac{\kappa}{\pi} e_b \exp\left(-\int_0^{r''} \kappa\, dr''\right)dr'$$

This equation is further solved to find the result,

$$\begin{aligned} I_{\theta\xi} &= \int_{r_o}^{r_o+\varepsilon} \frac{\kappa_o}{\pi} e_b \exp\left(-\int_{r_o}^{r'} \kappa_o dr''\right)dr' \\ &= \frac{\kappa_o e_b}{\pi} \int_{r_o}^{r_o+\varepsilon} \exp(-\kappa_o(r'-r_o))dr' \\ &= \frac{\sigma T^4}{\pi}[1-e^{-\tau}] \end{aligned} \tag{18}$$

Optically medially thin medium: When the system holds an optically medially thin (or thick) medium, Eq. (2) cannot analytically be solved as the above discussed cases; rather, a numerical method was employed for it. Without going into the details of its derivation (shown elsewhere [11]), but by knowing that the volume absorptance $\kappa(r)$ can be found from Eq. (5), the following result was used for the solution.

$$I_{\theta\xi} = \frac{15\,\sigma}{\pi^5} \sum_{i=1}^{M} \int_{\tau_{i-1}}^{\tau_i} \sum_{j=1}^{J} \kappa_{oij}\, T^5[F(4,a,x_{j-1}) - F(4,a,x_j)]d\tau \tag{19}$$

where, κ_{oij} is the volume absorptance defined in the ith subrange of r-domain and the jth subrange of λ-domain. The numerical results of Eq. (19) were obtained using Gaussian integration method.

RESULTS AND CONCLUSION

The present computational method enables an extensive parametric study of radiation heat transfer in a combustor with flame jets [2]. Since this summary paper is to primarily report the methodology of computation by using the authors' several new findings reported elsewhere [1, 2, 8, 10], only some representative results considered for a direct injection-type diesel engine are presented here. For this, in order to be consistent and to have better mutual comparisons, the same computational conditions employed for the previous results are considered here. The numerical values of f in Eq. (3) were, for soot, H_2O, CO_2 and fuel/air ratio, 3×10^{-6}, 0.01, 0.01 and 1.0, respectively; the distribution constants, a, b, and c were, for those species, 0.6, 2.36 and 2.0, accordingly. Note again that those constants and distribution made in each coordinate of Eq. (3) can be determined by computational or experimental method, or arbitrarily chosen for parametric studies. The engine details for the computation were: the chamber surface temperature, 500°K; the number of spray plumes, 4; the piston radius, R = 4.92 cm; the combustion chamber bowl radius, 3.44 cm; the compression ratio, 23; the engine speed, 1000 rpm; the surface spectral emissivity, 0.95; the fuel composition, $C_{16}H_{34}$; the time of computation in cycle, 40 degrees after top dead center. The results are shown in normalized forms: normalized radiation heat transfer, $Q/\sigma T^4$, where T is 2400°K and σ is the Stefan-Boltzmann constant; normalized directional intensity, $I_{\theta\xi}/\pi\sigma T^4$; normalized spectral radiation heat transfer, $Q_\lambda/\sigma T^4$.

The radiation heat transfer through a solid angle incident on the cylinder head, are shown in Fig. 2. Where there are four flame jets in the combustion chamber, radiation heat transfer flux incident on the locations along the radial direction varies depending upon the direction in the hemispherical volume of integration. The schematic drawing in the figure shows the spherical

coordinate identifying the direction of solid angles. Note that, for cases θ = 60° and 76.7°, heat transfer on r/R < 0.1 is in large from plume #1 and that beyond r/R = 0.1 from both plumes #1 and 2. The directional radiation intensity, $I_{\theta\xi}$ was combined with the spectral emissivity of the chamber wall, ε_λ = 0.95, to obtain radiation heat transfer through the cylinder head by integrating as, $Q = \int I_{\theta\xi} \cos\theta \sin\theta \, d\theta \, d\xi$ (Fig. 3). The net heat transfer computed with inclusion of wall emission at 500°K, reflection from the opposite-side walls are represented by "Net"; those obtained excluding the reflection is denoted by "No reflection"; and the heat flux incident on the surface without including wall effect are shown by "Spray plume". Explaining the results, the rapid reduction in heat transfer around r/R = 0.7 is caused by the presence of the piston bowl. The double hump in the plot may be surprising. In order to clarify this, an additional computation made for solid angle of zineith angle, θ = 39.7°, at varied azimuthal angles and locations on the cylinder head, is shown in Fig. 4. From the results, one finds that while the radiation heat flux incident on locations around the nozzle (r/R = 0) is from all of the four plumes, the flux on those near r/R = 0.1 is from one plume, i.e., the nearest plume to the location. If the computation is made for a single plume, the heat transfer should have asymptotically been approaching zero at r/R = 0. This trend is qualitatively compared with the experimental results obtained by using a single plume [12].

Since the distribution constants being used for Eq. (3) in the present analysis were chosen based on an in-cylinder soot measurement [13], it seems of interest to compute radiative heat transfer contributed by in-cylinder soot and gaseous species, i.e., mainly CO_2 and H_2O. Fig. 5 shows their spectrum-resolved radiation heat transfer smoothed over individual wave bonds in normalized form, $Q_\lambda/\sigma T^4$, with respect to normalized wave number, 6 μm/λ. It

appears clear that thermal radiation transmission caused by the presence of soot almost dominates the entire radiation process and the radiation by gaseous species is very small. The great portion of radiation by gas found around 6μm/λ is explained by the strong emission bands of H_2O at λ = 2.7 and CO_2 at λ = 2.7 and 4.3 μm. Since the spectral absorptance of surface can be incorporated with results like those in Fig. 5, the analysis may be made for combustors having various surface coatings with known spectral emissivity.

The main issue associated with the use of the present analysis method of radiation heat transfer may be justification of the species distribution described by Eq. (3). Since the distribution widely varies depending upon the fuel injector and combustor condition, it is difficult to exactly describe the variations by a single equation. Reported results suggest, however, the individual species distribution may be simplified by using exponential or normal (or skewed normal) distribution in each coordinate component of a cylindrical system, e.g., Eq. (3). It is found in the present study that the radiation heat analysis is greatly simplified when the distribution is made in such a form without resorting to the rather complex zonal method or the use of the geometric factors. Further, the use of the present method readily enables parametric analysis of radiation heat transfer, e.g., in order to identify a desirable injector suitable for a chosen combustor system.

ACKNOWLEDGEMENT

The present study has been sponsored by the U.S. Army Research Office, Contract No. DAAG 29-83-K-0043 (Scientific Program Officer, Dr. David M. Mann).

REFERENCES

1. Chang, S. L. and Rhee, K. T., "Coordinate Transformation Method for Radiation Heat Transfer Prediction in Soot Laden Combustion Products," being reviewed for publication.

2. Chang, S. L., Yang, X. L. and Rhee, K. T., "A Parametric Analysis of Radiation Heat Transfer in Direct Injection Diesel Combustion," International Symposium on Diagnostics and Modeling in Reciprocating Engines, September 4-6, 1985, Tokyo, Japan.

3. Dalzell, W. H. and Sarofim, A. F., "Optical Constants of Soot and Their Application to Heat Flux Calculation," Trans. of ASME, Vol. 9, pp. 100-104, 1969.

4. Lee, S. C. and Tien, C. L., "Optical Constants of Soot in Hydrocarbon Flame," 18th Symposium (Int'l) on Combustion, The Combustion Institute, pp. 1159-1165, 1981.

5. Edward, D. K. and Balakrishnan, A., "Thermal Radiation by Combustion Gases," Int'l J. of Heat Mass Transfer, Vol. 16, p. 25-40, 1973.

6. Takeuchi, K., Senda, J. and Shikuja, M., "Transient characteristics of Fuel Atomization and Droplet Size Distribution in Diesel Fuel Spray," SAE Paper 830449, 1983.

7. Kuo, T. W., Yu, R. C. and Shahed, S. M., "A Numerical Study of the Transient Evaporating Spray Mixing Process in the Diesel Environment," SAE Paper-831735, 1983.

8. Rhee, K. T. and Chang, S. L., "Empirical Equations for Adiabatic Flame

Temperatures for Some Fuel-Air Combustion Systems," Combustion Science and Technology, Vol. 44, pp. 75-88, 1985.

9. Grosshandler, W. L. and Modak, A., "Radiation from Nonhomogeneous Combustion Products," 18th Symposium (Int'l) on Combustion, The Combustion Institute, pp. 601-609, 1981.

10. Chang, S. L. and Rhee, K. T., "A Useful Integral Function and Its Application in Thermal Radiation Calculations," International Communication of Heat and Mass Transfer, Vol. 10, 1983.

11. Chang, S. L., "An Analytical and Numerical Method of Radiation Heat Transfer in Direct Injection-type Diesel Combustion," Ph.D. thesis, Rutgers University, 1984.

12. Tsuboi, T., Fukushima, M., Sato, T. and Oguri, T., "Thermal Radiation During Spray Combustion Behind Reflected Shock Waves," International Symposium on Diagnostics and Modeling in Reciprocating Engines, September 4-6, 1985, Tokyo, Japan.

13. Kittleson, D. B., Du, C. J. and Pipho, M., "Total Cylinder Sampling from a Diesel Engine: Part II - Particulate Measurement", SAE Paper 830243, 1983.

14. Papoulis, A., Probability, Random Variables, and Stochastic Processes, McGraw Hill Book Co., New York, 1965.

15. Schneider, P. J., Conduction Heat Transfer, Addison-Wesley Publishing Co. Inc., Reading, Mass., 1955.

16. Abramowitz, M. and Stegun, I. A., Handbook of Mathematical Functions, National Bureau of Standards, Applied Mathematic Series-55, U. S. Government Printing Office, Washington, D.C., 1964.

Appendix:

AN INVERSE ERROR FUNCTION

The error function, erf(x), although defined in several ways, is essentially equivalent to the following expression:

$$\mathrm{erf}(x) = \frac{2}{\sqrt{\pi}} \int_0^x e^{-t^2}\, dt = \frac{2}{\sqrt{\pi}} \sum_{n=0}^{\infty} (-1)^n \frac{x^{2n+1}}{n!(2n+1)} \qquad (A\text{-}1)$$

The equation is the integral of the so-called Gaussian or normal function and occurs frequently in the study of the general theory of probability [14], the analysis of transient heat flow in a semi-infinite solid [15], and the computation of radiation heat transfer with radiatively participating media [10], etc. For meeting the needs of such studies, the error function, its derivatives and integrals have been tabulated [16]. As found in the text, it was needed to obtain the inverse form of the error function, i.e., in Eq. (A-1), the value of x for a corresponding erf(x). The following derivation shows a new inverse error function in closed form:

When the error function, erf(x), is set equal to y, i.e., y = erf(x), its inverse form may be expressed, for the convenience of discussion,

$$x = \mathrm{erf}^{-1}(y) \qquad (A\text{-}2)$$

or,

$$x = \mathrm{fre}(y). \qquad (A\text{-}3)$$

By Taylor's expansion method, the inverse error function can be expressed as

$$x = \sum_{n=0}^{\infty} \frac{x^{(n)}(0)}{n!}\, y^n \qquad (A\text{-}4)$$

where, $x^{(n)}(0)$ is the nth derivative of x with respect to y at y = 0. In

order to find $x^{(n)}(0)$, the following steps are taken.

$$x'(y) = \frac{dx}{dy} = \left(\frac{dy}{dx}\right)^{-1}$$

$$= \left\{\frac{d}{dx}\left[\frac{2}{\sqrt{\pi}} \int_0^x e^{-t^2}\, dt\right]\right\}^{-1}$$

$$= \frac{\sqrt{\pi}}{2} e^{x^2},$$

$$x''(y) = \frac{d}{dy}[x'(y)] = \frac{d}{dx}[x'(y)]\left[\frac{dy}{dx}\right]^{-1}$$

$$= \frac{\pi}{2} x\, e^{2x^2},$$

$$x^{(3)}(y) = \frac{d}{dy}[x''(y)] = \frac{d}{dx}[x''(y)]\left[\frac{dy}{dx}\right]^{-1}$$

$$= \left[\frac{\pi}{2}(1 + 4x^2)\, e^{2x^2}\right]\left[\frac{\sqrt{\pi}}{2} e^{x^2}\right]$$

$$= \frac{\pi^{3/2}}{4}(1 + 4x^2)\, e^{3x^2},$$

$$x^{(4)}(y) = \frac{\pi^2}{4}(7x + 12x^3)\, e^{4x^2},$$

$$x^{(5)}(y) = \frac{\pi^{5/2}}{8}(7 + 92x^2 + 96x^4)\, e^{5x^2}$$

$$x^{(6)}(y) = \frac{\pi^3}{8}(127x + 652x^3 + 480x^5)\, e^{6x^2}$$

$$x^{(7)}(y) = \frac{\pi^{7/2}}{16}(127 + 3480x^2 + 10224x^4 + 5760x^6)\, e^{7x^2}, \text{ etc.}$$

Consequently, one can rewrite Eq. (4) as

$$x = fre(y) = \frac{\sqrt{\pi}}{2}\left(y + \frac{\pi}{2.3!} y^3 + \frac{7\pi^2}{4.5!} y^5 + \frac{127\pi^3}{8.7!} y^7 + \ldots\right). \qquad (A\text{-}5)$$

A close investigation of the above results indicates that a term $[\frac{dy}{dx}]^{-1}$ is repeated in each derivative and that the even derivatives become zero at y = 0. This leads to writing Eq. (5), the inverse error function, in a tidier form,

$$fre(y) = \sum_{n=0}^{\infty} f_n(0)(\frac{\sqrt{\pi}}{2} y)^{2n+1}/(2n+1)! \qquad |y| < 1 \qquad (A-6)$$

where, $f_n(0)$ is obtained from the reciprocally defined function, $f_n(t)$, expressed as

$f_o(t) = 1$, and

$$f_{n+1}(t) = f_n''(t) + 2(4n + 3) \times f_n'(t) + 2[2n+1 + 4(2n+1)(n+1)x^2] f_n(t). \qquad (n = 0,1,2,\ldots)$$

Among the analytical properties of the new inverse error function are

$fre(0) = 0$

$fre(-y) = -fre(y)$, and

$fre(1) = \infty$.

In addition, the convergence of Eq. (6) is demonstrated in Figure A-1.

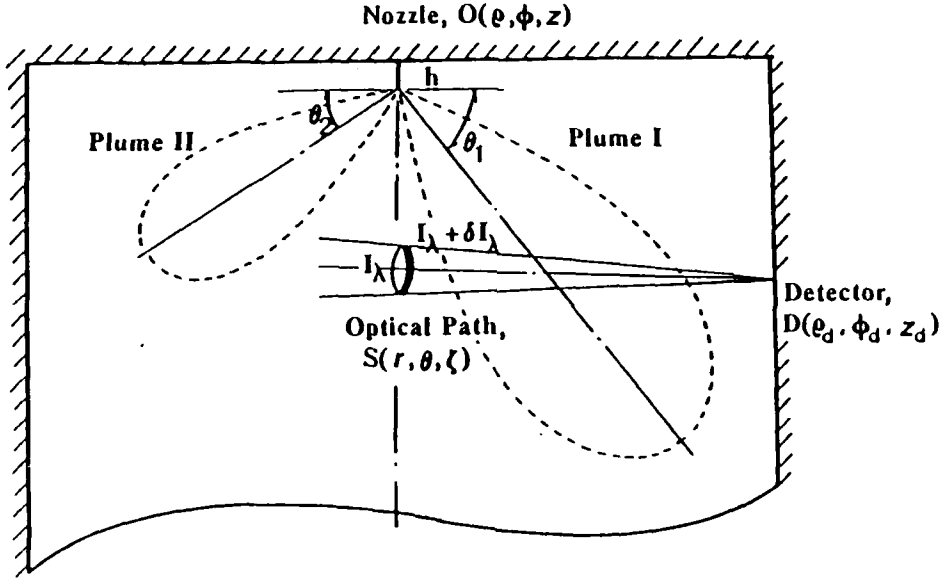
Nozzle, O(ϱ,ϕ,z)
h
Plume II
Plume I
θ_2
θ_1
$I_\lambda + \delta I_\lambda$
I_λ
Detector,
$D(\varrho_d, \phi_d, z_d)$
Optical Path,
$S(r, \theta, \zeta)$

Fig 1

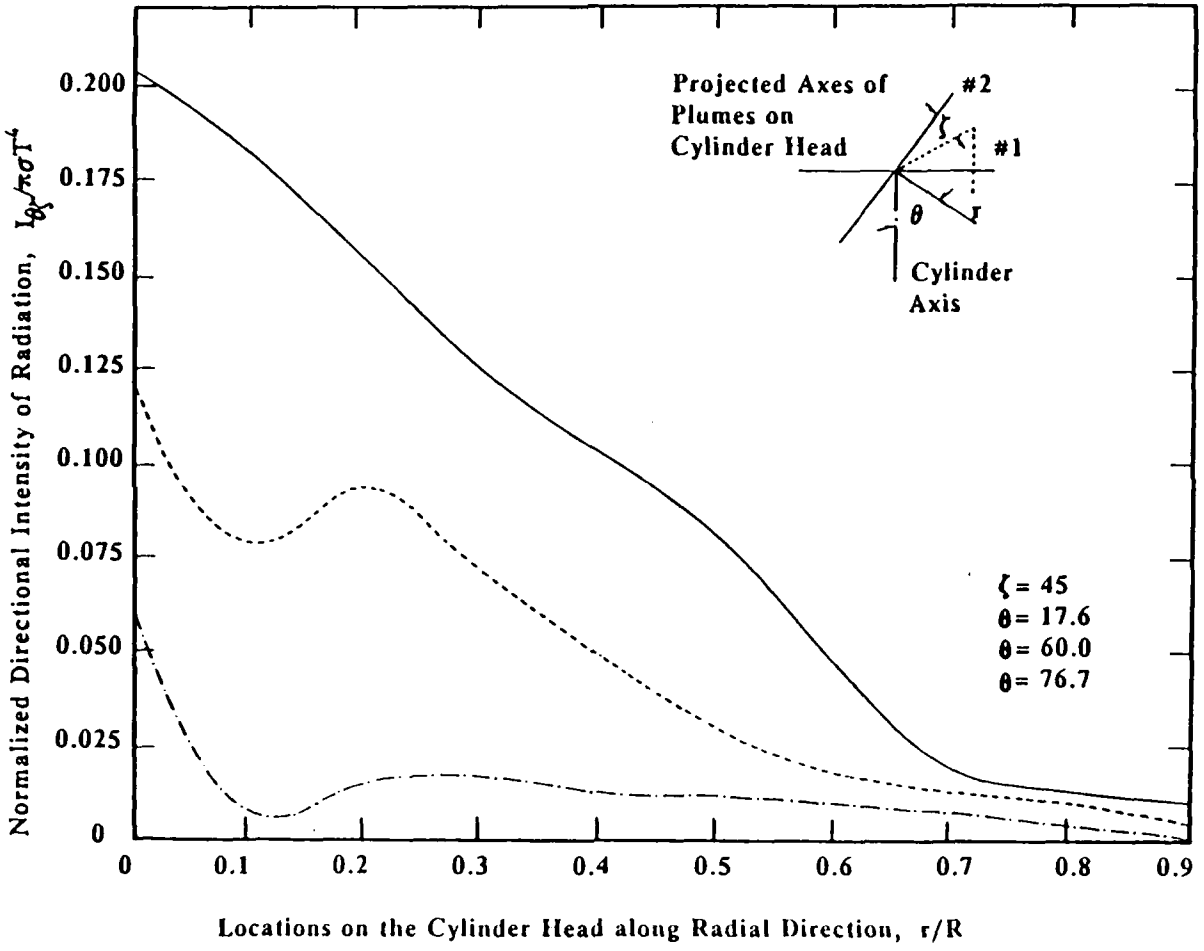
Projected Axes of Plumes on Cylinder Head
#2
#1
ζ
θ
Cylinder Axis
ζ = 45
θ = 17.6
θ = 60.0
θ = 76.7
Normalized Directional Intensity of Radiation, $I_{\theta\zeta}/\pi\sigma T^4$
0.200
0.175
0.150
0.125
0.100
0.075
0.050
0.025
0
0
0.1
0.2
0.3
0.4
0.5
0.6
0.7
0.8
0.9
Locations on the Cylinder Head along Radial Direction, r/R

Fig 2

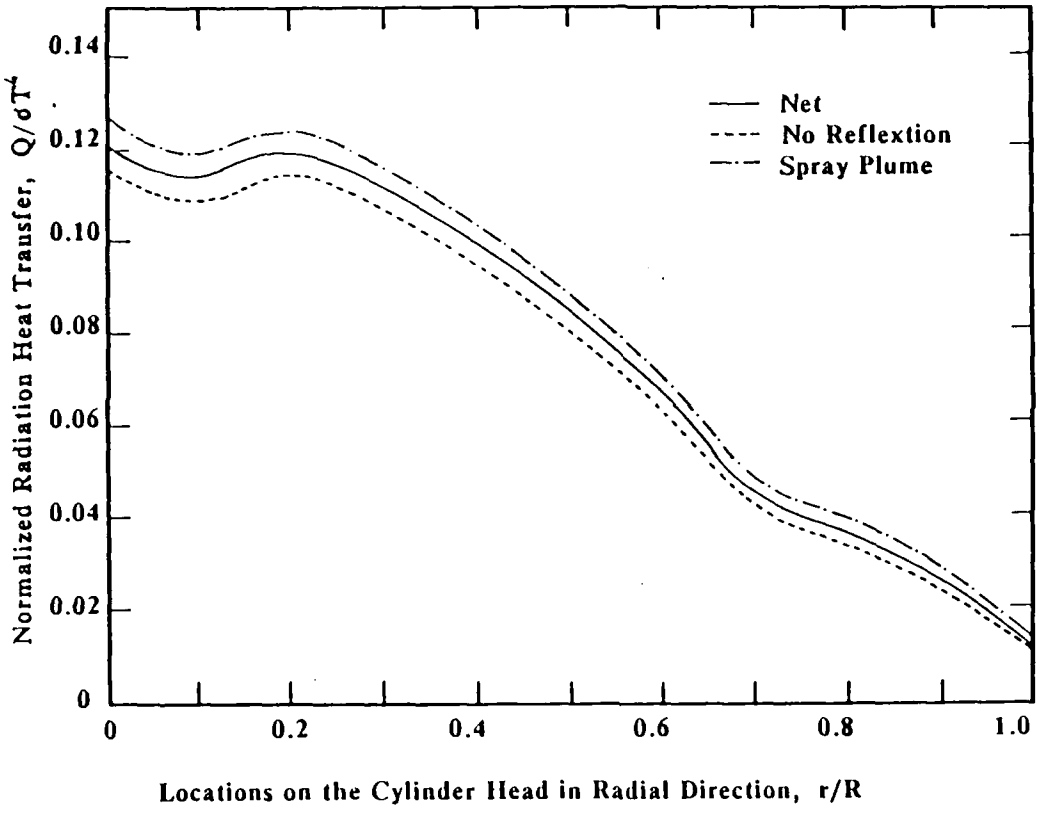
Net
No Reflextion
Spray Plume
Normalized Radiation Heat Trausfer, Q/σT⁴
0.14
0.12
0.10
0.08
0.06
0.04
0.02
0
0
0.2
0.4
0.6
0.8
1.0
Locations on the Cylinder Head in Radial Direction, r/R

Fig 3

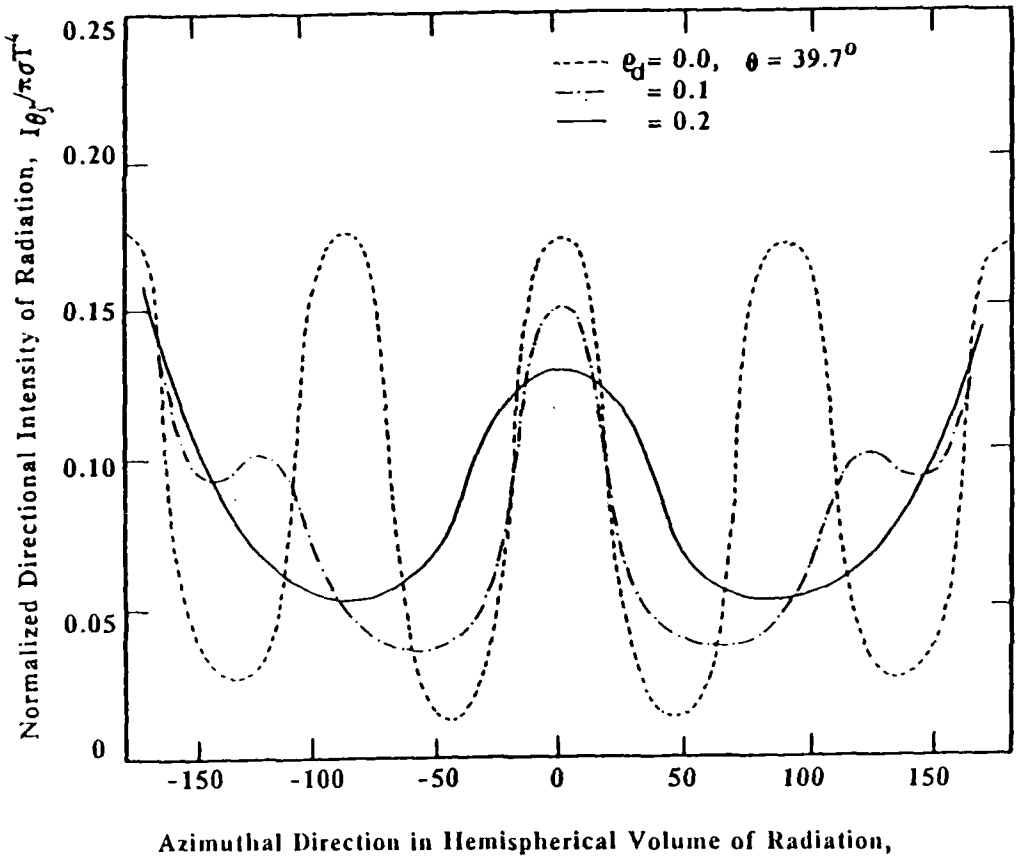
0.25
0.20
0.15
0.10
0.05
0
-150
-100
-50
0
50
100
150
ϱ_d= 0.0, θ = 39.7°
= 0.1
= 0.2
Normalized Directional Intensity of Radiation, $I\theta_s/\pi\sigma T^4$
Azimuthal Direction in Hemispherical Volume of Radiation,

Fig 4

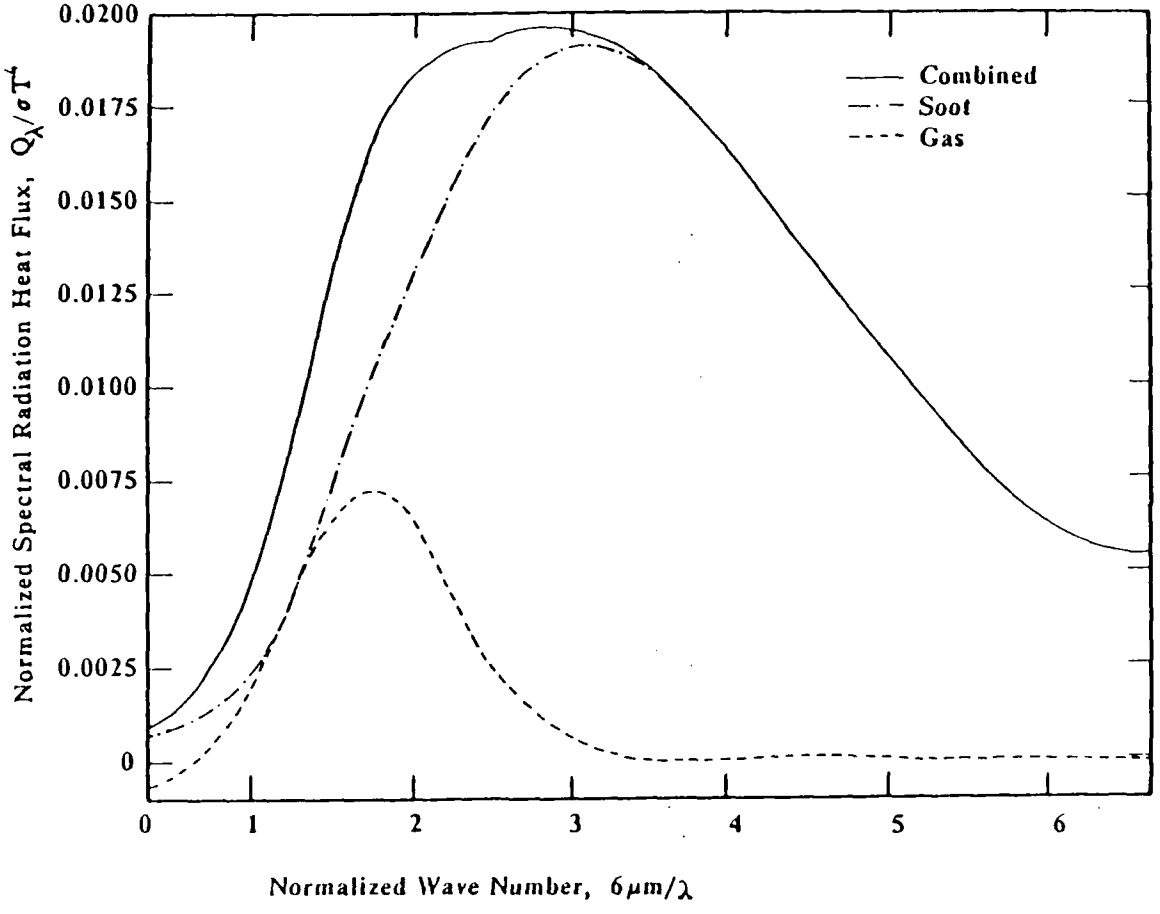
0.0200
0.0175
0.0150
0.0125
0.0100
0.0075
0.0050
0.0025
0
Normalized Spectral Radiation Heat Flux, $Q_\lambda/\sigma T^4$
Combined
Soot
Gas
0
1
2
3
4
5
6
Normalized Wave Number, $6\mu m/\lambda$

Fig 5

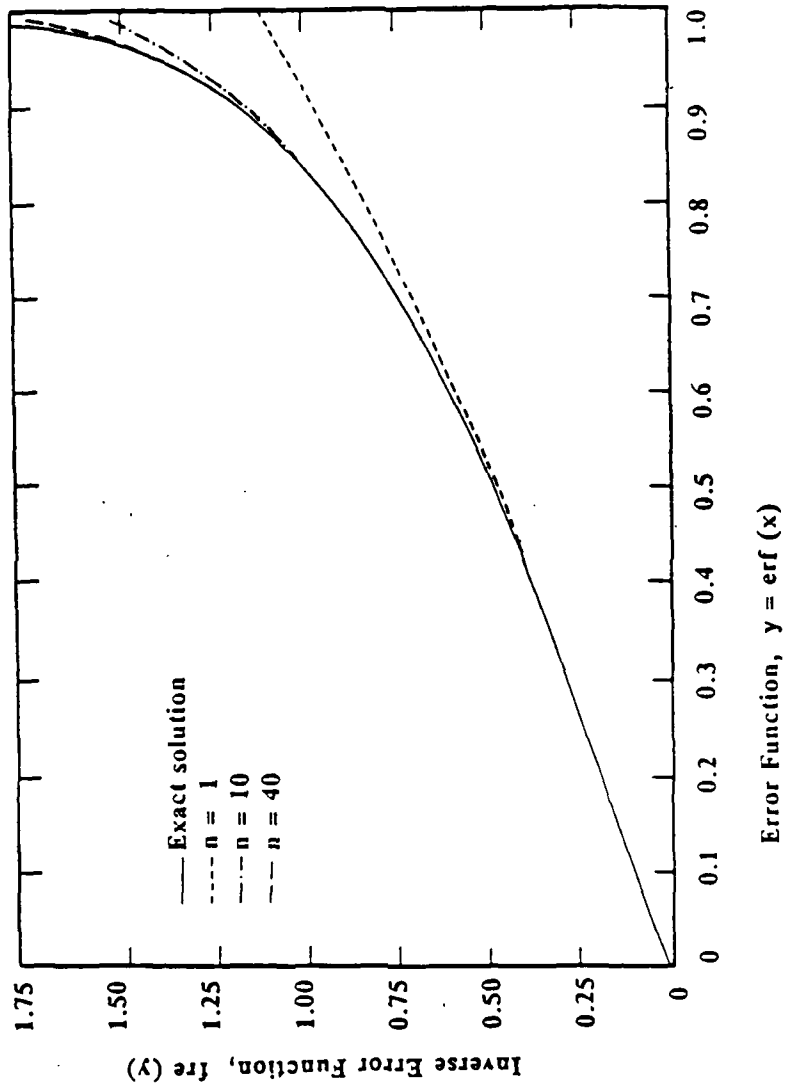
Inverse Error Function, Ire (y)
1.75
1.50
1.25
1.00
0.75
0.50
0.25
0
0
0.1
0.2
0.3
0.4
0.5
0.6
0.7
0.8
0.9
1.0
Error Function, y = erf (x)
Exact solution
n = 1
n = 10
n = 40

Fig A-1

Nomenclature

a	Species distribution constant or $(kT/hc)\int_0^r \kappa_o \, dr$
b	Species distribution constant
c	Species distribution constant or speed of light
f	Species distribution constant
h	Plank's constant
I	Radiation Intensity
k	Boltzman constant
q	Radiation heat flux
r	Optical path
R	Radius of cylinder
T	Temperature
ρ, ϕ, z	Components in cylindrical coordinate
r, θ, ξ	Components in spherical coordinate
J	Volume absorptance
λ	Wavelength
τ	Optical depth
σ	Stefan-Boltzman constant

Subscripts

a	Adiabatic
b	Blackbody
d	Detector
λ	Spectral

List of Figures

COORDINATE TRANSFORMATION METHOD FOR RADIATION HEAT TRANSFER PREDICTION IN SOOT LADEN COMBUSTION PRODUCTS

by

S. L. Chang and K. T. Rhee
Department of Mechanical and Aerospace Engineering
Rutgers, The State University of New Jersey
New Brunswick, New Jersey 08903

INTRODUCTION

Computational modeling of radiative heat transfer has recently become a more important means for the analysis of thermal loading of combustion chambers with luminous flames. This seems to arise due to both the renewed recognition of need for an extensive radiation heat transfer analysis to achieve a better design of many practical systems (e.g., furnace, turbine combustor and diesel engines) and promising new contributions from recent studies enabling more comprehensive modeling. In the modeling, however, several difficult problems are faced, mainly due to the directionality and spectral nature of radiative processes. Most serious problems to be solved in improving its modeling may be listed as follows:

(1) A viable computation of spectral volume absorptance of a mixture of combustion products;

(2) A more accurate computational method for integrating the equation of radiation heat transfer along individual optical paths in the hemispherical volume faced by each location of the reactor wall (hereafter called a detector) and over the wave length range of thermal radiation; and

(3) A detailed description of in-reactor distributions of combustion products and temperature in terms of a suitable coordinate system centered at an individual detector and its coupling with the above radiative transfer equation.

In the present paper, being mainly concerned with the last item of the list, a brief discussion is given for others in order to review the overall problem.

SPECTRAL VOLUME ABSORPTANCE OF SOOT/GAS MIXTURE

When the spectral volume absorptance of combustion products are calculated for the range of thermal radiation, the respective absorptances due to soot cloud and gas mixture are computed as well as their summation. The most widely accepted method of computing the absorptance of soot $\kappa_{\lambda.s}$, by using either Rayleigh limit expression [1] for median size of particles smaller than 0.1 micrometer, or Mie theory [2] for particles with greater sizes where it is required to know the size distribution to take into account scattering. Since practical combustion systems, in general, produce small-size soots, the Rayleigh expression is only considered here. The expression is independent of the size of the particles, inversely proportional to the wavelength λ, and proportional to the soot volume fraction, i.e.,

$$\kappa_\lambda = \frac{36\, n^2\, k(\pi/\lambda)\, f_v}{[n^2(1-k^2) + 2]^2 + 4\, n^4 k^2} \quad . \tag{1}$$

The optical constants, n, k, the real and imaginary parts of the refractive indices, were measured from the intensity of polarizing light reflected from the soot particles and the measurements were fitted to the dispersion equation [3,4]. It was reported that $\kappa_{\lambda.s}$ may slightly increase with wavelength and insignificantly varies with kind of soot and temperature. For computation of emissions from gaseous mixtures, the empirical wide band model proposed by Edwards and Balarkrishnan [5] has often been used [6-8]. The significance of the method is to find, instead of finding gray body absorptance of gas volumes,

the width of individual emission bands, A_λ, compared to blackbody spectrum to approximate the strength of original emission spectrum. This unique technique facilitates an evaluation of the spectral dependence of gas radiation. When emission bands overlap each other at a single spectrum, a separate correction is given [5]. With regard to the summation of both emissions due to soots and gases, even though any method has not fully been verified, several techniques have been used in the past: for an assumed homogeneous and gray body emission, by adding the gas emittance times the soot transmittance to soot emittance [9]; by adding the soot and gas emittances ε_s and ε_g, to find total emittance, ε_t, i.e., $\varepsilon_t = 1-(1-\varepsilon_g)(1-\varepsilon_s)$ [10]; by introducing a new approximation using a pentagamma functional form [11], etc. Unlike those for computation of gray body emittance of gas/soot mixture volume, the summation of spectral emissivity of such mixtures needs special consideration in order to evaluate the spectral dependence of radiation heat transfer. A new method of summing spectral volume absorptances has been used by the authors to find the spectral emittance of combustion products comprising both soot and gases for their recent studies [12]. In the computation of the spectral volume absorptance of a soot/gas mixture, the spectral volume absorptance of gaseous mixture, $\kappa_{\lambda.g}$ is expressed, for convenience of computation, in a form

$$\kappa_{\lambda.g} = C/\lambda \ . \tag{2}$$

Here, C was found from the relationship, $A_\lambda = \int_{\Delta\lambda} 1-\mathrm{Exp}(-C\ell/\lambda)d\lambda$ upon the computation of A_λ for each emission band by using the Edwards' wide band non-gray model. On the other hand, the volume absorptance due to soot suspending in the mixture, $\kappa_{\lambda.s}$, (Eq. 1) is used to find C' from the expression $\kappa_{\lambda.s} = C'/\lambda$. The spectral absorptance of soot/gas mixture, κ_λ, is then computed from the following:

$$\kappa_\lambda = (C+C')/\lambda \tag{3}$$

This method for quantifying spectral dependence of radiative processes of a combustion gas mixture with soot suspension is basically similar to one of those listed above for gray body radiation analysis. That is, a summation for individual spectral emissivity of such mixtures by using the new method, without exceeding blackbody emissivity at a spectrum upon the addition of both emissions, is quite equivalent to the following relationship:

$$\varepsilon_{t.\lambda} = 1-(1-\varepsilon_{g.\lambda})(1-\varepsilon_{s.\lambda}) \tag{4}$$

The validity of the new summation method, however similar to one often employed for gray body analysis, is not fully accepted at present, so that a future systematic experimental evaluation of summation is needed. Further, since the calculation of emittance as a thermal equilibrium mixture is made by computing the spectral volume absorptance instead of emittance as explained above, the assumption of Kirchhoff's law to hold for it in a system is more justified than a similar assumption made for gray body computations.

EQUATION OF RADIATION HEAT TRANSFER EQUATION

The equation of radiation heat transfer in radiatively participating fluids confined in a volume is well known. The governing equation of monochromatic radiation heat transfer is sought for the processes in combustors containing plumes of small size soot laden flames as shown in Fig. 1 where pertinent details are shown, e.g., geometric information and spectral reflectivity of wall surfaces, $\beta_{1\lambda}$, etc. Referring to Fig. 1, the governing equation of local spectral radiation intensity, $I_\lambda(r)$, is written as

$$I_\lambda(r) = \int_r^{r_o} \frac{\kappa_\lambda(r')}{\pi} e_{b\lambda}(r') \, \mathrm{Exp}\left(-\int_r^{r'} \kappa_\lambda(r'')dr''\right)dr' , \tag{5}$$

where, $e_{b\lambda} = \frac{2\pi hc^2}{\lambda^5 [Exp(hc/\lambda KT)-1]}$, κ_λ is the spectral volume absorptance at (r,θ,ζ), $c = 2.998 \times 10^{10}$ cm/sec, $h = 6.625 \times 10^{-27}$ erg-sec, and $k = 1.380 \times 10^{-16}$ erg/K. The heat flux along an optical path of a solid angle (θ,ζ) in the thermal radiation range may be, then, computed from

$$q_{\theta\zeta} = \int_0^\infty I_\lambda(0) \cos\theta \, d\lambda \tag{6}$$

The main difficulty in finding the solution of Eq. (5) resides in the fact that κ_λ is a function of both species concentrations and temperature and that both variables are a function of the location along the individual optical path, r. The present paper considers a new technique to describe the species distribution along individual optical paths and its coupling with Eq. (5). When such distribution details become available, a more realistic solution of Eq. (6) is accessible, as reported elsewhere [13].

The surface properties are combined with the radiation heat fluxes incident on individual locations of the combustor wall. The extinction coefficient, $\tau_\lambda = \int \kappa_\lambda \cdot dL$, along each optical path found from the computation as explained above and the spectral reflectivities, $\beta_{\lambda\cdot 1}$, are included in the expression for the radiosity of surface 1, $\beta_{\lambda 1}$, as

$$\beta_{\lambda 1} = \frac{(I_1 + \beta_{\lambda 1} \cos\theta_1 \, I_\lambda(0)) + \beta_{\lambda 1} \cos\theta_1 \, e^{-\tau_\lambda} \, (I_2 + \beta_{\lambda 2} \cos\theta_2 \, I_\lambda(0))}{1 - \beta_{\lambda 1} \beta_{\lambda 2} \cos\theta_1 \cos\theta_2 \, e^{-2\tau_\lambda}} \tag{7}$$

Upon implementation of computations by coupling Eq. (5) with Eq. (7), the net heat transferred through a chosen spectrum at a detector can be calculated.

IN-COMBUSTOR SPECIES DISTRIBUTION

Since an analysis of space- and spectrum-resolved radiation heat transfer in a combustor, as considered here, requires detailed distributions of in-reactor species and temperature, search of a useful technique for this is clearly warranted. Unfortunately, at present neither convenient means for obtaining in-combustor data sufficient for use in radiation heat transfer analysis has been available. The distributions may be obtained by either experimental or theoretical method. Some activity is underway in the direction of obtaining such information in the authors' laboratory. When the distribution becomes available, it is most convenient to express it in a coordinate system centered at the fuel injection nozzle.

Although, as explained above, the species distribution in plumes of combustors equipped with the fuel injection nozzle is not readily available, a new approach explained in the following may shed light in the search for a viable solution to the problem. It is found from some experimental and theoretical results in literature that the species distribution in non-axisymmetric plume of such systems [14,15] may conveniently be described by the following equation in a cylindrical coordinate:

$$F = F_o \exp(-a\rho - b\phi^2 - cz^2) \tag{8}$$

where F may represent either fuel/air ratio, or soot concentration, or CO_2 or H_2O concentrations; F_o, a, b and c are constants to be separately determined by either experimental or theoretical means for individual combustion units. This expression of plumes, however, deemed rather simple and probably less realistic, is considered to serve a suitable method for some parametric analysis of the confronting problem. Among the advantages of this approach is that the deformation of plume, e.g. in spiral direction, due to swirl motion while the fuel spray is

formed, may be reasonably described for both transient and steady combustion systems, i.e, by including it in ϕ-direction, as explained later.

The next task to be implemented for the final solution may be a proper coupling of, with Eq.(5), the details of in-combustor species distribution that may be obtained from the above method or others. Several techniques have been employed in finding a solution of the equation of radiation heat transfer (Eq. (5), namely, the Monte-Carlo method [10,16], the zonal method [17,18], the use of geometric factors [6,19], etc. Those methods did not rigorously implement the solution of Eq. (5), but sought for approximated solution and gray-body computation. Among the main reasons for this is that it is difficult to find species distribution along individual directions of integration in the hemispherical volume faced by the location where heat transfer is considered. The difficulty is compounded when the distribution varies with time as in transient-flow combustors.

COORDINATE TRANSFORMATION

In view of the discussion above on the overall problem in finding space- and spectral-resolved radiation heat transfer in combustors, it is highly desirable to find a more versatile method enabling us to find a better solution of Eq. (5). A new technique for the goal is presented in the following. The basic idea of the technique is to employ coordinate transformations for finding the species distribution along the individual optical direction, r, (Fig. 1) in an equational form by using the species distribution given in a coordinate with respect to the fuel injector. When such an equation in a suitable coordinate centered at detectors on the combustor wall becomes available, i.e. along individual optical direction with respect to the detector, a better computation of the space-resolved radiation heat transfer can be attempted.

As explained earlier, it was found to be convenient to express, in a cylindrical coordinate, the spray plumes of which geometry and others vary with time. The following discussion is concerned with description of the same plumes in a new coordinate system with respect to a detector of interest, consequently to make available the species distribution along individual optical paths centered at the detector. This goal is achieved by using a new coordinate transformation technique involving two main sets of coordinate systems, i.e., a cylindrical coordinate centered at the injection nozzle hole, O, for describing the spray plumes (ρ,ϕ,z) and a spherical coordinate (r,θ,ζ) for expressing the same plumes with respect to the detector located at D. Two transformation techniques are presented: (1) point-to-point transformation; and (2) distribution equation-to-distribution equation transformation. The former is considered to be particularly useful when some discrete point data are available in a coordinate with respect to the injection nozzle for expressing them in a new coordinate centered at a detector. The latter is developed for transforming a functional expression of the spray plume in a nozzle coordinate, e.g. Eq. (8), to find an equational spray description in a new detector coordinate.

(1) Point-to-point Transformations

MUTUALLY PARALLEL COORDINATES - When in-combustor species data is experimentally acquired [20], it is always likely that they become available in a set of discrete data points as opposed to in a form of continuous variation in species concentration of plumes. When one uses such discrete data points in computing radiation characteristics in a direction of optical path with respect to a detector, it is necessary to know a species distribution along individual optical paths for solving Eq. (5). For such needs, a new approach of using point-to-point coordinate transformation is introduced. To perform a coordinate transformation between these systems, two more intermediate coordinate systems,

X and Y, are introduced for the convenience of derivation. The axes of the coordinates under consideration are either parallel or perpendicular to each other in order to avoid the complexity of the derivation although cases with the mutually non-parallel coordinates are discussed later. The interim coordinate systems are listed in the following and shown in Fig. 2-(A).

a. Spray plume coordinate (cylindrical), C (ρ,ϕ,z)

b. X coordinate, X (x_1,x_2,x_3)

c. Y coordinate, Y (y_1,y_2,y_3)

d. Detection coordinate (spherical) S (r,θ,ζ)

Identifying the location of a detector at x_{1d}, x_{2d}, x_{3d}, a series of transformations are carried out to obtain

$$\rho^2 = r^2 \sin^2\theta + 2 r \rho_d \sin\theta \cos(\phi_d+\zeta) + \rho_d^2,$$

$$\phi = \tan^{-1}[(\rho_d \sin\phi_d - r \sin\theta \sin\zeta)/(\rho_d \cos\phi_d + r \sin\theta \cos\zeta)],$$

$$Z = Z_d - r \cos\theta , \qquad (9)$$

where, $\rho_d^2 = x_1^2 + x_2^2$, $\phi_d = \tan^{-1}(x_2/x_1)$, and $z_d = x_3$. Note that $\phi = \tan^{-1}(x_2/x_1)$ if $x_1 \geq 0$, $\phi = \tan^{-1}(x_2/x_1) + \pi$ if $x_1 < 0$ and $x_2 > 0$ and $\phi = \tan^{-1}(x_2/x_1) - \pi$ if $x_1 < 0$ and $x_2 < 0$.

MUTUALLY UNPARALLEL COORDINATES - However, since in many practical systems, e.g., diesel engines, the fuel is injected into the combustion chamber at an angle, θ_{in}, as shown in Figs. 1 and 2-(B), this has to be taken into consideration in the coordination transformation. In order to meet this need, an additional coordinate system having an angle of θ_{in} with respect to the cylinder coordinate (x_1,x_2,x_3) is introduced. The new coordinate (u_1,u_2,u_3) is not parallel to the detector coordinate (y_1,y_2,y_3). Their mutual relationship may be listed as follows:

$$x_1 = \rho \cos\phi,\ x_2 = \rho \sin\phi,\ x_3 = Z\ ;$$

$$u_1 = x_1 \cos\theta_{in} - x_3 \sin\theta_{in}\ ;$$

$$u_2 = x_2\ ;$$

$$u_3 = x_1 \sin\theta_{in} + x_3 \cos\theta_{in}\ ;$$

$$\rho_u^2 = u_1^2 + u_2^2\ ;$$

$$\theta_u = \tan^{-1}(u_2/u_1)\ ;\ \text{and}$$

$$z_u = u_3\ .$$

Further, an expression similar to Eq. (9) can be obtained as

$$\rho_u^2 = (\rho \cos\theta_{in} \cos\phi - z \sin\theta_{in})^2 + \rho^2 \sin^2\phi$$

$$\phi_u = \tan^{-1}[(\rho \sin\phi)/(\rho \cos\theta_{in} \cos\phi - z \sin\theta_{in})]$$

$$z_u = \rho \sin\theta_{in} \cos\phi + z \cos\theta_{in}\ .$$

Accordingly, the location of detector, initially identified by using the parallel coordinate (ρ,θ,z) can finally be rewritten in terms of the unparallel system (ρ_u,r_u,z_u) (see Fig. 2-(B) as,

$$\rho_u^2 = (\rho_d \cos\theta_{in} \cos\phi_d - z_d \sin\theta_{in})^2 + \rho_d^2 \sin^2\phi_d\ ,$$

$$\phi_u = \tan^{-1}[(\rho_d \sin\phi_d)/(\rho_d \cos\theta_{in} \cos\phi_d - z_d \sin\theta_{in})]\ \text{and}$$

$$z_u = \rho_d \sin\theta_{in} \cos\phi_d + z_d \cos\theta_{in}\ . \qquad (10)$$

Since it is readily found that the geometric configurations of the inclined plume vs. the coordinate (y_1,y_2,y_3) is equivalent to those of the similar plume with axis in x_1 vs. an equally inclined detector coordinate (u_1',u_2',u_3'), some pertinent conversion may be made. Converting the geometric details of a given solid angle initially represented by using (θ,ζ) into an expression in terms of corresponding unparallel coordinate (θ_u,ζ_u), the results obtained for the case of mutually parallel coordinate, Eq. (9), can directly be used. For this, the conversion for the solid angle is achieved by

$$\theta_u = \cos^{-1}[-\sin\theta \cos\zeta \sin\theta_{in} + \cos\theta \cos\theta_{in}]$$

$$\zeta_u = \tan^{-1}[\sin\theta \sin\zeta/(\sin\theta \cos\zeta \cos\theta_{in} + \cos\theta \sin\theta_{in})] \qquad (11)$$

The location of a data point originally identified in terms of the coordinate of plume of which axis is inclined by an angle of θ_{in} with respect to a perpendicular coordinate can, therefore, be expressed in terms of a spherical coordinate centered at a detector on the combustor wall by introducing Eqs. (9) and (10) into Eq. (11).

(2) Distribution-to-Distribution Transformations

WITHOUT SWIRL MOTION - As explained earlier, the details of in-combustor spray plume may be obtained in an equational form, e.g. Eq. (8), expressed with respect to the nozzle hole. The transformation of such distribution to individual distributions along an individual optical path at a detector is considered for a combustor without swirl motion. The logical step for this goal would have been introducing the corresponding terms of Eq. (9) into Eq. (8). Such transformation, however, results in an extremely complex form of Eq. (8) expressed in terms of the spherical coordinate at the detector. Furthermore, the new transformed distribution equation becomes too difficult to be used in Eq. (5). In order to alleviate the problem, an approximation technique was sought in such a way as to conveniently use its results in obtaining the solution of Eq. (5). It was found that use of the Taylor expansion method in the transformation not only greatly facilities the steps toward the final goal but also lead to very accurate results.

ρ-terms:

Letting $\chi \equiv r \sin\theta/\rho_d$, $A \equiv \cos(\phi_d + \zeta)$, with $f \equiv \rho/\rho_d$, one finds

$$f(\chi) = (1 + 2A\chi + \chi^2)^{1/2},$$

$$f'(\chi) = (A+\chi)/f \text{ , and}$$

$$f''(\chi) = [f^2(\chi) - (A+\chi)^2]/f^3$$

For $\chi = \chi_i + \varepsilon$ and $\varepsilon \ll 1$ the above may be rewritten as,

$$f(\chi) \cong f(\chi_i) + f'(\chi_i)\,\varepsilon + f''(\chi_i)\varepsilon^2/2$$

Further, since $\varepsilon = \chi - \chi_i$, $f(\chi)$ may be expressed as

$$f(\chi) = \rho/\rho_d \cong f_0 + f_1 + f_2\,\chi^2 \qquad (12)$$

where, $f_0 = f(\chi_i) - f'(\chi_i)\,\chi_i + f''(\chi_i)\,\chi_i^2/2$,

$f_1 = f'(\chi_i) - f''(\chi_i)\,\chi_i$, and

$f_2 = f''(\chi_i)/2$.

For $\chi \gg 1$, $f(\chi) = \rho/\rho_d \cong \chi + A$

φ terms:

From Eq. (9), having $f(\chi) = \tan(\phi)$

$$= (\sin\phi_d - \chi \sin\zeta)/(\cos\phi_d + \chi \cos\zeta),$$

one obtains

$$f'(x) = -\sin(\phi_d + \zeta)/(\cos\phi_d + x\cos\zeta)^2,$$

$$f''(x) = -2\, f'(x)\cos\zeta/(\cos\phi_d + x\cos\zeta),$$

$$\phi(x) = \tan^{-1}(f)$$

$$\phi'(x) = f'/(1+f^2), \text{ and}$$

$$\phi''(x) = [-2\, ff'^2 + (1+f^2)\, f'']/(1+f^2)^2.$$

Note, for $\cos\phi_d + x\cos\zeta = 0$, $\phi(x) = \pi/2$, $\phi'(x) = -\cos^2\zeta/\sin(\phi_d+\zeta)$ and $\phi''(x) = 0$. For $x = x_i+\varepsilon$ and $\varepsilon \ll 1$, $\phi(x)$ may be written as $\phi(x) \cong \phi(x_i) + \phi'(x_i)\,\varepsilon + \phi''(x_i)\,\varepsilon^2/2$.

In view of Eq. (8), one defines $\Phi(x) = \phi^2(x)$ to rewrite

$$\Phi(x) \cong \Phi(x_i) + \Phi'(x_i)\,\varepsilon + \Phi''(x_i)\,\varepsilon^2/2$$

where $\Phi'(x) = 2\phi(x_i)\,\phi'(x_i)$

$$\Phi''(x) = 2\phi(x_i)\,\phi''(x_i) + 2\phi'^2(x_i)$$

Further, since $\varepsilon = x-x_i$, Φ may be expressed

$$\Phi(x) \cong \Phi_o + \Phi_i\, x + \Phi_2\, x^2 \tag{13}$$

where, $\Phi_0 = \Phi(x_i) - \Phi'(x_i)\, x_i + \Phi''(x_i)\, x_i^2/2$

$$\Phi_1 = \Phi(x_i) - \Phi''(x_i)\, x_i$$

$$\Phi_2 = \Phi''(x_i)/2$$

For $x \gg 1$, $\phi(x) \cong -\zeta$, or $\Phi(x) \cong \zeta^2$.

z-terms:

Since z is a single first order polynomial function of r, the following is obtained from Eq. (9).

$$z^2 = z_d^2 - 2\, z_d\, r \cos\theta + r^2 \cos^2\theta \qquad (14)$$

Finally, by substituting terms in Eq. (8) with Eqs. (12), (13) and (14), one obtains

$$F = f_d\, e^{-[(r-r_o)/r_w]^2} \qquad (15)$$

where, $f_d = f_o\, e^{-(a_1 - b_1^2/4C_1)}$,

$r_o = b_1/2\, C_1$,

$r_w = (C_1)^{-1/2}$,

$a_1 = a\, \rho_o + b\, \Phi_o + C\, z_d^2$,

$b_1 = -[a\, \rho_1 + b\, \Phi_1]\, \sin\theta/\rho_d + 2\, Cz_d \cos\theta$, and

$c_1 = [a\, \rho_2 + b\, \Phi_2]\, \sin^2\theta/\rho_d^2 + C \cdot \cos^2\theta$.

When the above results are used in solving Eq. (5), it is found that the above approximation method generates better accuracy when the integral interval is divided into smaller subranges.

WITH SWIRL MOTION - The present coordinate transformation method is also considered for a combustor with swirl motion. With swirl motion, prior to the transformation, the spray plume distribution equation, Eq. (8), needs adjustments to take into account the bending of spray plume. Although the exact formation mechanism of bent sprays in the presence of gas swirl in the combustor is not properly understood at present, the following two probable cases are considered.

Droplet with Constant Axial Velocity:

It is assumed that (1) fuel droplets ejected from the nozzle hole to move at a constant axial velocity, v_f; (2) the angular velocity of the swirl, Ω, is constant along the axis of the plume; (3) the angular velocity of fuel droplets along the plume axis is the same as Ω. With the above, a point characteristic at a location (ρ,ϕ,Z) of no-swirl condition is found at a location $(\rho,\phi+\phi_s,Z)$, due to the swirl during a period of time Δt, according to

$$\phi_s = (\Omega/v_f)\rho,$$
$$\phi_s' = \Omega/v_f \text{ and}$$
$$\phi_s'' = 0.$$

In this case Eq. (8) becomes $F = F_o \exp[-a\rho - b(\phi-\phi_s)^2 - Cz^2]$. The transformation of the above equation into the detector coordinate expression is exactly identical except for a new set of equations in ϕ-terms. They are:

$$\Phi(x_i) = \psi^2(x_i),$$
$$\Phi'(x_i) = 2\psi(x_i)\,\psi'(x_i), \text{ and}$$
$$\Phi''(x_i) = 2\psi(x_i)\psi''(x_i) + 2\psi'^2(x_i), \qquad (16)$$

where, $\psi(x_i) = \phi(x_i) - \phi_s(x_i)$,
$\psi'(x_i) = \phi'(x_i) - \phi_s'(x_i)$ and
$\psi''(x_i) = \phi''(x_i) - \phi_s''(x_i)$.

Droplets with Specified Axial Velocity:

Melton [21] analyzed a case for the plume formation as

$$v_f = v_s/(1+\alpha\rho)$$

where, v_s is the exit velocity of the fuel droplet at the nozzle hole, α is about 0.085/Rs and Rs is the radius of the nozzle hole. Assumptions of the previous case are also similarly taken here for finding $\phi_s = \Omega \cdot t$, since $v_f = d\rho/dt = v_s/(1+\alpha\rho)$ and $\rho + \alpha\rho^2/2 = v_s\, t$.

Combining the above, one finds

$$\phi_s = (\Omega\rho/v_s)\ (1+\alpha\rho/2).$$

Letting $\phi_{s1} = (\Omega/v_s)\ (1+\alpha/2)$, the above equation may be expressed in terms of ϕ_{s1} to obtain

$$\phi_s = \phi_{s1}\ \rho(1+\alpha\rho/2)/(1+\alpha/2),$$

$$\phi_s' = \phi_{s1}(1+\alpha\rho)/(1+\alpha/2) \text{ and}$$

$$\phi_s'' = \phi_{s1}\ \alpha/(1+\alpha/2).$$

Substituting respective terms in Eq. (16) by the above results, the coordinate transformation of bending spray plumes, as specified here, can be achieved.

Regarding the plumes with their axis having an inclined angle of θ_{in}, the distribution-to-distribution transformation can be obtained by introducing Eqs. (11) and (12) into Eq. (15).

COMPUTATION OF RADIATION IN DIESEL COMBUSTION

The present method may readily be used for analysis of radiation heat transfer processes in combustors having jet flames. An analysis may be made over the entire wall of the reactor to introduce the results to implement a global analysis of the system heat transfer including convective and conduction heat transfers, which will enable prediction of the temperature distribution

into and over the wall. When an unsteady combustion reactor is considered, e.g., a diesel engine, the analysis will have to be made over the entire cycle period along with energy conversion process, as presently attempted in our laboratory. The present section, however, considers the computation of radiation heat transfer at a particular engine crank angle. Since more extensive results are reported elsewhere [22], only a few computations are described here. Among the assumptions employed due to the absence of either sufficient engine data or suitable engine modeling are (1) the values of constants in Eq. (8) are F_0 for soot, H_2O, CO_2 and burned fuel/air ratio, 8×10^{-6}, 0.01, 0.01, and 1.0, respectively; the distribution constants, a, b and c are 0.6, 2.36, and 2 for the above cases accordingly. (For example, the CO_2 distribution in the plume may be written as $F = \{0.01\ \mathrm{Exp} - [0.6(\rho/R) + 2.43(\phi/\phi_r) + 2.0(z/R)^2]\}$, where R is the piston radius and ϕ_r is π/(number of plumes), (2) other engine details are, the surface temperature, 500°K; the number of plumes, 4, the piston radius, 4.92 cm; the combustion chamber bowl radius, 3.44 cm, and the fuel composition $C_{16}H_{34}$, (3) the computation of the temperature distribution is computed by using the equilibrium adiabatic temperature relationship to the fuel/air ratio (e.g., using a new method [23]), etc. The computed radiation heat flux is presented presented in terms of the following nondimensionalized terms: the normalized spectral energy, $Q_\lambda/Q_{b\lambda}$, and the normalized directional radiation intensity, $I(\rho,\phi,z)/I_b$, where, $Q_{br} = \sigma T_r^4$, T_r = 2,400°K, $I_b = Q_{br}/\pi$, and σ is the Stefan-Boltzman constant ($5.670\times10^{-8} W/m^2\ K^4$).

Shown here are the following case analyses: (1) the spectral radiation heat incident upon locations on the cylinder head along the axis of a spray plume at r = 0.0R, 0.5R and 0.9R (Fig. 3), (2) the normalized directional radiation intensity streaming into the injection nozzle tip (ρ = 0.0, ϕ = 0.0) along the direction of zenith angle in the hemispherical volume faced by the tip (Fig. 4

and (3) the normalized directional radiation intensity along the locations on the cylinder head right above the axis of the spray plume in directions of zenith angle, θ = 17.6, 60.0 and 76.7 in the hemispherical volume faced by each location (Fig. 5). Without discussing the details of the results, one may readily find from the above illustration that improved radiation heat transfer computations can be achieved by employing the present new coordinate transformation method in its modeling.

ACKNOWLEDGMENT

The present work has been supported by the U.S. Army Research Office, Contract No. DAAG29-83-K-0042 (Scientific Program Officer, Dr. David M. Mann).

NOMENCLATURE

- A band absorptance
- a constant determining species distribution
- B radiosity
- b constant determining species distribution
- c speed of light or constant determining species distribution
- e Plank's emission power
- F species distribution function
- f soot volume fraction or transformation function
- h Plank's constant
- I radiation intensity
- k Boltzman constant or imaginary part of reflective index
- n real part of the reflective index
- Q black body radiation
- q radiation heat flux

R radius of cylinder

T temperature

t time

v velocity

x component of cartesian coordinate X

y component of cartesian coordinate Y

α constant for plume injection speed

β reflectivity of cylinder wall

γ,θ,ζ components in spherical coordinate, C

ε emittance

θ angle of optical path with respect to normal

κ volume absorptance

λ wavelength

ρ,ϕ,Z components in cylindrical coordinate, S

τ extinction coefficient

Φ transformation function

Ω angular speed

Subscripts

b blackbody

d detector

g gas

in inclined

o constant

s soot

t total

u unparallel

λ spectral

θs optical path of solid angle

REFERENCES

1. Bard, S. and Pagni, P. J., "Carbon Particles in Small Pool Fire Flame," J. Heat Transfer, 103, pp. 357-362, 1981.

2. Plass, G. N., "Mie Scattering and Absorption Cross Section for Absorbing Particles," Applied Optim., 5, pp. 279-285, 1966.

3. Dalzell, W. H. and Sarofin, A. F., "Optical Constants of Soot and Their Application to Heat Flux Calculation," Trans. of ASME, Vol. 9, pp. 100-104, 1969.

4. Lee, S. C. and Tien, C. L., "Optical Constants of Soot in Hydrocarbon Flame," 18th Symposium (Int.) on Combustion, The Combustion Institute, pp. 1159-1165, 1981.

5. Edward, D. K. and Balakrishnan, A., "Thermal Radiation by Combustion Gases," Int. J. Heat Mass Transfer, Vol. 16, pp. 25-40, 1973.

6. Chang, S. L. and Rhee, K. T., "Computation of Radiation Heat Transfer in Diesel Combustion," SAE Paper-831332, 1983, also in SAE Transactions.

7. Chang, L. C., Yang, K. T. and Lloyd, J. R., "Radiation-Natural Convection Interactions in Two-Dimensional Complex Enclosure," J. Heat Transfer, Vol.105, pp. 89-95, Feb. 1983.

8. Buckius, R. O. and Tien, C. L., "Infrared Flame Radiation," Int. J. Heat Mass Transfer, Vol. 20, pp. 93-106, 1977.

9. Yuen, W. W. and Tien, C. L., "A Simple Calculation Scheme for the Luminous Flame Emissivity, 16th Symposium (Int.) on Combustion, The Combustion Institute, pp. 1481-1487, 1976.

10. Siegel, R. and Howell, J. R., The Radiation Heat Transfer, 2nd Edition, McGraw-Hill Book Co., 1981.

11. Grosshandler, W. L. and Modak, A. T., "Radiation from Non-homogeneous Combustion Products," 18th Symposium (Int.) on Combustion, The Combustion Institute, pp. 601-609, 1981.

12. Chang, S. L. and Rhee, K. T., "An Analytical and Numerical Modeling of Radiation Heat Transfer in Combustion Having Jet Flames," Proc. of Fourth Int. Conf. on Applied Numerical Modeling, Taiwan, Dec. 28-31, 1984.

13. Chang, S. L. and Rhee, K. T., in preparation.

14. Takeuchi, K., Senda, J. and Shikuja, M., "Transient Characteristics of Fuel Atomization and Droplet Size Distribution in Diesel Fuel Spray," SAE Paper-830449, 1983.

15. Kuo, T. W., Yu, R. C. and Shahed, S. M., "A Numerical Study of the Transient Evaporating Spray Mixing Process in the Diesel Environment," SAE Paper-831735, 1983.

16. Steward, F. R. and Cannon, P., "The Calculation of Radiative Heat Flux in a Cylindrical Furnace Using the Monte Carlo Method," Int. J. Heat Mass Transfer, Vol. 14, No. 2, pp. 245-262, 1971.

17. Hottel, H. C. and Sarofin, A. F., Radiative Transfer, McGraw-Hill Book Co., New York, 1967.

18. Menguc, M. P., Viscanta, R. and Ferguson, C. R., "Multidimensional Modeling of Radiative Heat Transfer in Diesel Engines," SAE Paper-850503, 1983.

19. Chapman, M., Friedman, M. C. and Aghan, A., "A Time-Oependent Spatial Model for Radiant Heat Transfer in Diesel Engines," SAE Paper-831725, 1983.

20. Whitehouse, N. D. and Abdul-Hadt, M.A., "The Distribution of Soot in the Cylinder of a Quiescent Combustion Chamber Diesel Engine," Proc. Inst. Mech. E., Vol. 196, No. 24,1982.

21. Melton, R. B., Jr., "Diesel Fuel Injection Viewed as a Jet Phenomenon," SAE Paper 710132, 1971.

22. Chang, S. L., Yang, X. L. and Rhee, K. T., "A Parametric Analysis of Radiation Heat Transfer in Direct Injection Diesel Combustion," International Symposium on Diagnostics and Modeling in Reciprocating Engines, September 4-6, 1985, Tokyo, Japan.

23. Rhee, K. T. and Chang, S. L., "Empirical Equations for Adiabatic Flame Temperature for Some Fuel-Air Combustion Systems," Combustion Science and Technology, Vol. 44, 1985, p. 75.

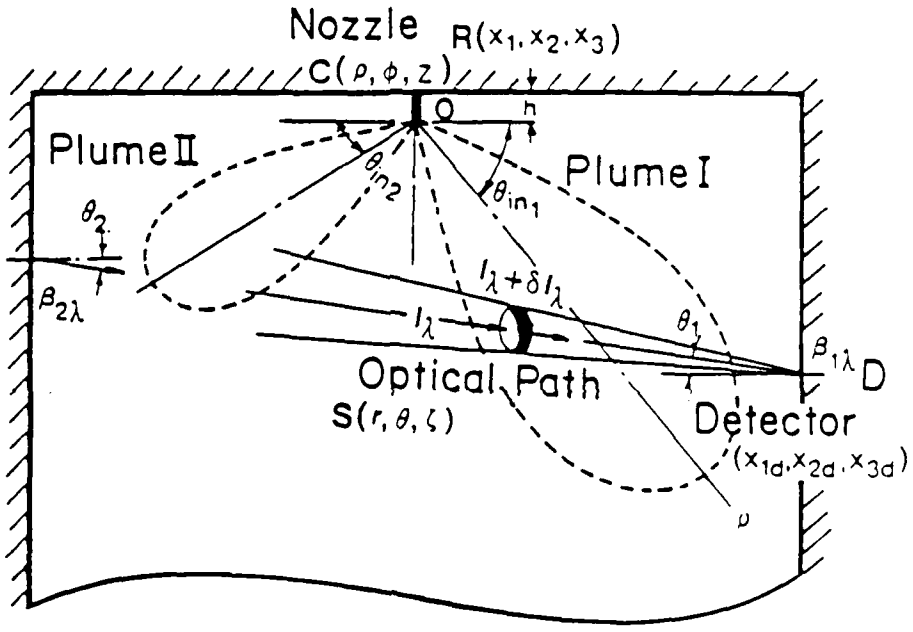

Fig. 1. Soot laden flames in a combustion chamber

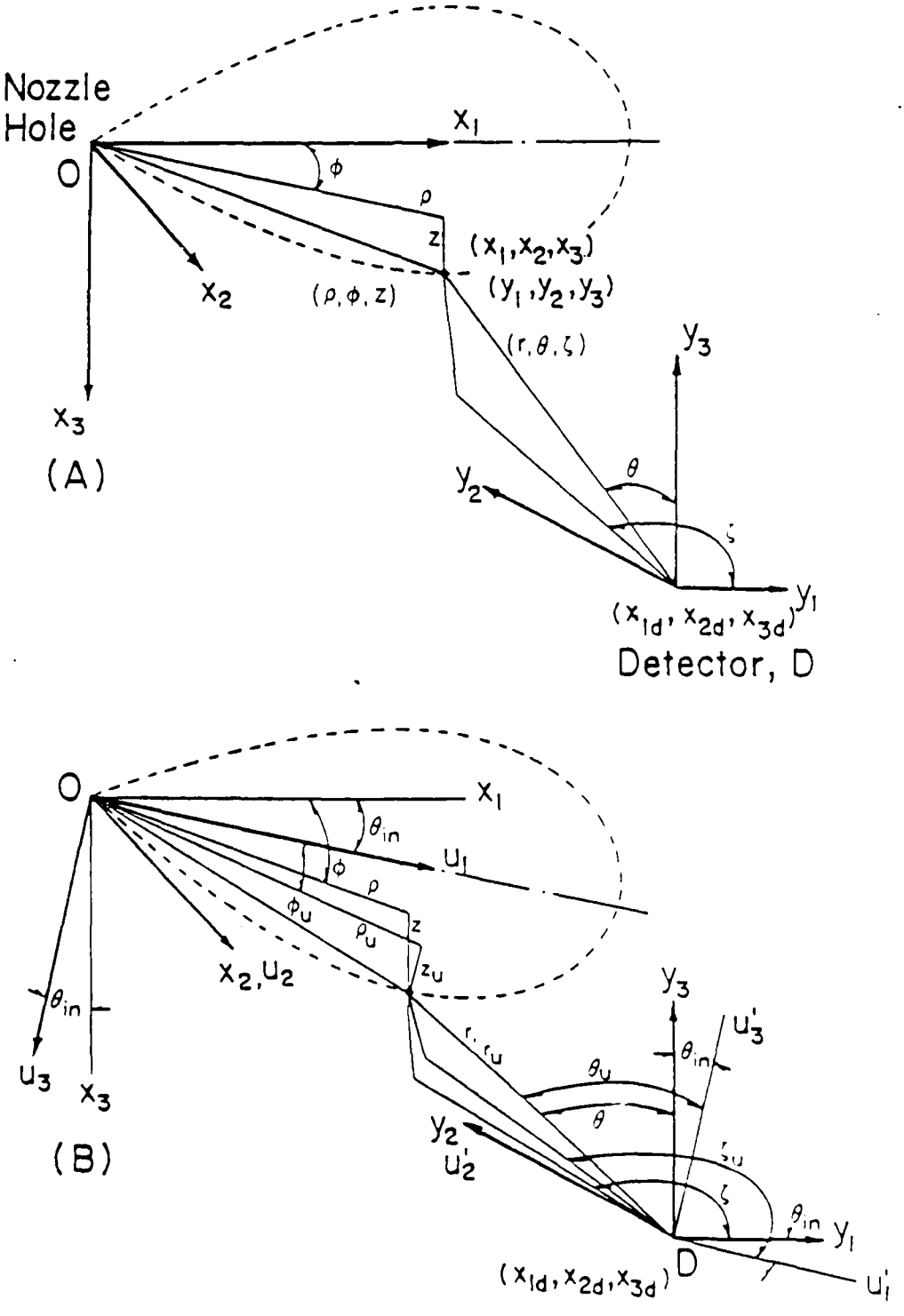

Fig. 2. Detector location with respect to flame plume.
(A) Parallel Coordinate and (B) Unparallel Coordinate

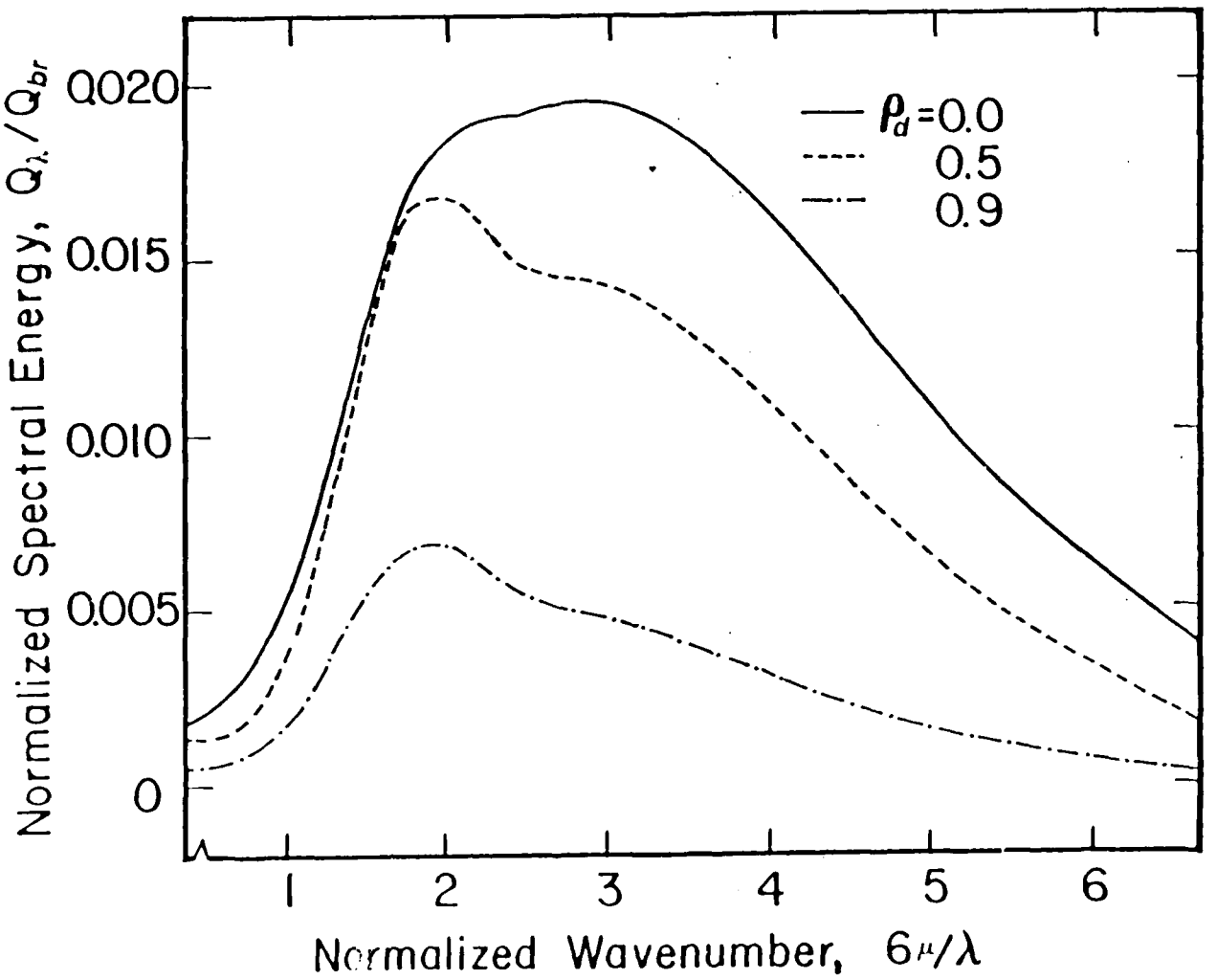

Fig. 3. Spectral radiation energy incident upon detectors located on the cylinder head at r = 0.0R, r = 0.5R and r = 0.9R.

AD-A168 979 RELATIONSHIP OF IN-CYLINDER GASEOUS AND PARTICULATE 2/2
CONCENTRATION TO RADI..(U) RUTGERS - THE STATE UNIV NEW
BRUNSWICK N J DEPT OF MECHANICAL.. K T RHEE ET AL.
UNCLASSIFIED 15 APR 86 ARO-19869.13-EG DAAG29-83-K-0042 F/G 21/2 NL

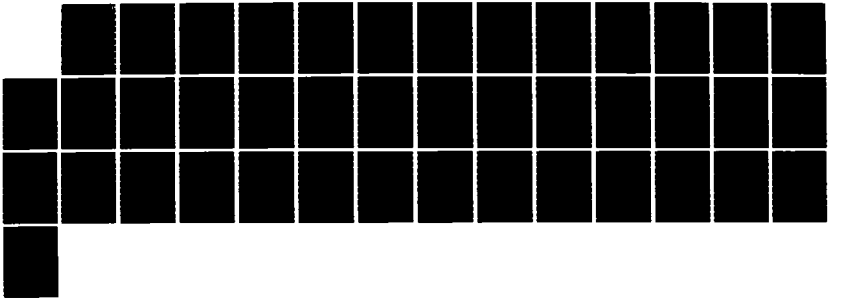

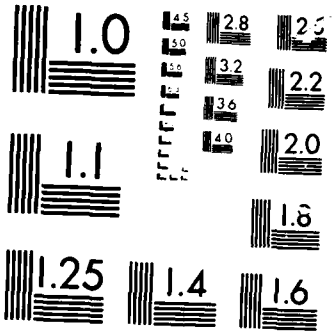
1.0
1.1
1.25
1.4
1.6
1.8
2.0
2.2
2.8
3.2
3.6
4.0

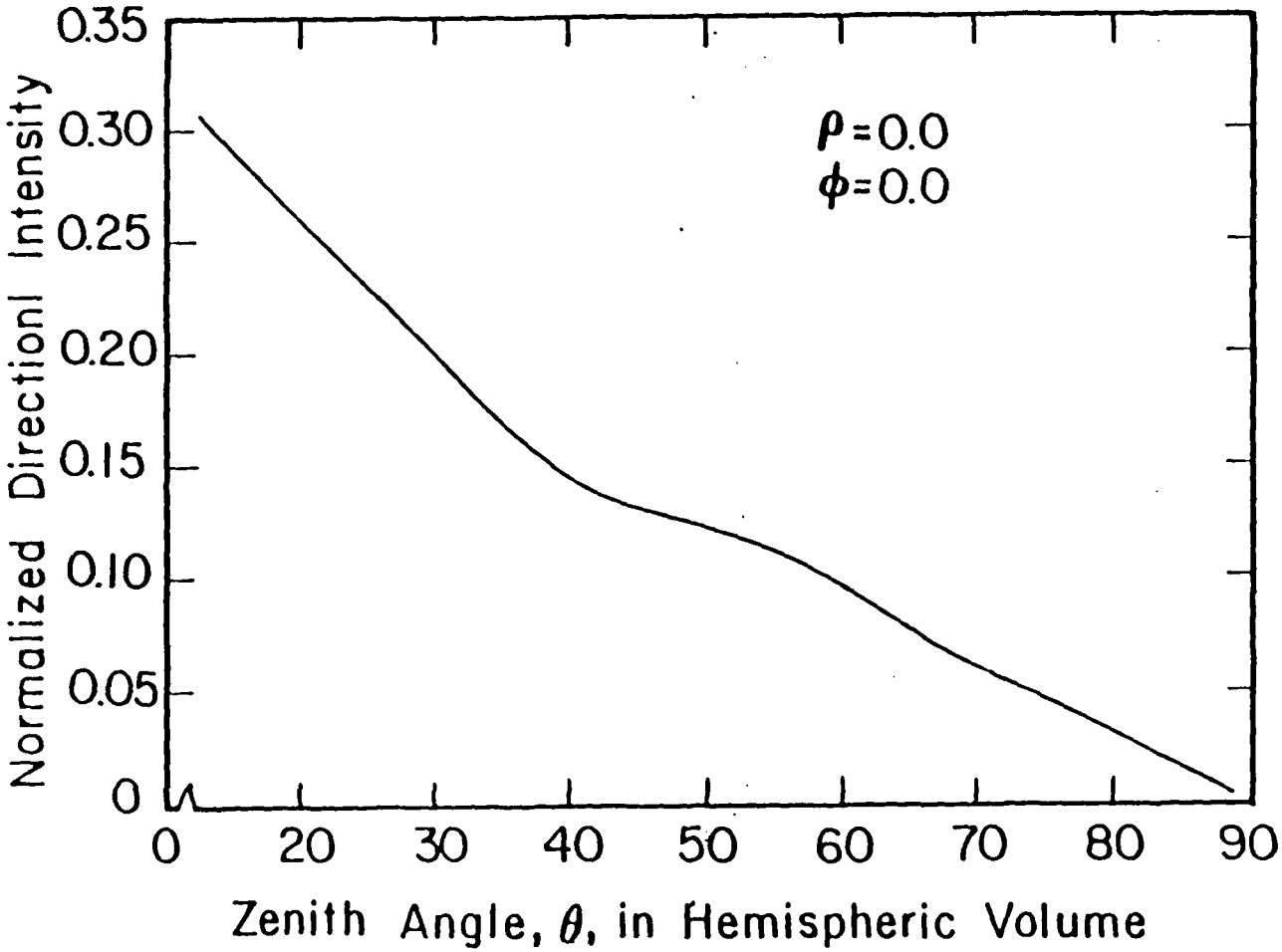

Fig. 4. Directional radiation intensity at the injection nozzle streaming through individual direction of zenith angle.

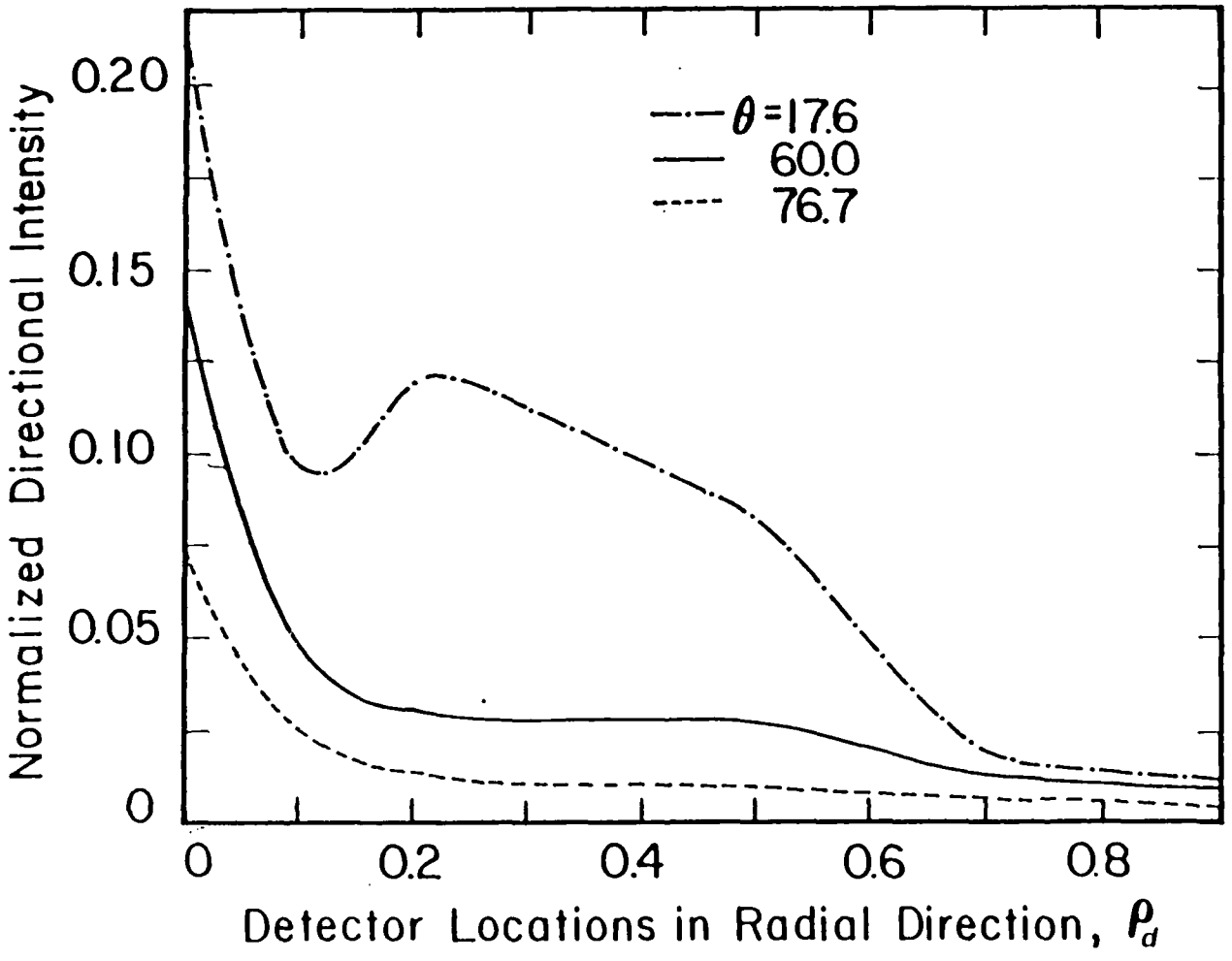

Fig. 5. Directional radiation intensity upon the cylinder head along the axis of the flame plume.

Appendix-VII. A New Integral Function for Radiation Modeling

INT. COMM. HEAT MASS TRANSFER 0735-1933/83/040329-05$03.00/0
Vol. 10, pp. 329-333, 1983 ©Pergamon Press Ltd. Printed in the United States

A USEFUL INTEGRAL FUNCTION AND ITS APPLICATION IN THERMAL RADIATION CALCULATIONS

S.L. Chang and K.T. Rhee
Department of Mechanical and Aerospace Engineering
Rutgers University
New Brunswick, New Jersey 08903

(Communicated by J.P. Hartnett and W.J. Minkowycz)

ABSTRACT

A new integral function has been discovered. The present function is found to be useful in computing the spectral emissivity of an isothermal volume containing either soot or gaseous species, or both. Examples of its application are discussed herein.

Introduction

In the application of the Planck formula for computing the energy radiated from an isothermal source, it is necessary to find the emissivity of the source. The emissivity, ϵ, is expressed in terms of its spectral emissivity, ϵ_λ, as follows

$$\epsilon = \int_0^\infty \epsilon_\lambda E_{b\lambda}(T)d\lambda/\sigma T^4 \tag{1}$$

where $E_{b\lambda}(T)$ is the Planck radiation function

$$E_{b\lambda}(T) = \frac{2\pi hc^2}{\lambda^5[\exp(hc/\lambda KT)-1]}$$

c, K and h, constants.

In the past, the determination of ϵ_λ has been made for various radiating sources by either experimental or theoretical means, e.g., for solid surface [1], gases [2,3], soot suspension in transparent gases [4,5], and combustion products [6,8]. For the computation of ϵ_λ of an isothermal volume with an optical length, L, containing radiating gases and/or soot, the following equation was employed [1]

$$\epsilon_\lambda = 1 - e^{-\kappa_\lambda L} \tag{2}$$

where κ_λ is the spectral volume absorption coefficient.

Regarding the emissivity by soot, ε_s, one may introduce eq.(2) into eq.(1) to find

$$\varepsilon_s = 1 - \int_0^\infty e^{-\kappa_\lambda L} E_{b\lambda}(T)d\lambda/\sigma T^4 \tag{3}$$

Although significant progress has been made on the determination of κ_λ [3-8], researchers have resorted to numerical methods in finding a solution of eq.(3) with additional assumptions. A common assumption made in the past [6,9] is the relationship, $\kappa_\lambda = \kappa_0 f_v/\lambda^d$, where, κ_0, the constant; f_v, the soot volume fraction; and d, the number chosen close to 1. This allowed one to obtain the final equation of emissivity including the hexagamma function

$$H(L) = -\int_0^\infty t^4 e^{-Lt}/(1-e^{-t})dt \tag{4}$$

where L represents the space variable. Consequently, the final equation was numerically solved, e.g., using Simpson's rule [6,9].

The New Integral Function and Applications

The present paper offers an exact solution of eq.(3). The spectral absorption coefficient of an isothermal volume containing soot that was found, by using the dispersion theory [4,5,7] and the Rayleigh-limit, was introduced into eq.(3). It was followed by a rearrangement to obtain the following tidy equation

$$\varepsilon_s = 1 - \frac{15}{\pi^4}\int_0^\infty e^{-ax}\frac{x^3}{e^x-1}\,dx \tag{5}$$

where

$$x = hc/\lambda KT\ ,$$

$$a = \frac{36\pi n^2 k}{[n^2-nk^2+2]+4n^4k^2} f_v L \frac{KT}{ch}\ ,\ \text{and}$$

$n+ink$, the complex refractive index.

An exact solution of eq.(5) has been discovered by the authors in a closed form by defining a more general expression of indefinite integration, F(m,a,x)

$$F(m,a,x) = -\int \frac{e^{-ax}x^m}{e^x-1}\,dx \quad (a \geq 0,\ m,\ \text{positive integer})$$

$$= -\int x^m e^{-(a+1)x}(1-e^{-x})^{-1}\,dx$$

$$= - \int x^m e^{-(a+1)x} \sum_{n=0}^{\infty} e^{-nx} \, dx$$

$$= - \sum_{n=1}^{\infty} \int e^{-(n+a)x} x^m \, dx \, .$$

By using the Heaviside linear differential inversion operator, D, the authors found

$$F(m,a,x) = - \sum_{n=1}^{\infty} \left\{ \frac{1}{D} \left[e^{-(n+a)x} x^m \right] \right\}$$

$$= - \sum_{n=1}^{\infty} \left\{ e^{-(n+a)x} \left[\frac{1}{D-(n+a)} \, x^m \right] \right\}$$

$$= \sum_{n=1}^{\infty} \left\{ \frac{e^{-(n+a)x}}{(n+a)} \left[\sum_{i=0}^{\infty} \left(\frac{D}{n+a} \right)^i x^m \right] \right\} .$$

Finally, the indefinite solution was obtained as

$$F(m,a,x) = \sum_{n=1}^{\infty} \left\{ e^{-(n+a)x} \sum_{i=0}^{m} \left[\frac{\Gamma(m+1)}{\Gamma(m-i+1)} \, (n+a)^{-i-1} \, x^{m-i} \right] \right\} \tag{6}$$

where Γ is the gamma function defined as

$$\Gamma(m+1) = m\Gamma(m) \text{ and } \Gamma(1) = 1.$$

The definite integral in eq.(5), therefore, becomes

$$\int_{x_1}^{x_2} \frac{e^{-ax} x^m}{e^x - 1} \, dx = F(m,a,x_1) - F(m,a,x_2). \tag{7}$$

In fact, the solution for the hexagamma function, eq.(4), can be readily found as

$$H(L) = - [F(4,L,0) - F(4,L,\infty)].$$

The new solution can be conveniently used even in the computation of the gas emissivity, that employs the use of the band model [2,6] to have

$$\epsilon_{g,i} = \frac{15}{\pi^4} \int_{\text{band } i} \frac{x^3}{e^x - 1} \, dx. \tag{8}$$

Although the solution of eq.(8) may be approximated by using tabulated values of Debye functions [10] or other approximations [11], the new solution, eq.(6), offers a more convenient and accurate result, i.e.,

$$\epsilon_{g,i} = \frac{15}{\pi^4} \left[F(3, 0, x_{u,i}) - F(3, 0, x_{l,i}) \right] .$$

Here, u and l indicate the upper and lower bound of the band.

In addition, it was found that the new solution enables the authors to construct an extensive three-dimensional model of radiation in diesel combustion as long as κ_λ in eq.(3) is known in terms of L.

Acknowledgment

The research has been supported by the U.S. Department of Transportation, contract no. DT-RS-S6-80C-00029 and the U.S. Army Research Office, contract no. DAAG29-83-K-0042.

Nomenclature

a	function defined by eq.(5)
c	speed of light
D	Heaviside linear differential inversion operator
d	number chosen close to 1
$E_{b\lambda}$	Planck's spectral black body radiation function
F	indifinite integral function defined by eq.(6)
f_v	soot volume fraction
g	subscript denoting gas
H	hexagamma function defined by eq.(4)
h	Planck's constant
K	Boltzmann's constant
L	space variable
m	positive integer
n+ink	complex refractive index
s	subscript denoting soot
T	temperature
t	variable used in eq.(4)
x	variable defined by eq.(5)
ε	emissivity
Γ	gamma function
σ	Stefan-Boltzman constant
κ_λ	spectral volume absorption coefficient
κ_g	constant

References

1. E.M. Sparrow and R.D. Cess, Radiation Heat Transfer, Augmented Edition, McGraw-Hill, New Yerk (1978)

2. D.K. Edwards and A. Balakrishnan, J. of Heat Mass Transfer 16, 525 (1973).

3. A. Balakrishnan and D.K. Edwards, J. of Heat Transfer 96, 37 (1974).

4. W.H. Dalzell and A.F. Sarofim, J. of Heat Transfer 9, 100 (1969).

5. S.C. Lee and C.L. Tien, 18th Symp. (Int.) on Combustion, The Combustion Institute, 1159 (1981).

6. W.L. Grosshandler and A.T. Modak, 18th Symp. (Int.) on Combustion, The Combustion Institute, 601 (1981).

7. S.L. Chang and K.T. Rhee, to be published in SAE.

8. S.L. Chang and K.T. Rhee, Eastern Section of The Combustion Institute, Technical Meeting, 18 (1982).

9. R.O. Buckius and C.L. Tien, Int. J. of Heat Mass Transfer 20, 93 (1977).

10. M. Abramowitz and I.A. Stegun, Handbook of Mathematical Function, National Bureau of Standards (1982).

11. M.A. Bramson, Optical Physics and Engineering, Plenum Press

Appendix-VIII. Blackbody Radiation Functions

INT. COMM. HEAT MASS TRANSFER 0735-1933/84 $3.00 + .00
Vol. 11, pp. 451-455, 1984 ©Pergamon Press Ltd. Printed in the United States

BLACKBODY RADIATION FUNCTIONS

S.L. Chang and K.T. Rhee
Department of Mechanical and Aerospace Engineering
Rutgers University
New Brunswick, New Jersey 08903

(Communicated by J.P. Hartnett and W.J. Minkowycz)

ABSTRACT

The present paper reports an exact solution of the fractional function of blackbody radiation. The new equation is expressed as

$$F_{o-\lambda T} = \int_o^{\lambda T} \frac{E_{b\lambda}(T)}{\sigma T^5}\, d(\lambda T) = \frac{15}{\pi^4} \sum_{n=1}^{\infty} \left[\frac{e^{-nx}}{n} \left(x^3 + \frac{3x^2}{n} + \frac{6x}{n^2} + \frac{6}{n^3}\right) \right]$$

where $x \equiv hC_o/\lambda kT$.

Introduction

It is often necessary to calculate the fraction of the total radiation emission from a blackbody that is emitted in a given wave length interval or band. This fraction, for a given temperature, T and the wavelength interval from o to λ, may be expressed as

$$F_{o-\lambda T} \equiv \frac{\int_o^{\lambda} E_{b\lambda}\, d\lambda}{\int_o^{\infty} E_{b\lambda}\, d\lambda} = \int_o^{\lambda T} \frac{E_{b\lambda}}{\sigma T^5}\, d(\lambda T) = f(\lambda T) \qquad (1)$$

where, $E_{b\lambda}$ is the Plank radiation function

$$E_{b\lambda} = \frac{2\pi h C^2}{\lambda^5[\exp(hC_o/\lambda kT)-1]}$$

C, C_o, k and h are constants.

Due to the unavailability of an exact solution of eq. (1) in the past and its frequent uses in radiation heat transfer computations, $F_{o-\lambda T}$ has been numerically obtained and its tabulated values for different λT are found in most of the fundamental heat transfer textbooks. In addition, for the computer solution of various types of radiation problems, Pivovonsky and Nagel [2] and Wiebelt [3] have presented polynomial curves fitted to the function, e.g.,

$$F_{o-\lambda T} = \frac{15}{\pi^4} \sum_{m=1,2,..} \frac{e^{-mv}}{m^4} (\{[(mv+3)mv+6]mv+6\}) \qquad \text{for } v \geq 1,$$

$$F_{o-\lambda T} = 1 - \frac{15}{\pi^4} v^3 (\frac{1}{3} - \frac{v}{8} + \frac{v^2}{60} - \frac{v^4}{5040} + \frac{v^6}{272160} - \frac{v^8}{13305600}) \qquad \text{for } v < 2$$

where $v \equiv \frac{C_2}{\lambda T}$ and $C_2 = 14388$ μm.K.

The New Blackbody Radiation Functions

The present paper reports an exact solution of eq. (1). The solution has been derived by a direct application of the new integral function that the authors have recently presented demonstrating its usefulness in thermal radiation calculations. The reported integral is expressed as [4]

$$\int_{x_1}^{x_2} \frac{e^{-ax} x^m}{e^x-1} dx = F(m,a,x_1) - F(m,a,x_2) \qquad (2)$$

where, $F(m,a,x) = \sum_{n=1}^{\infty} \{e^{-(n+a)x} \sum_{i=1}^{m} [\frac{\Gamma(m+1)}{\Gamma(m-i+1)} (n+a)^{-i-1} x^{m-i}]\}$,

$\Gamma(m+1) = m\Gamma(m)$ and $\Gamma(1) = 1$.

Since the speed of light, $C_o = \nu\lambda$, where ν is the wave number, eq. (1) can be rewritten as

$$F_{o-\lambda T} = \int_o^{\lambda T} \frac{E_{b\lambda}}{\sigma T^5}\, d(\lambda T) = 1 - \int_o^{\nu} \frac{E_{b\nu}}{\sigma T^4}\, d\nu \qquad (3)$$

where, $E_{b\nu} = \dfrac{2\pi h\nu^3}{C_o^2[\exp(\frac{h\nu}{kT})-1]}$.

And since $\int_o^{\infty} E_{b\nu}\, d\nu/\sigma T^4 = 1$, by using eq. (2) with m = 3 and a = 0, we find

$$\frac{\int_o^{\infty} E_{b\nu}\, d\nu}{\sigma T^4} = \frac{2\pi k^4}{\sigma C_o^2 h^3} \int_o^{x} \frac{x^3}{e^x-1}\, dx$$

$$= \frac{2\pi k^4}{\sigma C_o^2 h^3} \cdot 3! \cdot \sum_{n=1}^{\infty} \frac{1}{n^4}$$

$$= \frac{2\pi k^4}{\sigma C_o^2 h^3} \cdot 3! \cdot \frac{\pi^4}{90} = 1 \ .$$

Hence, $$\sigma = \frac{2}{15} \frac{\pi^5 k^4}{C_o^2 h^3} \ . \qquad (4)$$

The integral in the righthand side of eq. (3), therefore, can be expressed by using eqs. (2) and (4), with $x \equiv hC_o/\lambda kT$, as

$$\int_o^{\nu} \frac{E_{b\nu}}{\sigma T^4}\, d\nu = \frac{15}{\pi^4} \int_o^{x} \frac{x^3}{e^x-1}\, dx$$

$$= 1 - \frac{15}{\pi^4} \sum_{n=1}^{\infty} \left[\frac{e^{-nx}}{n} \left(x^3 + \frac{3x^2}{n} + \frac{6x}{n^2} + \frac{6}{n^3}\right) \right] \ . \qquad (5)$$

Finally, from the relationships in eqs. (3) and (5), we find the exact form of the fractional function of the blackbody radiation as

$$F_{o-\lambda T} = \frac{15}{\pi^4} \sum_{n=1}^{\infty} \left[\frac{e^{-nx}}{n} \left(x^3 + \frac{3x^2}{n} + \frac{6x}{n^2} + \frac{6}{n^3}\right) \right] \quad (6)$$

where, $x = hC_o/\lambda kT$.

Figure 1 demonstrates the convergence of the new blackbody functions with n.

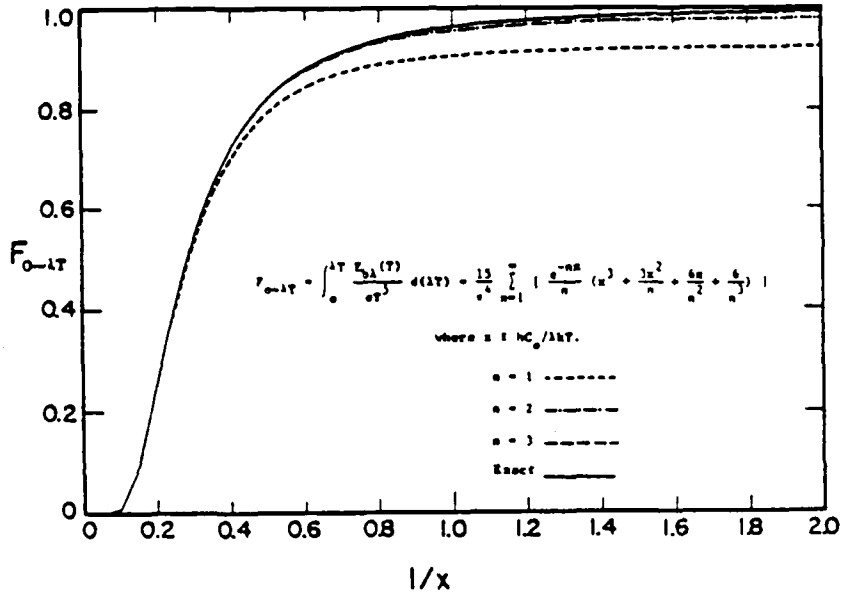

Fig. 1 Blackbody Radiation Functions

Acknowledgement

The present research has been supported by the U.S. Army Research Office, Contract no. DAAG29-83-K-0042.

Nomenclature

a	function used in eq. (2)
C_o	speed of light
$E_{b\lambda}$	Plank's spectral blackbody radiation function
F	integral function defined by eq. (2)

$F_{o-\lambda T}$	fractional function of the blackbody radiation
h	Plank's constant
k	Boltzman's constant
m	positive integer
n	variable used in eq. (5)
T	temperature
x	variable defined in eq. (6)
Γ	gamma function
σ	Stefan-Boltzman constant
λ	wavelength
υ	wavenumber

References

1. Dunkle, R.V., Trans. ASME, 76, 549 (1954)

2. Pivovonsky, M. and Nagel, M.R., Tables of Blackbody Radiation Functions, The Macmillan Co., N.Y. (1961)

3. Wiebelt, J.A., Engineering Radiation Heat Transfer, Holt, Rinehart and Winston, Inc., N.Y. (1966)

4. Chang, S-L. and Rhee, K.T., Int. Com. Heat Mass Transfer, 10, 329 (1983)

Appendix-X. Adiabatic Flame Temperature Computation (I)

Combustion Science and Technology, 1983, Vol. 35, pp. 203–206
0010-2202/83/3504-0203$18.50/0

SHORT COMMUNICATION

Adiabatic Flame Temperature Estimates of Lean Fuel/Air Mixtures

S. L. CHANG and K. T. RHEE *Department of Mechanical and Aerospace Engineering, Rutgers University, The State University of New Jersey, New Brunswick, NJ 08903*

(*Received May 6, 1983, in final form May 20, 1983*)

Abstract—This paper reports new formulas of adiabatic flame temperature. They are functionally expressed in terms of fuel/air ratio, reaction pressure, and the number of carbon atoms in the individual fuel. Among the fuels presently considered for the formulas are members of paraffin, aromatic and olefin families, acetylene, alcohols, and hydrogen.

INTRODUCTION

The combustion reactions in many air-breathing engines take place at high temperatures. When the energy released in such reactions is completely used to heat the combustion products, the product temperature may attain the highest level. At such a temperature, however, the combustion products dissociate into fractions of molecule, *e.g.*, atom and free radicals, by up to several percentage points. Since the dissociation reaction is highly endothermic, the processes substantially lower the flame temperature, consequently achieving the equilibrium adiabatic flame temperature, T_a.

NASA-Lewis pioneered the computation of T_a and thermodynamic equilibrium composition of combustion products of various fuels (Gordon and McBride, 1971). Among the same computational approaches taken by others for the equilibrium data of gaseous hydrocarbon–air systems are those for modeling the combustion processes in internal combustion engines (Olikara and Borman, 1975) and for computing radiation heat transfer in diesel combustion (Chang and Rhee, 1983). In computing the equilibrium data of a specific fuel–air system, eleven gaseous species were considered beside the fuel, including seven dissociation reactions with known individual equilibrium constants, a stoichiometric equation and an energy equation. Due to the highly nonlinear nature of the problem, the solution was numerically found by using Newton's iteration method (Gordon and McBride, 1971; Olikara and Borman, 1975). Although the authors employed a new numerical method for the solution that substantially reduced the computation time, one of the more time-consuming steps for a recent report (Chang and Rhee, 1983) was still that for finding T_a at each nodal point with a burned fuel/air ratio in the combustion volume. In order to simplify the computational process of T_a in their more involved on-going computational model of diesel combustion, the authors have developed simple formulas of T_a for various fuel–air systems.

NEW FORMULAS OF ADIABATIC FLAME TEMPERATURE

This paper reports the new formulas of T_a for an individual family of fuels expressed in terms of the fuel air ratio and the reaction pressure. The formulas were determined by using the least-squares method for computed results obtained from the above-mentioned method with variation of fuel (gas state), fuel air ratio, and pressure. Note that the present formulas may not be useful for those beyond the lean flammability because the flame does not virtually exist in the mixtures, and that the formulas for those richer than stoichiometric are not considered due to the unavailability of the equilibrium dissociation equations for such mixtures. The new formula of T_a of a fuel–air system leaner than stoichiometric under reaction pressure, P, is expressed as,

$$T_a = a[1 - b \cdot \ln\phi - c \cdot (\ln\phi)^2]\ (^\circ\mathrm{K})$$

where $a = a_1 + a_2 \cdot \ln(P/P_0)$

$b = b_1 - b_2 \cdot \ln(P/P_0)$

$c = c_1 + c_2 \cdot \ln(P/P_0)$

$$\phi = \frac{\text{Fuel volume fraction}}{(\text{Fuel volume fraction})_{\text{stoich}}}$$

$P_0 = 1$ atm

$a_1, b_1, \ldots$ are coefficients of each family of fuels given in the following.

1) Paraffin family, C_nH_{2n+2} $(1 \leqslant n \leqslant 16)$

$$a_1 = 2295.0 + 9.5 \ln(n - 0.99)$$
$$a_2 = 13.2 + 0.7 \ln(n - 0.97)$$
$$b_1 = 0.544 - 0.0019 \ln(n - 0.99)$$
$$b_2 = 0.018 + 0.0009 \ln(n - 0.96)$$
$$c_1 = 0.070 - 0.003 \ln(n - 0.98)$$
$$c_2 = 0.0169 + 0.0008 \ln(n - 0.97)$$

2) Olefin family, C_nH_{2n} $(2 \leqslant n \leqslant 16)$

$$a_1 = 2377.0 - 17.9 \ln(n - 1.85)$$
$$a_2 = 19.9 - 1.4 \ln(n - 1.89)$$
$$b_1 = 0.512 + 0.0085 \ln(n - 1.89)$$
$$b_2 = 0.025 - 0.0014 \ln(n - 1.86)$$
$$c_1 = 0.035 + 0.0083 \ln(n - 1.89)$$
$$c_2 = 0.023 - 0.0013 \ln(n - 1.86)$$

3) Aromatic family, C_nH_{2n-6} $(6 \leqslant n \leqslant 22)$

$$a_1 = 2378.0 - 15.3 \ln(n - 5.36)$$
$$a_2 = 21.0 - 1.6 \ln(n - 5.29)$$
$$b_1 = 0.518 + 0.006 \ln(n - 5.51)$$
$$b_2 = 0.027 - 0.002 \ln(n - 5.24)$$
$$c_1 = 0.034 + 0.008 \ln(n - 5.38)$$
$$c_2 = 0.025 - 0.0016 \ln(n - 5.27)$$

4) Alcohol family, $C_nH_{2n+1}OH$ $(2 \leq n \leq 8)$

$$a_1 = 2153.5 + 60.2 \ln(n - 1.51)$$
$$a_2 = -0.5 + 5.2 \ln(n + 0.11)$$
$$b_1 = 0.641 - 0.030 \ln(n + 3.4)$$
$$b_2 = 0.0004 + 0.0066 \ln(n + 0.02)$$
$$c_1 = 0.193 - 0.041 \ln(n + 3.5)$$
$$c_2 = -0.0002 + 0.0066 \ln(n + 0.09)$$

5) Hydrogen, H_2

$a_1 = 2412.2$
$a_2 = 17.9$
$b_1 = 0.473$
$b_2 = 0.021$
$c_1 = 0.0217$
$c_2 = 0.0191$

6) Acetylene, C_2H_2

$a_1 = 2562.9$
$a_2 = 42.3$
$b_1 = 0.390$
$b_2 = 0.0426$
$c_1 = -0.0819$
$c_2 = 0.0379$

A comparison of computed T_a and approximated T_a by the present formula of paraffin–air systems at reaction pressure of 100 atm can be seen in Figure 1. In almost all the cases with the formula, the discrepancy between the two sources of value was less than one percent. The formula enables one to find the adiabatic flame temperature of a wide range of fuels, fuel air ratio, and reaction pressures even by using a simple pocket calculator.

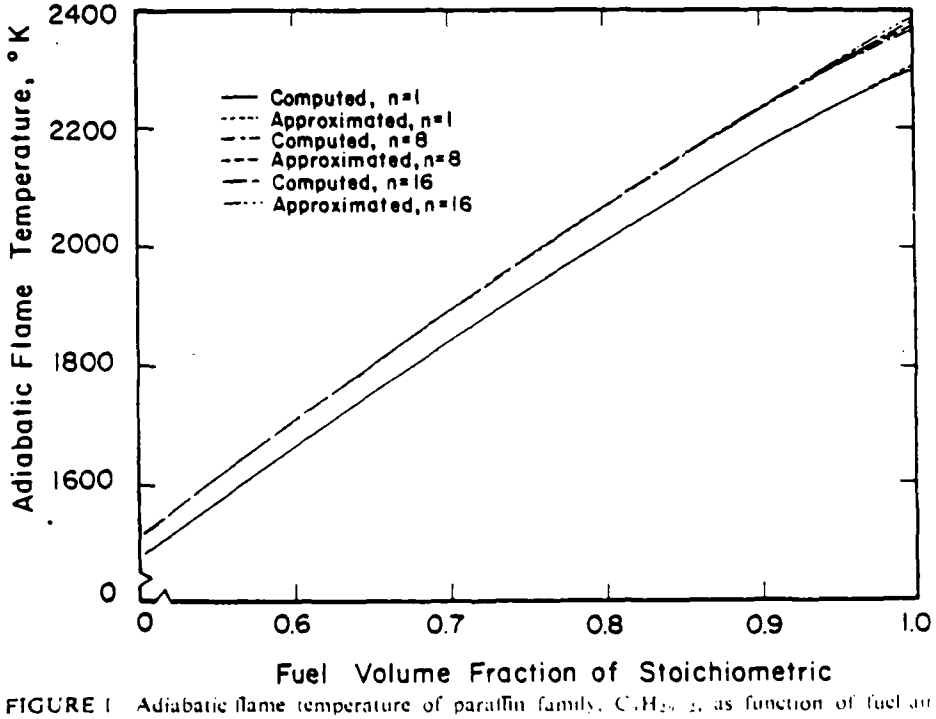

FIGURE 1 Adiabatic flame temperature of paraffin family, C_nH_{2n+2}, as function of fuel air ratio and number of carbon atoms of fuel for reaction pressure of 100 atm.

ACKNOWLEDGEMENTS

This research has been sponsored by the U.S. Department of Transportation, Contract No. DTRS 5680-C-00029 and U.S. Army Research Office, Contract No. DAAG 29-83-K-0042.

REFERENCES

Chang, S. L., and Rhee, K. T. (1983). Computation of Radiation Heat Transfer in Diesel Combustion, to be presented at SAE International Off-Highway Meeting in September, 1983.

Gordon, S., and McBride, B. J. (1971). Complex Chemical Equilibrium Calculation, NASA SP-273.

Olikara, C., and Borman, G. L. (1975). A Computer Program for Calculating Properties of Equilibrium Combustion Products with Some Application to I.C. Engines, SAE Paper 750468.

4-25-84

Combustion Science and Technology, 1984, Vol. 55, pp. 555–555
0010-2202/84/5555-5555$18.50/0

Erratum

(*Received April 25, 1984*)

Chang, S. L., and Rhee, K. T. (1983). Adiabatic flame temperature estimates of lean fuel-air mixtures. Short Communication, *Combustion Science and Technology* 35, 203.

In our recent paper we reported new formulas for adiabatic flame temperature (AFT) expressed in terms of the fuel-air ratio (entering at 298 K), the reaction pressure, and the number of carbon atoms in the individual fuel. Recently, Gülder (1) has performed a close study of the formulas, which lead us to discover a numerical error in copying the acetylene heat of formulation in the computer code. In addition, there was an editorial error in our computer program of the AFT for alcohol-air mixtures. The correct formulas for both cases are given below. In the meantime, the authors have completed additional work (2) to find new improved formulas of the AFT similar to the previous ones with inclusion of the initial temperature as a variable.

Acetylene, C_2H_2	Alcohol family $C_nH_{2n}OH$ $(2 \le n \le 8)$
$a_1 = 2573.1$	$a_1 = 2276.8 + 12.6 \ln(n + 1.51)$
$a_2 = 44.5$	$a_2 = 12.65 + 1.147 \ln(n + 0.11)$
$b_1 = 0.374$	$b_1 = 0.4677 + 0.0261 \ln(n + 3.4)$
$b_2 = 0.439$	$b_2 = 0.0173 + 0.0013 \ln(n + 0.02)$
$c_1 = -0.0948$	$c_1 = -0.0272 + 0.0122 \ln(n + 3.5)$
$c_2 = -0.0386$	$c_2 = 0.0163 + 0.0013 \ln(n + 0.09)$

REFERENCES

1. Gülder, Ö. L., private communication.
2. Chang, S. L., and Rhee, K. T., to be published.

Appendix-XI. Adiabatic Flame Temperature Computation (II)

Combust. Sci. and Tech., 1985, Vol. 44, pp. 75–88
0010-2202/85/4402-0075 $18.50/0

Empirical Equations For Adiabatic Flame Temperatures For Some Fuel–Air Combustion Systems

K. T. RHEE and S. L. CHANG *Department of Mechanical and Aerospace Engineering, Rutgers, The State University of New Jersey, New Brunswick, New Jersey 08903*

(*Received May 2, 1984; in final form June 6, 1984*)

Abstract—A new simple formula for calculating the adiabatic flame temperature of fuel air mixtures has been developed. The formula is usable in a wide range of both fuel and reaction variables. Among the fuels considered for the formula are members of the paraffin, aromatic, olefin and alcohol families, and hydrogen and acetylene. The formula is functionally expressed in terms of the fuel air ratio, the reaction pressure, the initial mixture temperature and the number of carbon atoms in the individual fuel. By using the formula, the adiabatic flame temperature for a designated fuel and reaction condition can be found within an accuracy of one percent.

INTRODUCTION

The computation of the equilibrium adiabatic flame temperature is often performed in the analysis of various airbreathing combustion devices. Due to its complexity, however, researchers have resorted to computer operation for its computation in the past (Gordon and McBride, 1971; Olikara and Borman, 1975; Chang and Rhee, 1983). The computation for a typical fuel–air system considers eleven gaseous species besides fuel, in simultaneously solving the following equations: seven dissociation reaction equations with the respective temperature-dependent equilibrium constants; a stoichiometric equation and an energy equation.

In spite of a considerable reduction in computer time by the use of a new numerical method for the solution, one of the more time-consuming steps for a recent paper (Chang and Rhee, 1983) was still that for finding the adiabatic flame temperature in each nodal point with a burned fuel/air ratio in the combustion volume. In order to facilitate its involved computation, the authors recently introduced simple formulas for adiabatic flame temperature estimates (Chang and Rhee, 1983). They are expressed in terms of fuel air ratio (entering at 298 K), reaction pressure, and the number of carbon atoms in the individual fuels. For a similar goal, graphs for adiabatic flame temperature of hydrocarbon fuel–air mixtures were introduced by others (Glassman and Clark, 1983). As a continuation of the previous endeavor, the authors have developed a new improved formula for adiabatic flame temperature which additionally includes the initial reactant temperature as a variable and generate more accurate results. In addition, as an exploratory procedure in the development of more accurate and consistent formulas of adiabatic flame temperature, factors controlling the temperature in the First Law relation were reviewed. Some findings seem to be worth reporting, along with the newly developed formula.

Adiabatic Flame Temperature of Fuel–Air Combustion

It is generally expected that the energy released in a combustion reaction is best represented by the adiabatic flame temperature (Gaydon and Wolfhard, 1970). In

the calculation of the heat of reaction, as a convenient and logical procedure, the heat of formation at the standard state, ΔH°_{298}, of chemical substances are used. To a good approximation, in many cases, it is possible to determine ΔH°_{298} of a molecule by adding the energy of bonds forming the molecule. The heat of reaction (or heat of combustion), Q_p, of a fuel may be determined by using ΔH°_{298} of substances involved in the reaction as follows

$$-Q_p = \sum_{i\text{-products}} \nu_i(\Delta H^\circ_{298})_i - \sum_{j\text{-reactants}} \nu_j(\Delta H^\circ_{298})_j. \tag{1}$$

For a closer look at the above relationship of common fuels, the molar quantities of ΔH°_{298} and Q_p at a reference temperature of 298°K are plotted against the number of carbon atoms, N_c, in individual fuels as shown in Figures 1 and 2, respectively. A brief look at the Figures and Eq. (1) shows, although not new, that ΔH°_{298} of fuel is much smaller than the corresponding Q_p in magnitude and that for the respective fuel family there is no mutually comparable trend between ΔH°_{298}–N_c and Q_p–N_c relationships. This indicates that ΔH°_{298} for fuels may not play a great role in determining the adiabatic flame temperature, T_a. For the purpose of comparison

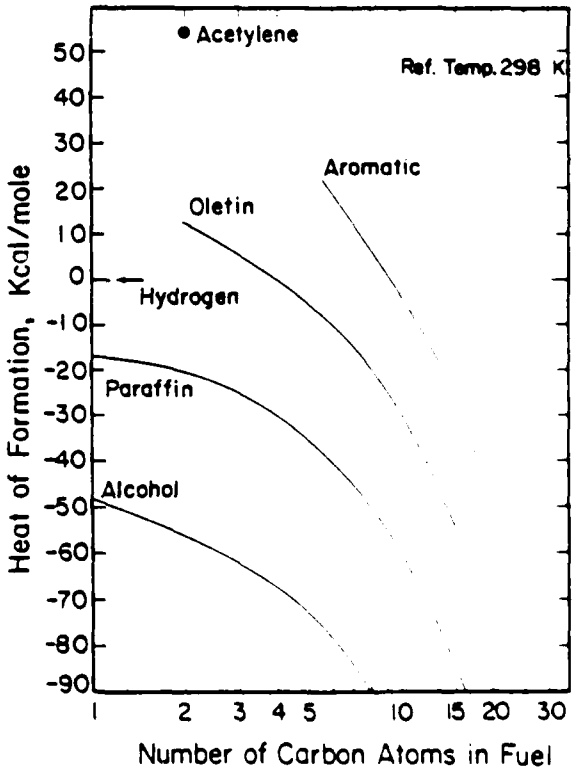

FIGURE 1 Molar heat of formation of fuels vs. number of carbon atoms in fuel

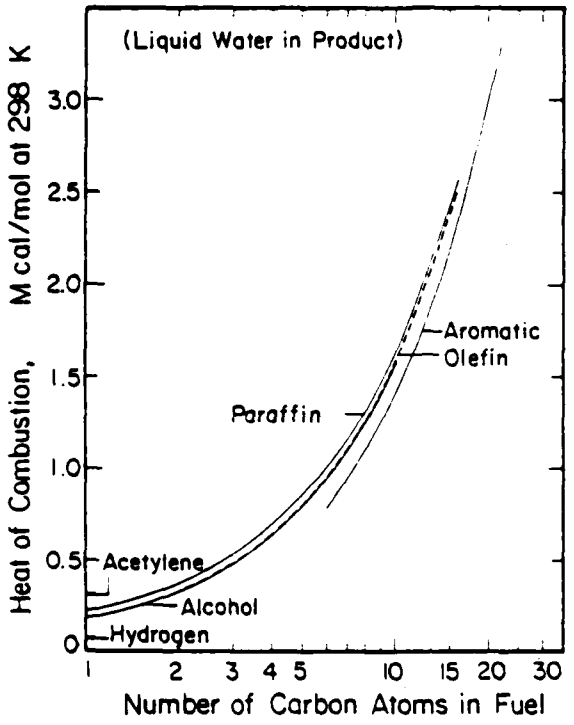

FIGURE 2 Molar heat of combustion of fuel–air vs. number of carbon atoms in fuel.

and then finding the possibility of using Q_p as a parameter in the new formulas of T_f, the relationship of T_a to V_e is reviewed for fuel–air mixtures (initially at 298 K and reacting at 1 atm) at a fuel volume fraction of stoichiometric, $\phi = 1$ (in addition, for alcohol, $\phi = 0.75$), as shown in Figure 3. Putting aside the mutual irrespectivity between the ΔH_{298}–V_e and T_a–V_e relationships, the similar irrespectivity between the Q_p–V_e and T_a–V_e relationship could be surprising. But one soon finds that Q_p may not be a proper indicator for T_a by recognizing that Q_p is used up, in a highly nonlinear manner, in heating the products and the endothermic dissociation reaction as

$$\sum_{i\text{-products}} [(H^\circ_{T_a} - H^\circ_{298}) + \Delta H^\circ_{298}]_i - \sum_{j\text{-reactants}} \nu_j [(H^\circ_{T_i} - H^\circ_{298}) + \Delta H^\circ_{298}]_j = -Q_p, \qquad (2)$$

where T_i indicates the initial temperature of reactants, ν is the number of moles of each species, and Q_p becomes zero in an equilibrium. Further, since the analysis of the open thermodynamic systems is more conveniently performed by using mass thermodynamic quantities than molar basis, the mass quantities of ΔH_{298} and Q_p may be worth investigating as shown in Figures 4 and 5. Unlike the hitherto-held notion that ΔH_{298} may not well represent T_a, it is rather unexpected to find a mutual similarity in the trend existing between the ΔH_{298} (mass)–V_e and T_a–V_e relationships except for the alcohol fuel family; no such trend exists between the Q_p (mass)–V_e and T_a–V_e relationships. Although there is no explanation that can be given for the

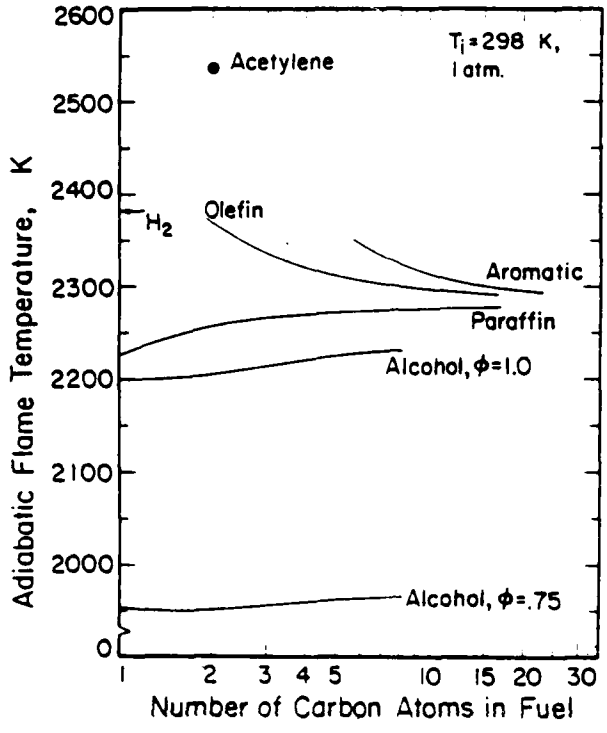

FIGURE 3 Adiabatic flame temperature of fuel air mixture with ϕ = 1 (entering at 298 K and reacting at 1 atm) vs. number of carbon atoms in fuel.

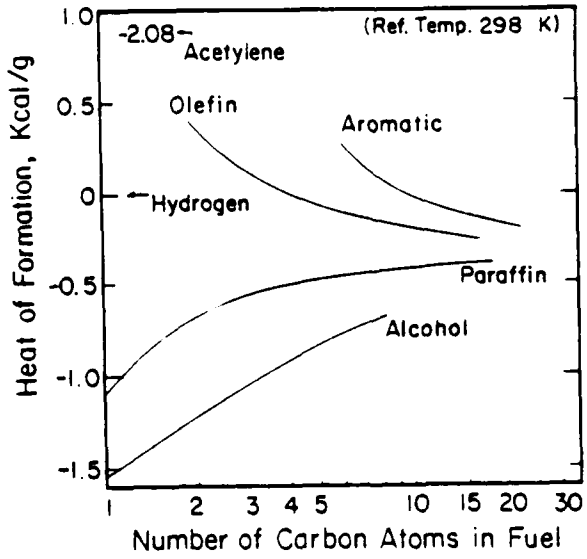

FIGURE 4 Mass heat of formation of fuels vs. number of atoms in fuel

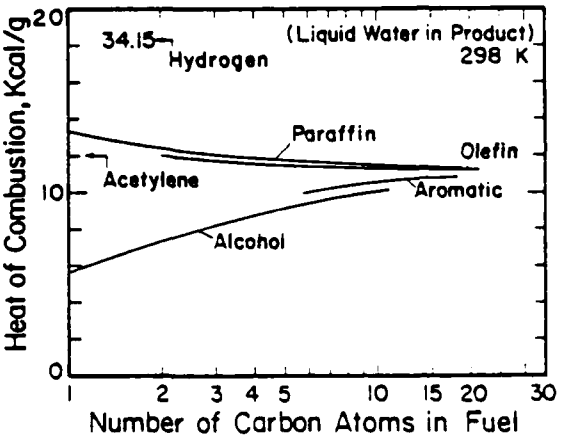

FIGURE 5 Mass heat of combustion of fuels vs. number of carbon atoms in fuel.

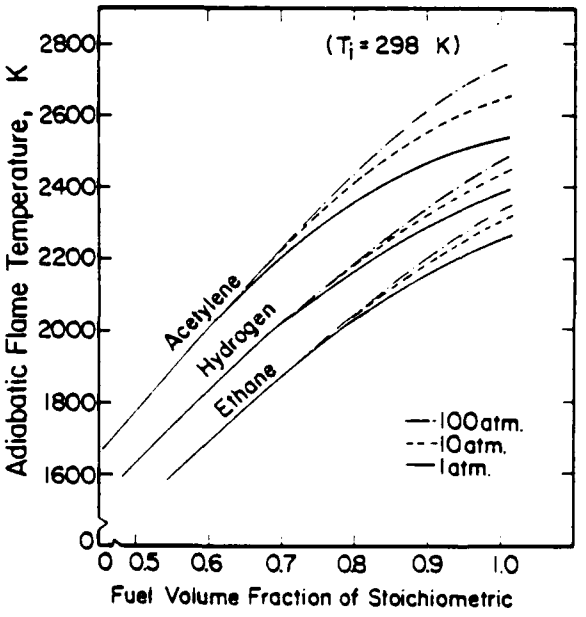

FIGURE 6 Effect of fuel/air ratio and reaction pressure on adiabatic flame temperature.

unexpected mutual similarity, this trend seems to support choosing ΔH_{298} as a parameter in the construction of T_a-graphs introduced by Glassman and Clark (1983). In search of a proper formula of T_a, however, the close relationship of ΔH_{298} to T_a found in the present study is not used due to the inability to include the alcohol family.

In parallel with the above-mentioned approach, an extensive parametric study of T_a has been carried out for the following major variables by the numerical method for T_a mentioned earlier: the fuel/air ratio; the reaction pressure and the initial temperature of reactants; and the number of carbon atoms in individual fuels. Some of the results are summarized in the following forms: adiabatic flame temperature vs. fuel volume fraction of stoichiometric at varied reaction pressure (Figure 6); adiabatic flame temperature vs. initial mixture temperature for representative fuels at reaction pressure of 1 atm (Figure 7); and adiabatic flame temperature vs. reaction pressure with varied initial mixture temperature (Figure 8).

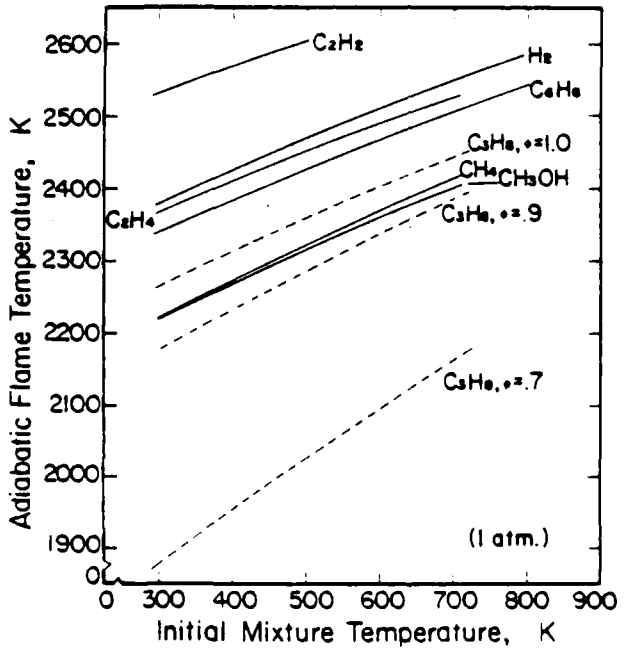

FIGURE 7 Adiabatic flame temperature of various fuels (with $\phi = 1.0$ reacting at 1 atm) vs. initial mixture temperature.

Among the important characteristics of the results, already well known, are the following.

1) The higher the reaction pressure, the higher the adiabatic flame temperature. This is due to the more reverse of dissociation reactions (Chang and Rhee 1983) at

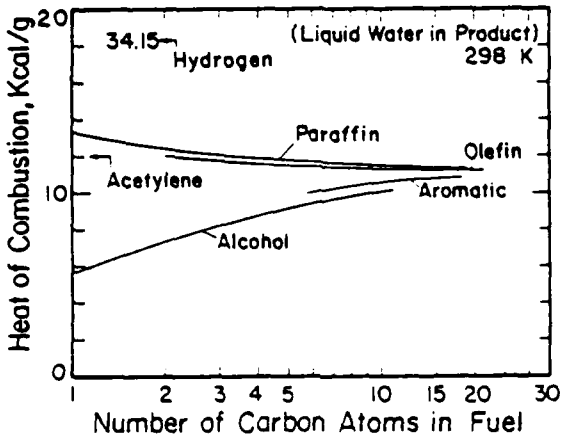

FIGURE 5 Mass heat of combustion of fuels vs. number of carbon atoms in fuel.

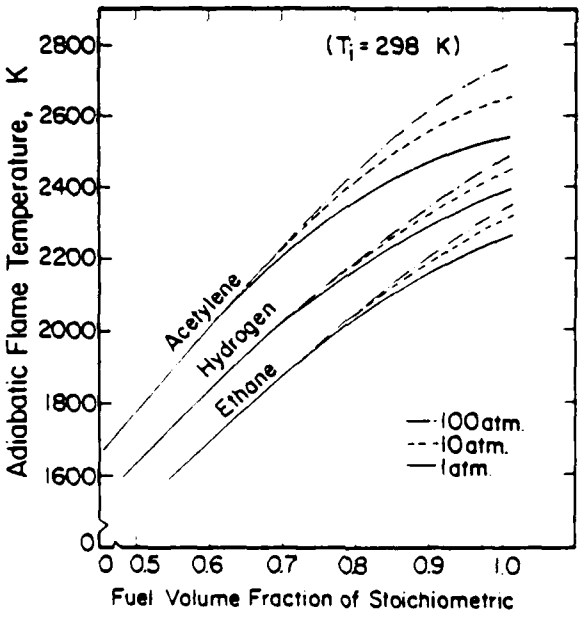

FIGURE 6 Effect of fuel air ratio and reaction pressure on adiabatic flame temperature

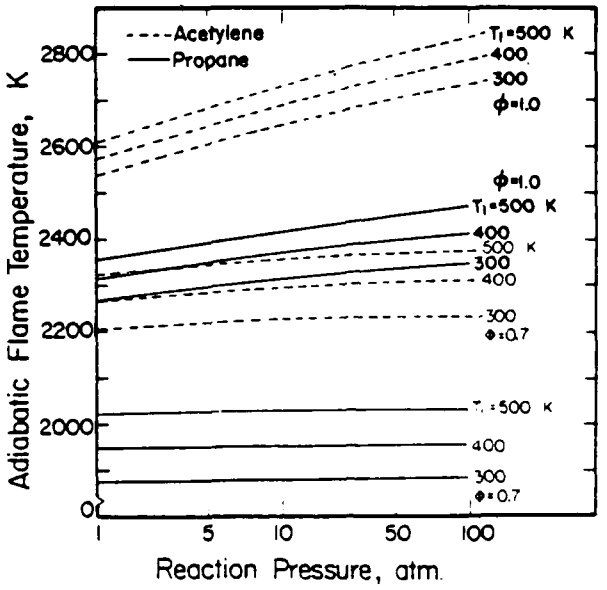

FIGURE 8 Effect of reaction pressure and initial mixture temperature on adiabatic flame temperature.

higher reaction pressure, in particular,

$$CO_2 \rightarrow CO + \tfrac{1}{2}O_2$$
$$H_2O \rightarrow H_2 + \tfrac{1}{2}O_2$$
$$\tfrac{1}{2}H_2 \rightarrow H$$
$$\tfrac{1}{2}O_2 \rightarrow O, \quad \text{and}$$
$$\tfrac{1}{2}N_2 \rightarrow N.$$

2) The higher the adiabatic flame temperature of the mixture, the greater the effect of reaction pressure on the temperature. The effect is greater because of the greater tendency of dissociation at higher flame temperature.

3) An increment in the initial mixture temperature by ΔT is reflected in the adiabatic flame temperature by an amount much smaller than ΔT; this tendency is greater in higher initial mixture temperature and for mixtures with higher flame temperature. This is explained by the greater tendency of dissociation at higher flame temperatures, and the change in heat capacity with temperature and composition.

A careful review of results (refer to Figures 3, 7 and 8) revealed that the adiabatic flame temperature could be expressed in terms of the above-mentioned major variables by using the least-squares fit method, as similarly attempted by the present authors (Chang and Rhee, 1983). The main task for this was to identify its equational form.

New Formulas for Adiabatic Flame Temperature

The search for new formulas for T_a of fuel-air systems was made in such a way as to meet the following requirements: (1) a simple form of equation, (2) convenient

and easy to use; (3) accuracy within one percent; (4) applicable within the flammability limit of individual fuels but leaner than stoichiometric; (5) applicable in the range of initial mixture temperature from 298°K to the self-ignition temperature of individual fuels, (6) applicable, at least, in the range of reaction pressure from 1 atm to 100 atm, and (7) mixtures in gas state.

Upon performing a considerable amount of computational work in correlating T_a to the previously described main variables, largely through the trial and error approach, the authors have found the following equational form which offers a considerable flexibility in use and to meet most of the abovementioned requirements. The new formula of T_a is

$$T_a = A_1[1 + A_2 \ln \phi + A_3(\ln \phi)^2], \tag{3}$$

where

$$A_i = A_{i1} + A_{i2} \ln P + A_{i3}(\ln P)^2 \quad (i = 1, 2, 3) \tag{4}$$

$$A_{ij} = A_{ij1} + A_{ij2} \ln T + A_{ij3}(\ln T)^2 \quad (j = 1, 2, 3) \tag{5}$$

$$A_{ijk} = A_{ijk1} + A_{ijk2} \ln N_c + A_{ijk3}(\ln N_c)^2 \quad (k = 1, 2, 3) \tag{6}$$

T_a, the estimated adiabatic flame temperature (°K)
ϕ, the burned fuel volume fraction of stoichiometric
P, the nondimensional form of reaction pressure (p) defined as $P = p$/1 atm, and
T, the nondimensional form of initial mixture temperature (T_i) defined as $T = T_i/298°K$.

The correlation coefficients in the above equations were determined for the following cases to offer more convenience in use: (1) for individual fuel families ($0.5 \le \phi \le 1.0$); (2) for hydrogen with fuel/air ratio ranges, $0.14 \le \phi < 0.6$ and $0.6 \le \phi \le 1.0$, respectively; (3) for acetylene with fuel/air ratio ranges, $0.31 \le \phi < 0.6$ and $0.6 \le \phi \le 1.0$, respectively, and (4) for individual fuels with respective fuel/air ratio ranging from lean flammability to stoichiometric. For the sake of convenience one could use one of the coefficient matrices for individual fuel families in Table I instead of one for individual fuels in Table II, or vice versa. Note that if the coefficient matrix in Table II is used, Eq. (6), which implements the variation in the number of carbon atoms in the fuel, is not required in the computation, making it simpler. In addition, the coefficients for lean mixtures of hydrogen and acetylene fuels are zero since there is almost no effect of the reaction pressure on T_a for the cases.

Use of New Formulas for T_a Estimate

Complex as it may look at first glance, the use of the coefficient matrix for computing T_a is relatively simple on a pocket calculator as well as in computer coding as a part of combustion modeling. In order to familiarize oneself with its use, the typical combinations of fuel/air ratio and reaction condition are summarized in Table III by listing the coefficients needed for each case.

It is expected that the use of the present formulas for the T_a estimate will help facilitate various analyses of air breathing combustion systems. It will be useful in

TABLE 4
Coefficients for individual fuel family, A_{ijkl}

	kl	A_{1111}	A_{2111}	A_{1211}	A_{1121}	A_{2211}	A_{2121}	A_{1221}	A_{2221}	A_{2222}
Paraffin	11	2247.78	0.5052	0.0063	20.8399	0.0363	0.0431	1.6977	−0.00284	−0.00327
(C_nH_{2n+2})	21	144.242	0.1564	0.1246	13.4898	0.0261	0.0307	1.2510	−0.00194	−0.00199
	31	86.050	−0.0944	0.0222	12.6555	0.0141	−0.0325	0.2995	0.00313	0.00495
	12	43.946	0.0209	0.0322	5.0616	0.0067	0.0072	−0.2937	−0.00027	−0.00018
	22	−12.414	0.0127	0.0141	1.4937	−0.0012	0.0039	0.0675	0.00058	0.00100
	32	−3.6738	0.0141	0.0242	−2.4395	−0.0062	−0.0075	0.3309	0.00038	0.00025
	13	−9.4911	0.0045	0.0067	−1.0551	0.0014	−0.0015	0.0640	0.00006	0.00005
	23	2.5880	0.0026	0.0029	−0.3276	0.0002	0.0008	−0.0120	−0.00012	−0.00021
	33	0.8213	0.0030	0.0050	0.5002	0.0013	0.0016	−0.0690	−0.00008	−0.00005
Olefin	11	2445.33	0.3755	−0.1522	43.8478	0.0583	0.0616	−2.6837	−0.00291	−0.00242
(C_nH_{2n})	21	95.551	0.1696	−0.1227	14.6219	0.0077	0.0034	0.4020	0.00139	0.00326
	31	78.176	0.0226	0.0788	4.6301	−0.0280	0.0131	1.0069	0.00275	0.00310
	12	−98.360	0.0731	0.0810	−11.4967	0.0087	0.0053	0.4011	−0.00025	−0.00086
	22	22.026	0.0055	0.0186	0.8774	0.0125	0.0212	−0.5547	−0.00184	−0.00279
	32	2.0714	−0.0366	−0.0465	3.1225	0.0030	−0.0011	−0.1465	0.00075	0.00172
	13	18.429	0.0139	0.0153	2.1809	0.0016	0.0008	0.0706	0.00006	0.00018
	23	4.0817	0.0015	0.0041	0.2094	−0.0025	0.0041	0.1073	0.00035	0.00053
	33	0.3300	0.0068	0.0085	0.5750	0.0005	0.0004	0.0239	0.00016	−0.00034
Aromatic	11	2561.86	0.3023	0.2732	60.8042	0.0764	0.0780	3.1974	−0.00267	−0.00144
(C_nH_{2n-6})	21	58.079	0.1954	0.1412	13.5457	−0.0085	−0.0325	0.6227	0.00442	0.00799
	31	77.557	0.0295	0.1620	−2.0899	−0.0405	−0.0542	1.4531	0.00217	0.00132
	12	156.39	0.1093	0.1448	20.1755	−0.0183	0.0143	0.6486	0.00040	−0.00137
	22	41.553	0.0094	0.0071	1.7489	0.0214	0.0371	1.1526	−0.00351	−0.00541
	32	1.6917	0.0642	0.0911	6.5573	0.0098	0.0049	0.3363	0.00097	0.00274
	13	24.927	0.0178	0.0232	3.2207	0.0028	0.0021	−0.0988	0.00008	0.00024
	23	6.5429	0.0010	0.0018	−0.3584	−0.0036	−0.0062	0.1934	0.00057	0.00088
	33	−0.1716	0.0103	0.0144	1.0012	0.0014	0.0005	0.0420	−0.00018	−0.00048
Alcohol	11	2238.05	0.4275	−0.0500	22.7574	0.0381	0.0436	−1.8038	−0.00285	−0.00311
(ROH)	21	136.127	0.1550	0.1222	14.1682	0.0246	0.0264	1.2266	−0.00153	−0.00121
	31	84.343	0.0740	0.0060	10.9700	−0.0195	−0.0383	0.5128	0.00345	0.00507
	12	30.390	0.0510	0.0237	1.7181	0.0033	0.0048	−0.1039	−0.00019	−0.00028
	22	−1.887	−0.0125	0.0150	0.6029	0.0011	0.0018	0.0127	0.00002	0.00001
	32	1.4652	0.0087	0.0070	0.4058	0.0003	0.0014	0.0872	0.00009	0.00019
	13	3.2582	0.0136	0.0077	0.0350	0.0003	0.0007	0.0057	0.00004	0.00007
	23	0.3686	0.0025	0.0032	0.0918	0.0005	0.0009	0.0077	0.00004	0.00007
	33	0.2052	0.0033	0.0033	0.0380	−0.0002	0.0	0.0061	−0.00002	0.00005

TABLE II
Coefficients for individual fuel, A_{ijk}

	k	A_{11k}	A_{21k}	A_{111k}	A_{112k}	A_{221k}	A_{122k}	A_{113k}	A_{213k}	A_{313k}
Hydrogen	1	2471.50	0.5562	0.1035						
$0.13 \le \phi \le 0.6$	2	177.180	−0.0596	−0.0093	0	0	0	0	0	0
	3	152.454	−0.0457	−0.0106						
Hydrogen	1	2392.94	0.3889	0.1443	32.0662	0.0521	0.0678	−2.4776	−0.00365	−0.00424
$0.6 \le \phi \le 1.0$	2	126.287	−0.1453	−0.1174	14.5362	0.0170	0.0122	−1.1117	−0.00040	0.00124
	3	80.335	−0.0493	0.0449	11.8463	0.0219	−0.0484	0.3428	0.00339	0.00561
Acetylene	1	2806.75	0.6271	0.1392						
$0.31 \le \phi \le 0.6$	2	185.066	−0.0501	−0.0072	0	0	0	0	0	0
	3	96.924	−0.0773	−0.0311						
Acetylene	1	2541.56	0.2425	−0.3472	55.4202	0.0470	0.0265	−2.0261	0.00115	0.00571
$0.6 \le \phi \le 1.0$	2	84.929	−0.0504	0.0391	6.6827	−0.0267	−0.0667	0.5768	0.00390	0.00719
	3	79.973	0.0100	0.1122	6.5091	−0.0051	0.0112	0.1499	−0.00194	−0.00665
Methane	1	2244.55	0.5068	0.0083	20.5269	0.0359	0.0427	−1.6769	−0.00282	−0.00325
(CH_4)	2	145.021	0.1557	0.1238	13.3841	0.0261	0.0309	−1.2535	−0.00198	−0.00205
	3	86.320	−0.0954	−0.0238	12.7909	−0.0137	−0.0320	0.2808	0.00311	0.00493
Ethane	1	2279.32	0.4902	−0.0163	24.3821	0.0410	0.0481	−1.9074	−0.00304	−0.00341
(C_2H_6)	2	135.518	−0.1652	−0.1344	14.5457	0.0253	0.0281	−1.2037	−0.00154	−0.00130
	3	83.445	−0.0842	−0.0050	10.9817	−0.0185	−0.0378	0.5250	0.00340	0.00514
Propane	1	2287.23	0.4863	−0.0228	25.3971	0.0424	0.0496	−1.9605	−0.00309	−0.00344
(C_3H_8)	2	133.141	−0.1675	−0.1368	14.7857	0.0248	0.0269	−1.1852	−0.00140	−0.00105
	3	82.736	−0.0818	−0.0007	10.4890	−0.0195	−0.0390	0.5931	0.00346	0.00514
Butane	1	2290.04	0.4852	−0.0252	25.7801	0.0428	0.0501	−1.9773	−0.00309	−0.00343
(C_4H_{10})	2	132.051	−0.1690	−0.1386	14.9854	0.0249	0.0270	−1.1922	−0.00139	−0.00102
	3	82.592	−0.0806	−0.0015	10.1903	−0.0202	−0.0399	0.6345	0.00351	0.00520
Pentane	1	2292.55	0.4840	−0.0272	26.1144	0.0433	0.0505	−1.9950	−0.00310	−0.00343
(C_5H_{12})	2	131.256	−0.1700	−0.1397	15.0468	0.0249	0.0269	−1.1824	−0.00136	−0.00099
	3	82.411	−0.0796	−0.0032	10.0376	−0.0207	−0.0406	0.6533	0.00355	0.00525

Table II –continued

	k	A_{11k}	A_{21k}	A_{31k}	A_{12k}	A_{22k}	A_{32k}	A_{13k}	A_{23k}	A_{33k}
Hexane	1	2294.10	0.4832	−0.0286	26.3413	0.0436	0.0509	−2.0076	−0.00312	−0.00345
(C_6H_{14})	2	130.819	−0.1703	−0.1398	15.0022	0.0246	0.0262	−1.1628	−0.00129	−0.00087
	3	82.235	−0.0793	0.0038	10.0214	−0.0207	−0.0404	0.6518	0.00351	0.00518
Heptane	1	2295.29	0.4827	−0.0295	26.4884	0.0437	0.0510	−2.0138	−0.00312	−0.00343
(C_7H_{16})	2	130.372	−0.1709	−0.1406	15.0840	0.0247	0.0265	−1.1653	−0.00131	−0.00091
	3	82.212	−0.0787	0.0049	9.8907	−0.0211	−0.0410	0.6687	0.00356	0.00525
Octane	1	2296.17	0.4821	−0.0304	26.6138	0.0439	0.0512	−2.0203	−0.00312	−0.00344
(C_8H_{18})	2	130.125	−0.1710	−0.1405	15.0791	0.0245	0.0261	−1.1573	−0.00127	−0.00084
	3	82.110	−0.0786	0.0051	9.8686	−0.0211	−0.0409	0.6696	0.00355	0.00521
Hexadecane	1	2299.40	0.4806	−0.0331	27.0291	0.0444	0.0517	−2.0375	−0.00313	−0.00344
($C_{16}H_{34}$)	2	129.047	−0.1722	−0.1419	15.2180	0.0245	0.0259	−1.1574	−0.00124	−0.00078
	3	81.948	−0.0772	0.0074	9.6046	−0.0217	−0.0417	0.7062	0.00359	0.00525
Ethylene	1	2389.09	0.4170	−0.1060	37.3064	0.0532	0.0584	−2.4486	−0.00304	−0.00288
(C_2H_4)	2	108.231	−0.1722	−0.1325	15.0497	0.0147	0.0085	−0.7123	0.00034	0.00166
	3	79.397	−0.0437	0.0519	6.4574	−0.0261	−0.0435	0.9141	0.00316	0.00404
Propylene	1	2354.81	0.4427	−0.0778	33.2814	0.0503	0.0567	−2.3146	−0.00315	−0.00321
(C_3H_6)	2	115.809	−0.1746	−0.1397	15.4394	0.0192	0.0161	−0.9154	−0.00030	0.00069
	3	80.130	−0.0562	0.0362	7.4652	−0.0253	−0.0442	0.8786	0.00365	0.00469
Butene	1	2342.84	0.4514	−0.0679	31.8970	0.0492	0.0559	−2.2591	−0.00316	−0.00329
(C_4H_8)	2	118.517	−0.1749	−0.1413	15.4933	0.0205	0.0183	−0.9761	−0.00051	0.00039
	3	80.454	−0.0608	0.0302	7.8805	−0.0247	−0.0439	0.8506	0.00350	0.00482
Pentene	1	2334.46	0.4573	−0.0612	30.9477	0.0483	0.0552	−2.2182	−0.00316	−0.00332
(C_5H_{10})	3	120.472	−0.1748	−0.1421	15.5272	0.0216	0.0203	−1.0241	−0.00070	0.00007
	3	80.680	−0.0639	0.0261	8.1530	−0.0244	−0.0441	0.8364	0.00358	0.00501
Hexene	1	2329.22	0.4609	−0.0570	30.3762	0.0478	0.0548	−2.1954	−0.00317	−0.00336
(C_6H_{12})	2	121.752	−0.1746	−0.1424	15.4755	0.0220	0.0211	−1.0414	−0.00077	−0.00002
	3	80.779	−0.0660	0.0233	8.3728	−0.0240	−0.0438	0.8197	0.00358	0.00504
Heptene	1	2325.49	0.4635	−0.0540	29.9573	0.0474	0.0545	−2.1755	−0.00317	−0.00337
(C_7H_{14})	2	122.590	−0.1745	−0.1425	15.4771	0.0223	0.0217	−1.0603	−0.00082	−0.00011
	3	80.943	−0.0674	0.0213	8.5045	−0.0237	−0.0435	0.8085	0.00358	0.00506

Table II continued

	k	A_{11k}	A_{21k}	A_{31k}	A_{12k}	A_{22k}	A_{32k}	A_{13k}	A_{23k}	A_{33k}
Octene (C_8H_{16})	1	2322.68	0.4654	−0.0518	29.6471	0.0471	0.0542	−2.1615	−0.00316	−0.00337
	2	123.273	−0.1744	−0.1427	15.4845	0.0227	0.0223	−1.0760	−0.00089	−0.00022
	3	81.005	−0.0685	0.0199	8.5895	−0.0237	−0.0435	0.8046	0.00361	0.00512
Hexadecene ($C_{16}H_{32}$)	1	2312.80	0.4722	−0.0439	28.5524	0.0461	0.0533	−2.1095	−0.00316	−0.00341
	2	125.542	−0.1740	−0.1431	15.4871	0.0236	0.0241	−1.1265	−0.00106	−0.00048
	3	81.412	−0.0721	0.0150	8.8956	−0.0231	−0.0432	0.7862	0.00364	0.00524
Benzene (C_6H_6)	1	2363.62	0.4397	−0.0902	35.2324	0.0529	0.0594	−2.3589	−0.00313	−0.00311
	2	111.079	−0.1817	−0.1475	15.4907	0.0180	0.0137	−0.8084	0.00001	0.00119
	3	80.028	−0.0517	0.0460	6.3786	−0.0276	−0.0470	0.9883	0.00352	0.00465
Toluene (C_7H_8)	1	2349.92	0.4494	−0.0777	33.4945	0.0513	0.0582	−2.3020	−0.00316	−0.00323
	2	114.623	−0.1811	−0.1483	15.6560	0.0199	0.0169	−0.9076	−0.00030	0.00072
	3	80.219	−0.0573	0.0382	6.9166	−0.0268	−0.0467	0.9610	0.00361	0.00489
Ethyl benzene (C_8H_{10})	1	2343.42	0.4537	−0.0717	32.6413	0.0505	0.0575	−2.2721	−0.00317	−0.00328
	2	116.444	−0.1804	−0.1483	15.6303	0.0206	0.0183	−0.9400	−0.00041	0.00053
	3	80.315	−0.0598	0.0345	7.2895	−0.0262	−0.0463	0.9264	0.00361	0.00496
Propylbenzene (C_9H_{12})	1	2338.09	0.4572	−0.0669	31.9658	0.0499	0.0569	−2.2499	−0.00318	−0.00331
	2	117.887	−0.1798	−0.1480	15.6592	0.0212	0.0194	−0.9750	−0.00053	0.00035
	3	80.473	−0.0620	0.0312	7.5033	−0.0259	−0.0459	0.9137	0.00364	0.00503
Butylbenzene ($C_{10}H_{14}$)	1	2334.00	0.4599	−0.0632	31.4380	0.0493	0.0565	−2.2289	−0.00318	−0.00334
	2	119.078	−0.1791	−0.1476	15.6457	0.0216	0.0201	−1.0023	−0.00061	0.00023
	3	80.516	−0.0638	0.0285	7.7199	−0.0254	−0.0455	0.8989	0.00364	0.00507
Amylbenzene ($C_{11}H_{16}$)	1	2330.91	0.4618	−0.0604	31.0280	0.0489	0.0561	−2.2110	−0.00318	−0.00335
	2	119.943	−0.1786	−0.1472	15.6674	0.0220	0.0208	−1.0257	−0.00069	0.00011
	3	80.615	−0.0650	0.0266	7.8526	−0.0252	−0.0453	0.8892	0.00366	0.00511
Hexylbenzene ($C_{12}H_{18}$)	1	2328.39	0.4634	−0.0581	30.7054	0.0485	0.0557	−2.1991	−0.00318	−0.00336
	2	120.631	−0.1783	−0.1472	15.6897	0.0224	0.0215	−1.0457	−0.00076	−0.00000
	3	80.717	−0.0659	0.0253	7.9445	−0.0251	−0.0454	0.8853	0.00369	0.00518

Table II--continued

	k	A_{11k}	A_{21k}	A_{31k}	A_{12k}	A_{22k}	A_{32k}	A_{13k}	A_{23k}	A_{33k}
Hexadecylbenzene	1	2316.25	0.4709	−0.0475	29.1657	0.0469	0.0542	−2.1354	−0.00317	−0.00341
($C_{22}H_{38}$)	2	124.097	−0.1761	−0.1455	15.5301	0.0233	0.0234	−1.0939	−0.00096	−0.00032
	3	81.146	−0.0707	0.0178	8.6311	−0.0238	−0.0440	0.8130	0.00366	0.00522
Methanol	1	2238.70	0.4266	−0.0508	22.8315	0.0382	0.0437	−1.8079	−0.00285	−0.00311
(CH_3OH)	2	135.938	−0.1550	−0.1222	14.1737	0.0245	0.0263	−1.2232	−0.00152	−0.00119
	3	84.317	−0.0736	0.0065	10.9430	−0.0196	−0.0384	0.5142	0.00345	0.00507
Ethanol	1	2255.58	0.4590	−0.0351	23.7136	0.0400	0.0464	−1.8613	−0.00297	−0.00328
(C_2H_6O)	2	135.208	−0.1624	−0.1312	14.5154	0.0253	0.0276	−1.2216	−0.00153	−0.00121
	3	83.501	−0.0797	0.0012	10.7504	−0.0196	−0.0191	0.5638	0.00350	0.00518
Propanol	1	2267.87	0.4671	−0.0334	24.6321	0.0413	0.0481	−1.9122	−0.00302	−0.00334
(C_3H_8O)	2	133.514	−0.1658	−0.1351	14.7514	0.0252	0.0274	−1.2101	−0.00147	−0.00113
	3	82.971	−0.0795	0.0026	10.4372	−0.0203	−0.0400	0.6090	0.00355	0.00525
Butanol	1	2274.80	0.4710	−0.0328	25.1700	0.0421	0.0490	−1.9426	−0.00305	−0.00337
($C_4H_{10}O$)	2	132.547	−0.1674	−0.1369	14.8266	0.0250	0.0270	−1.1859	−0.00139	−0.00102
	3	82.668	−0.0793	0.0033	10.2905	−0.0205	−0.0403	0.6201	0.00354	0.00522
Pentanol	1	2279.27	0.4731	−0.0328	25.5236	0.0425	0.0496	−1.9616	−0.00307	−0.00339
($C_5H_{12}O$)	2	131.904	−0.1684	−0.1379	14.9009	0.0249	0.0267	−1.1800	−0.00136	−0.00096
	3	82.495	−0.0791	0.0039	10.1536	−0.0207	−0.0405	0.6386	0.00354	0.00522
Hexanol	1	2282.29	0.4746	−0.0327	25.7601	0.0429	0.0499	−1.9735	−0.00308	−0.00340
($C_6H_{14}O$)	2	131.512	−0.1691	−0.1389	14.9093	0.0248	0.0267	−1.1696	−0.00134	−0.00094
	3	82.333	−0.0789	0.0045	10.1308	−0.0208	−0.0408	0.6396	0.00355	0.00523
Heptanol	1	2284.64	0.4755	−0.0328	25.9485	0.0431	0.0501	−1.9838	−0.00309	−0.00341
($C_7H_{16}O$)	2	131.077	−0.1698	−0.1395	15.0517	0.0249	0.0268	−1.1852	−0.00135	−0.00095
	3	82.115	−0.0786	0.0050	9.9265	−0.0212	−0.0412	0.6747	0.00360	0.00529
Octanol	1	2286.42	0.4763	−0.0328	26.0857	0.0433	0.0504	−1.9899	−0.00310	−0.00341
($C_8H_{18}O$)	2	130.846	−0.1700	−0.1398	15.0015	0.0247	0.0264	−1.1679	−0.00131	−0.00088
	3	82.198	−0.0786	0.0051	9.9834	−0.0211	−0.0410	0.6606	0.00356	0.00523

a wide range of applications since the formula is expressed in terms of the major variables determining T_a: the fuel/air ratio, the reaction pressure, the initial mixture temperature, and the number of carbon atoms in individual fuels. The accuracy of the formula may be as great as one percent at either of the lower or upper limits of fuel/air ratio considered for the formula but much smaller otherwise.

TABLE III
Coefficient matrix needed in individual cases

Mixture and reaction cond.	Use of matrix	Coefficients of fuel family in (I)–(IV)	Coefficients of individual fuels in (V)–(VII)
$\phi = 1.0$,	$p = 1$ atm, $T_i = 298°K$	A_{111l} $(k = 1, 2, 3)$	A_{111}
$\phi = 1.0$,	$p = 1$ atm, $T_i \neq 298°K$	A_{11kl} $(k = 1, 2, 3;\ l = 1, 2, 3)$	A_{11k} $(k = 1, 2, 3)$
$\phi = 1.0$,	$p \neq 1$ atm, $T_i = 298°K$	A_{1jll} $(j = 1, 2, 3;\ l = 1, 2, 3)$	A_{1jl} $(j = 1, 2, 3)$
$\phi = 1.0$,	$p \neq 1$ atm, $T_i \neq 298°K$	A_{1jkl} $(j = 1, 2, 3;\ k = 1, 2, 3;\ l = 1, 2, 3)$	A_{1jk} $(j = 1, 2, 3;\ k = 1, 2, 3)$
$\phi \neq 1.0$,	$p = 1$ atm, $T_i = 298°K$	$A_{1111}, A_{2111}, A_{3111}$ $(l = 1, 2, 3)$	A_{111} $(i = 1, 2, 3)$
$\phi \neq 1.0$,	$p = 1$ atm, $T_i \neq 298°K$	A_{11kl} $(i = 1, 2, 3;\ k = 1, 2, 3;\ l = 1, 2, 3)$	A_{11k} $(i = 1, 2, 3;\ k = 1, 2, 3)$
$\phi \neq 1.0$,	$p \neq 1$ atm, $T_i = 298°K$	A_{ijll} $(i = 1, 2, 3;\ j = 1, 2, 3;\ l = 1, 2, 3)$	A_{ijl} $(i = 1, 2, 3;\ j = 1, 2, 3)$
$\phi \neq 1.0$,	$p \neq 1$ atm, $T_i \neq 298°K$	A_{ijkl} $(i, j, k, l = 1, 2, 3)$	A_{ijk} $(i, j, k = 1, 2, 3)$

ACKNOWLEDGEMENTS

The suggestion to include the initial mixture temperature as a variable which was offered by Mr. C. Amann and Dr. Ö. Gülder is appreciated. This research has been sponsored by the U.S. Army Research Office, Contract No. DAAG 29-83-K-0042.

REFERENCES

Chang, S. L., and Rhee, K. T. (1983). Computation of radiation heat transfer in diesel combustion, SAE Paper 831332, also in *SAE Transactions*.

Chang, S. L., and Rhee, K. T. (1983). Adiabatic flame temperature estimates of lean fuel/air mixtures. *Combustion Science and Technology* 35, 203.

Gaydon, A. G., and Wolfhard, H. G. (1970). *Flames, Their Structures, Radiation and Temperature*, 3rd Ed., Chapman and Hall, Ltd., p. 98.

Glassman, I., and Clark, G. (1983). Universal hydrocarbon-air temperature graphs, Fall Meeting of the Eastern States Section of the Combustion Institute, Paper 12, 1983.

Gordon, S., and McBride, B. J. (1971). Complex chemical equilibrium calculation, NASA SP-273.

Olikara, C., and Borman, G. L. (1975). A computer program for calculating properties of equilibrium combustion products with some application to IC engines, SAE Paper 750468.

Appendix-XII.

A Parametric Analysis of Radiation Heat Transfer in Direct Injection Diesel Combustion

S.L. Chang, X.L. Yang and K.T. Rhee
Department of Mechanical and Aerospace Engineering
Rutgers, The State University of New Jersey
New Brunswick, New Jersey 08903

ABSTRACT

Radiation heat transfer in a direct injection-type diesel engine is investigated by a computational parametric analysis for various engine and combustion variables. A new model has been developed to compute the spectral radiation heat flux incident on various locations in the combustion chamber and to incorporate it with the spectral emissivity of the chamber wall surface. The model mainly differs from previous ones in several ways: (1) it uses the in-cylinder species distribution; (2) a new coordinate transformation method is introduced, instead of using geometric factors or the zonal method; (3) it computes the spectral volume absorptance of the combustion products through optical paths; (4) a new formulation and integration method are employed for the governing equation of radiation heat flux; etc. The main purpose of the present paper is to report some of results from a parametric analysis carried out by using the new computational model.

A NEW MODEL

A better modeling of radiation heat transfer is desired for a more comprehensive analysis of thermal loading of a diesel engine. A rigorous way of computing the radiation heat flux incident on a particular location of the combustion chamber wall will be implementing the equation of radiation heat transfer as accurately as possible. The equation calls for the detailed distributions of optical and thermal properties along individual optical paths in the hemispherical volume faced by the location. Several difficult issues remain to be overcome in achieving the above goals for a long time. They are the proper use of the in-cylinder species and temperature distributions in the modeling, the computation of optical and thermal properties of the species along the individual optical paths, the accurate implementation of the equation of monochromatic radiation heat transfer, to name a few. Each problem is discussed elsewhere by proposing the authors' solution. However, a brief description of the authors' methods for the individual problems are made in the following. Note that the main purpose of the present paper is to report results from a parametric analysis made in the present numerical method, which are not included in others.

In order to properly evaluate the space-resolved nature of the radiation heat transfer in diesel combustion, it is important to determine the instantaneous in-cylinder species and temperature distributions. It cannot be overemphasized that an assumption of uniform species distribution in diesel combustion is incapable of properly evaluating the spatial dependence of heat transfer. Such space-resolved distribution data, which may be found by using either experimental methods [1-3] or computational means, presently are not sufficient for an extensive analysis of the radiation process, in particular, for a parametric study of the process. As an alternative, a plume equation which seems to reasonably express the instantaneous species distribution has been introduced for radiation heat transfer analysis as [4],

$$f = f_0 \exp(-a\phi - b\phi^2 - cz^2) \qquad (1)$$

where f represents the local burned fuel/air ratio or CO_2 or H_2O concentrations, etc., and f_0, a, b, c are the ones to be respectively determined at each engine crank angle by using the above mentioned methods. For simplicity but perhaps as one of the only presently available alternatives, the burned fuel air ratio may be used for computing the instantaneous local temperature distribution [5]. The above plume equation enables one to choose plume geometries of varied species distributions. Therefore, the above equation can be used in a parametric analysis of radiation heat transfer in a combustion chamber when one chooses plume details as independent variables, i.e., by varying values of the constants in the equation.

Even though the in-cylinder species distribution is given, very likely in a coordinate system with respect to the injection nozzle, it is needed to find the species distribution along the optical paths centered at the location of which incident heat flux is sought. Because of its complexity, simplified methods have been employed in previous radiation computations; uses of geometric factors [5,6], zonal method [7], etc. A new coordinate transformation method is introduced for finding an accurate species distribution along each optical path centered at individual locations over the combustion chamber, when the in-cylinder distribution is given with respect to the nozzle hole [8]. A short summary of the method is given here: Referring to Fig. 1 which shows plumes

distributed in a cylindrical coordinate centered at the nozzle hole, R, one wants to find the species distribution along an optical path faced by a particular location on the wall (called a detector for simplicity's sake), D.

A new equation was derived for this purpose as shown in the following (Fig. 1) or for a given property distribution with respect to the nozzle as shown in Eq. (1), the property distribution along an optical path (r,θ,ζ), s, is expressed as,

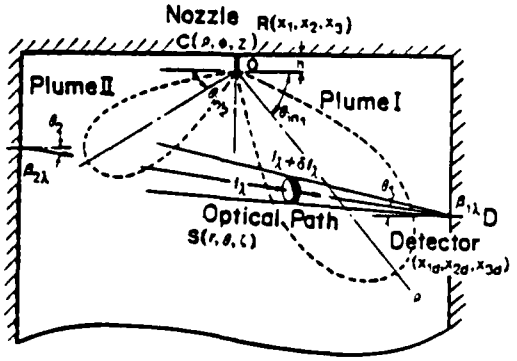

Fig. 1. A Schematics of Flame Plumes in a Combustion Chamber

$$s = s_d\, e^{-[r-r_c)/r_w]^2} \qquad (2)$$

where,

$$s_d = f_v\, e^{-(a_1-b_1^2/4c_1)}$$

$$r_c = b_1/2c_1$$

$$r_w = (c_1)^{-1/2}$$

$$a_1 = a\rho_d + b\phi_d + cz_d^2$$

$$b_1 = -[a\rho_1+b\phi_1]\sin\vartheta/\rho_d + 2c\, z_d\cos\theta$$

$c_1 = [a\rho_2+b\phi_2]\sin^2\theta/\rho_d^2 + c\cos^2$ and ρ_i and ϕ_i (i = 0,1, and 2) are second order polynomials expressed by using Taylor's expansion in terms of $x = r\sin\theta/\rho_d$, r, ϑ, and the plume angle ϑ_{in} (refer to Fig. 1).

Upon the determination of the species distribution along the individual optical paths, the radiation heat flux incident on the detector through each path is computed. In order to achieve this, the following two steps have to be taken, i.e., to compute the thermal and optical properties of the species and to implement integration of the equation of radiation by combining all the above results. The computations of optical properties along each path were made by finding radiation from both soot and gases respectively: Rayleigh-limit expression and the dispersion equation are used for finding the monochromatic volume absorptance of soots [5,9] and the non-gray semiempirical band model proposed by Edwards and Balakrishnan [5,10] is employed for computing gas volume absorption. The summation of radiations from both contributions, $\epsilon_{t,\lambda}$, are made equivalent to $\epsilon_{t,\lambda} = 1-(1-\epsilon_{g,\lambda})(1-\epsilon_{s,\lambda})$, where $\epsilon_{g,\lambda}$ and $\epsilon_{s,\lambda}$ are the spectral emissivity due to the presence of gaseous species and soot, respectively. Notice that the monochromatic property variation is a function of the distance along each optical path. Regarding the equation of radiation heat transfer, the following equation was derived. In reference to Fig. 1, when the distribution of the total volume absorptance, $\kappa_\lambda(r)$, is found, the governing equation of local directional spectral radiation intensity, $I_\lambda(r)$, is written as

$$I_\lambda(r) = \int_r^{r_0} \frac{\kappa_\lambda(r')}{\tau} e_{b\lambda}(r')\exp(-\int_r^{r'} \kappa_\lambda(r'')dr''dr'.$$

The heat flux along an optical path of a solid angle (θ,ζ) in the thermal radiation range may be, then, found from

$$q_{\theta\zeta} = \int_0^\infty I_\lambda(0)\cos\theta\, d\lambda \qquad (3)$$

where κ_λ is the spectral volume absorptance at (r,θ,ζ). Combining Eq. (2) with the above equation, a better implementation of its computation has been made by using Gaussian integration method [11].

Due to the repeated computation of the adiabatic flame temperature based on the local burned fuel/air ratio along the individual optical paths, a convenient way was sought to find the temperature values. A simple form of equation was developed in a direction of its proper coupling with Eq. (3) for facilitating the subsequent solution. The new equation of the adiabatic flame temperature, T_a, is functionally related to several variables, i.e., the fuel volume fraction of stoichiometric, Λ, the reaction pressure p, the initial temperature of mixture, T, and the number of carbon atoms in the fuel, I, as shown in the following [12]:

$$T_a = A_1[1+ A_2\ln\Lambda + A_3(\ln\Lambda)^2] \qquad 0.5 < \Lambda \le 1.0 \qquad (4)$$

where A_1, A_2 and A_3 are functionally expressed in terms of p, T and I. The constants in those expressions for most of practially used fuel/air systems are given in the above reference.

In addition, the spectral surface reflectivity is incorporated with the spectral radiation heat flux incident on each detector over the combustion chamber wall. By defining the extinction coefficient, τ, along the optical path and giving the spectral surface reflectivities, ρ_1 and ρ_2 (see Fig. 1), the radiosity of the surface 1, B_1, is expressed as

$$B_1 = \frac{(I_1+\beta_{\lambda 1}\cos\theta_1 I_{op})+\beta_{\lambda 1}\cos\theta_1 e^{-\tau}(I_2+\beta_{\lambda 2}\cos\theta_2 I_{op})}{1-\beta_{\lambda 1}\beta_{\lambda 2}\cos\theta_1\cos\theta_2 e^{-2\tau}} \quad (5)$$

where $I_i = \epsilon_i \sigma T_i^4$ $(i = 1,2)$ and $\beta_\lambda = 1-\epsilon_\lambda$.

PARAMETRIC ANALYSIS OF DIESEL RADIATION HEAT TRANSFER

Since the details of instantaneous in-cylinder events are not known due to either the insufficient experimental data or the limitations in combustion modeling, several assumptions are taken in the present computational analysis. The main assumptions are: (1) the system for each computed entity is isolated; (2) the species in the system attains an equilibrium at successive moments; (3) the temperature distribution is that of the adiabatic flame temperature determined by the burned local fuel/air ratio and cylinder pressure; (4) the fuel is injected into the combustion chamber at an inclined angle, θ_{in} = 150°; (5) the scattering in the radiation is negligible; and (6) the standard values of constants for convenience of comparison in Eq. (1) are, f_0 for soot, H_2O, CO_2 and fuel/air ratio, 8 x 10^{-6}, 0.01, 0.01 and 1.0, respectively. In addition, the distribution constants a, b, and c are 0.6, 2.36 and 2 accordingly. For example, the fuel/air ratio distribution, may be written as $= (1.0 \exp -[0.6(\rho/R) + 2.43(\theta/\theta_r) + 2.0(z/R)^2]$, where R is the piston radius and θ_r is π/(the number of plumes). Further, the analysis was made for the following engine details; the surface temperature, 500°K; number of spray plumes, 4; piston radius, 4.92 cm; combustion chamber bowl radius, 3.44 cm and the fuel composition, $C_{16}H_{34}$.

The computation was carried out to evaluate the following: the apparent emissivity (or normalized radiation heat transfer), $\epsilon_a = q/q_r$; the spectral emissivity (or normalized spectral radiation heat transfer), $\epsilon_\lambda = q_\lambda/q_{r\lambda}$; the spectral apparent emissivity (or normalized relative spectral radiation heat transfer), $\epsilon_{\lambda a} = q_\lambda/q_{r\lambda}$, where $q_r = \sigma T_r^4$, T_r = 2400°K; λ_r = 6.0 μm; and $\sigma = 2\pi^5 k^4/15c^2h^3$, c = 2.998x$10^{10}$ cm/sec, h = 6.625x10^{-27} erg-sec, and k = 1.380x10^{-16} erg/K. Additionally, in order to evaluate the effect of the presence of the combustion chamber wall on the radiation, three different computations of heat flux were evaluated (as shown in results): Net, computation of radiation on heat flux through the wall with inclusion of the emission of the spray plumes, the absorption and emission of the wall and the reflection from the surroundings; No Reflection, computation including the emission of the spray plumes plus the absorption and emission of the wall but excluding the reflection and emission from the opposite walls; and Spray Plume, computation of radiation streaming out of the spray plumes only.

The results obtained by using the above conditions and assumptions are shown in the following for various parameters with relevant explanations.

Location of Detector (ρ_d, ϕ_d, z_d). A computation was carried out for heat fluxes through the locations on the cylinder head across a plume at ρ_d = 0.5 and along the direction of a plume axis (ϕ_d = 0) and their results are shown in Figs. 2 and 3 respectively. The trend shows the radiation flux quite similarly follows the species

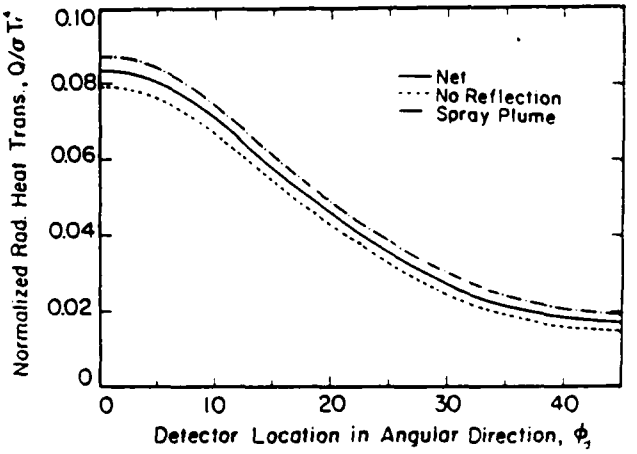

Fig. 2. Radiation Heat Flux Through a Cylinder Wall Along the Axial Direction of a Plume

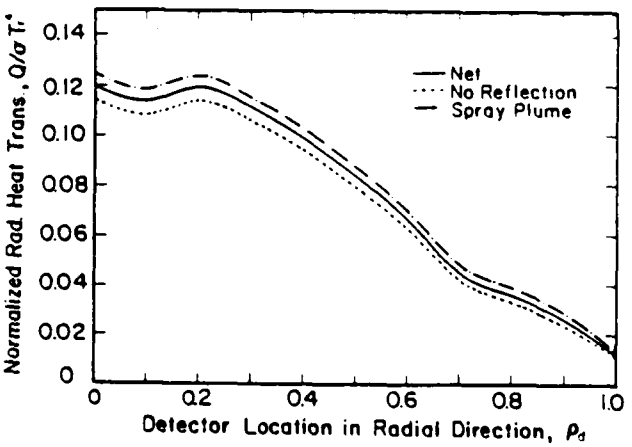

Fig. 3. Radiation Heat Flux Through a Cylinder Wall Along the Circumferential Direction Across a Plume

distribution in the corresponding plume. This suggests the greatest portion of heat flux incident on a detector comes from the radiation source right beneath the detector, as indicated by the directional cosine in Eq. (3). A similar conclusion was made in the authors' preliminary radiation modeling of diesel combustion [5]. The local minimum around ρ_d = 0.1 may be of surprise. In order to find its reason, the net directional radiation intensity was calculated at different locations along the axis (ϕ_d = 0) by varying the azimuthal angle (ζ) of integration with an zineith

angle of $\theta = 39.7°$, as shown in Fig. 4: The reason for the minimum at $\rho_d = 0.1$ is readily explained form the figure by finding that while the radiation heat flux incident on the detector at the nozzle ($\rho_d = 0$) is from all of the four plumes, the heat flux on the detector at $\rho_d = 0.1$ is from the species from one plume, i.e., the nearest plume.

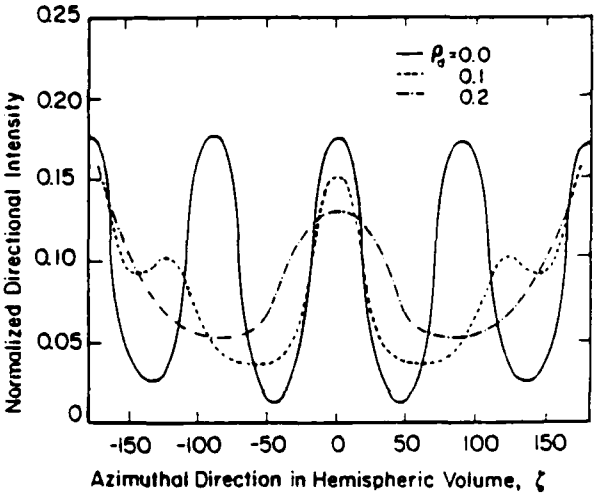

Fig. 4. Net Directional Intensity Incident on Zineith Angle of 39.7 deg in the Hemispheric Volume (r, θ, ζ) Faced by Detectors Along a Plume Axis

The radiation heat flux incident on the piston surface (with the cup depth of 0.74 cm) for $\phi = 0$ was calculated as shown in Fig. 5. The trend of results is predictable; the local minimum at $\rho_d = 0$ is caused by the weak emission species right underneath the nozzle; the abrupt change around $\rho_d = 0.7$ is due to the presence of the piston bowl bank.

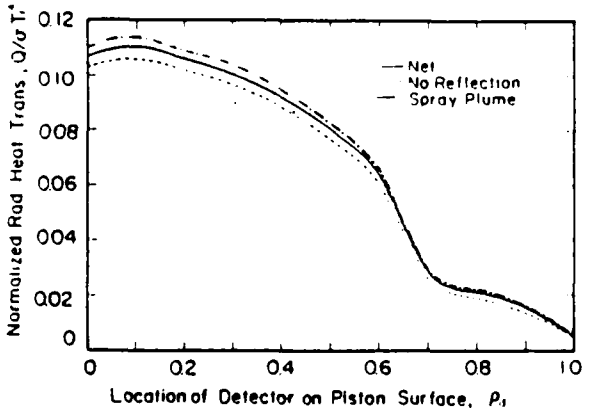

Fig. 5. Radiation Heat Flux Through a Piston Surface Along the Axial Direction of a Plume

A similar computation was conducted for the heat flux incident on the side wall of the piston cup as shown in Fig. 6. The strongest heat flux was not found for the straight end of the plume ($\phi_d = 0$) but for $\phi_d = 10$. The humps in the curve were found to occur due to the geometric configuration of other plumes from a similar analysis to results in Fig. 4.

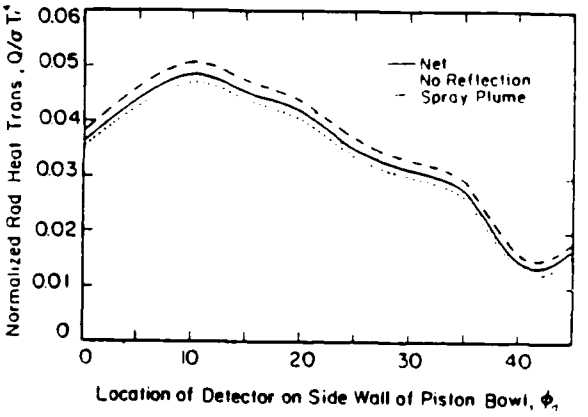

Fig. 6. Radiation Heat Flux Through a Piston-Cup Side Wall

The heat flux on the cylinder linear ($\rho_d = 1$) may be of interest: Computation was made for $z_d = -0.044$ as shown in Fig. 7. The decrease in heat flux with ϕ_d was expected because the species concentration near the detector becomes leaner with increase in ϕ_d. The relatively flat curve between $\phi_d = 10°$ and $\phi_d = 35°$ indicates the increasing effect of the neighboring plume on the heat flux. Note that the heat flux striking the cylinder wall at $\rho_d = 1$ is stronger than that at the similar location on the cylinder head. Also note that the heat flux, in general, is much stronger on the cylinder head (Fig. 3) than the cylinder liner (Fig. 7).

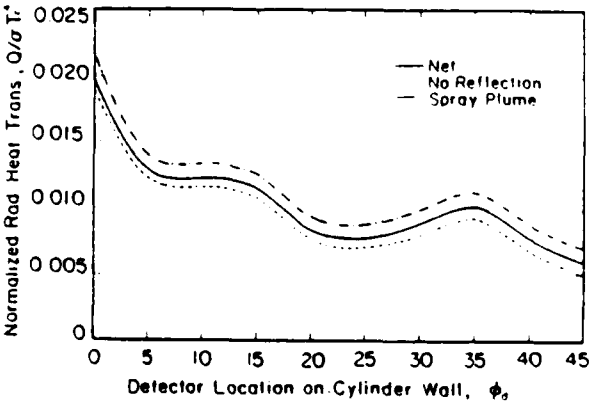

Fig. 7. Radiation Heat Flux Through a Cylinder Liner Along the Circumferential Direction

Surface Emissivity. In Figs. 2 and 3, the energy-spray plume is greatest and the energy-net is greater than the energy-no reflection. This result may be conveniently explained by the following example. At $\rho_d = 0$, since the detection

surface absorbs 95% of the incident energy (with reflection of 5%) and emits an amount of energy (T_w = 500°K) equivalent to 1.4% of radiation energy from the spray plume (q_{sp}), the energy-no reflection is 93.6% of the energy-spray plume. Computational results show the energy-net is 96.8% of q_{sp}; the difference of the two, 3.2% (96.8%-93.6%) of q_{sp} is, therefore, the energy reflected from the opposite surface walls. Since, from this example, 5% of reflection and 1.4% of emission from the chamber surfaces result in a 3.2% of increment of the energy detected by a location of the chamber, it may be concluded the following: A net energy equivalent to about one half of the energy leaving a surface will arrive at the same surface when incorporated the emission from the opposite wall with the extinction along the optical paths.

The effect of the above trend may be inferred for different surface emissivities from the results shown in Fig. 8. The decrease of heat flux-net with decrease in emissivity is caused by the increase in reflectivity. At the present, the spectral emissivity of the wall is being incorporatedinto the analysis for further investigation as a continuing activity at Rutgers.

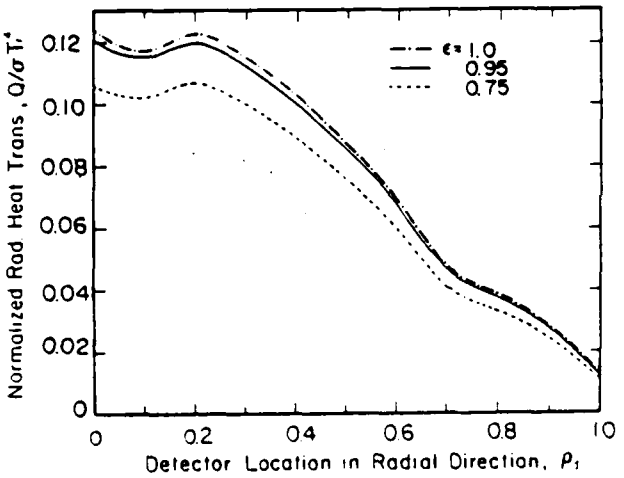

Fig. 8. Effect of Surface Emissivity on Radiation Heat Flux Through a Cylinder Head

Soot Concentration. The radiation heat flux increases with the soot concentration in the plume as shown in Fig. 9. The increase is greater in the lower concentration range than that high concentration. The reason for the convergence of the emissivity at high soot concentration is due to the exponential function relationship of the emissivity to the volume absorptance. Another loqk at Fig. 9 will lead one to find the local minimum in heat flux does not occur for low soot concentrations. The result is more evidence to explain the unique receiving geometric configuration at the injection nozzle for some cases.

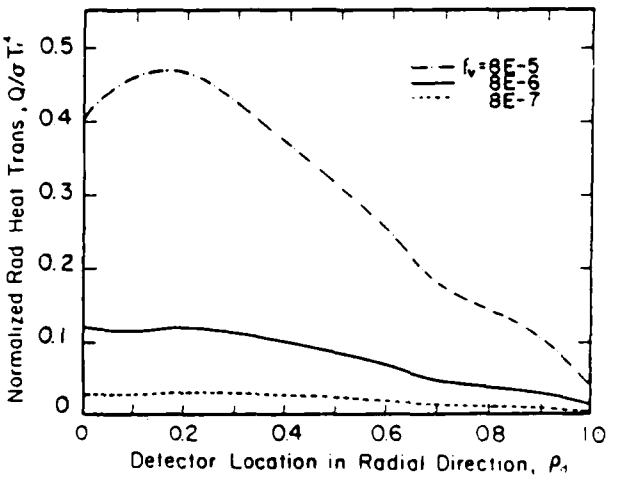

Fig. 9. Soot Concentration Variation Effect on Radiation Heat Flux Through a Cylinder Head

Soot and Gas Radiation. As expected from the authors' previous study [5], it is found that the soot radiation is much stronger than the gas radiation (Fig. 10). The direct summation of soot radiation and gas radiation exceeds the computed combined radiation. While its reason may be explained by looking into the method of combination [4,8], it can also be seen from the fact that some gas emission is absorbed by soots and that soot radiation is similarly attenuated by the presence of the gas species.

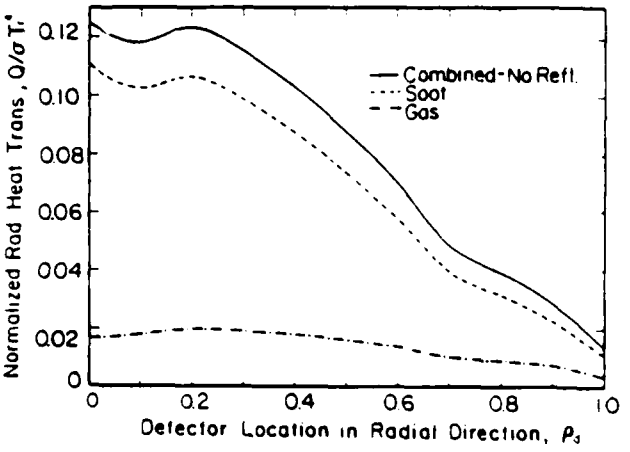

Fig. 10. Comparison of Radiation Heat Fluxes Due to Soot and Gaseous Species

In order to investigate predominant wave bands of radiation, a wave number-resolved computation was made as shown in Fig. 11. There are three distinctively strong bands of gas radiations at λ = 1, 3 and 10 μm (recall that the normalized wave number = $\lambda/6$ μ). In fact, each band consists of many small bands of CO_2 and H_2O in the plume. Over the spectra of radiation, one finds that soot radiation is dominant in short wavelength, λ < 2 μm, while the gas radiation

becomes important in longer wavelengths, $\lambda > 4$ μm (Fig. 12).

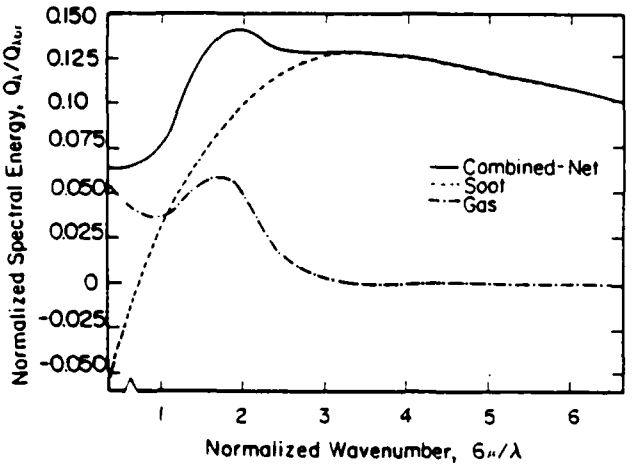

Fig. 11. Spectral Radiation Heat Flux Due to Soot and Gaseous Species

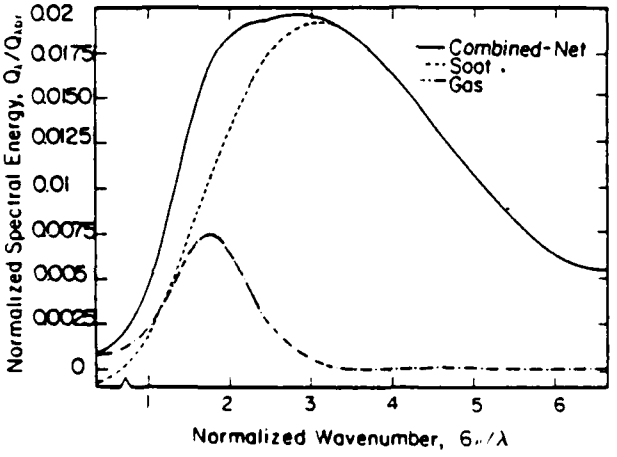

Fig. 12. Relative Spectral Radiation Heat Flux Due to Soot and Gaseous Species

Pressure. The effect of pressure on radiation heat transfer was studied assuming the injection processes and the gas motions are not affected. Figure 13 shows the computational results of the pressure effect on spectrum-resolved radiation heat flux at $\theta_d = 0$. The variation of the spectral radiation with pressure is somewhat noticeable at the long wavelength region ($\lambda > 3$ μm) where the gas radiation is important. Since the flame temperature is relatively insensitive to the pressure variation, the results in Fig. 13 only show the pressure broadening effect on the gas radiation in diesel combustion.

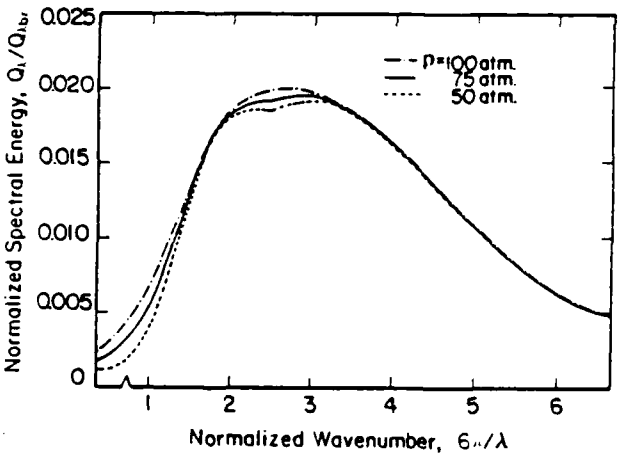

Fig. 13. Pressure Broadening Effect on Diesel Radiation Heat Transfer

Surface Temperature. The weak effect of the chamber surface temperature variation on the radiation heat transfer is shown in Fig. 14. There is some reduction in the energy-net due to the stronger surface emission at higher surface temperature. Such an effect will be greatly increased in some local places where the surface temperature, however, is extremely high in the engine combustion chamber.

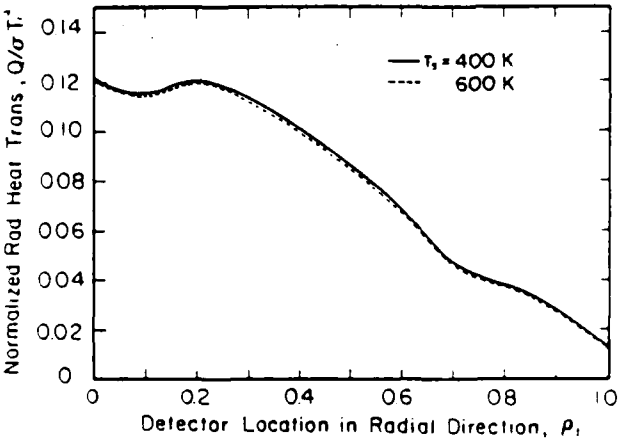

Fig. 14. Surface Temperature Effect on Diesel Radiation Heat Transfer

Burned Fuel/Air Ratio vs. Soot Concentration vs. Flame Temperature. In order to mutually compare parameters greatly affecting the radiation heat transfer, Figs. 14, 15 and 16 are offered. Several important points found from the results may be in order: the effect on the radiation heat transfer is much greater with the relative variation of the fuel/air ratio than that of the soot concentration. The greater effect of the fuel/air variation is caused by the corresponding changes in CO_2 and H_2O concentrations and the adiabatic flame temperature. Note that the temperature effect on volume absorptance is the quadruple power dependency of temperature and the soot concentration effect on it is the linear

relationship of soot concentration.

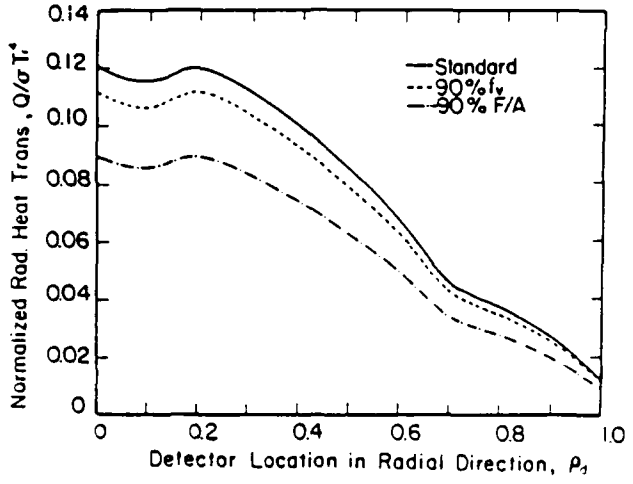

Fig. 15. Comparison of Effects on Diesel Radiation Heat Transfer Due to Variations in the Soot Concentration and the Fuel/Air Ratio

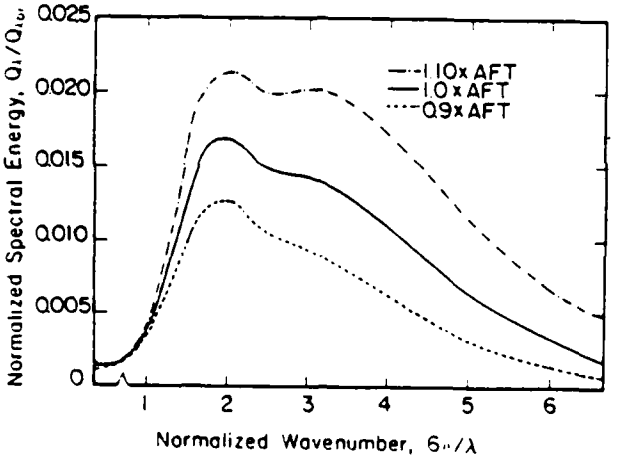

Fig. 16. Comparison of Effects on Relative Spectral Radiation Heat Transfer Due to Variations in the Soot Concentration and the Fuel/Air Ratio

Since the adiabatic flame temperature is not realistic, at all, in diesel combustion, the sensitivity of radiation heat transfer to the temperature variation is worth investigating. Note that the actual flame temperature in diesel combustion may either higher or lower than the adiabatic flame temperature due to the post-reaction compression, heat transfer, etc. Figure 15 shows the effect of temperature on the radiation heat flux. Note that there is an assumption of no change in gaseous species concentrations in this variation, unlike in the fuel/air ratio variation. As mentioned above, because of the quadruple dependence of temperature on the volume absorptance and due to the weak effect of the variation in gaseous species concentrations on the radiation, the impact of temperature variation on the process is concluded to be very high as shown in the results. Figure 16 shows the stronger effect of the temperature variation on the radiation heat transfer at shorter wavelengths. This may be well explained by Plank's radiation function.

SUMMARY

A new radiation heat transfer model of direct injection diesel combustion has been developed. The model has been used for a parametric analysis of radiation transmission in a diesel engine. Some of the results may be misleading due to the lack of sufficient combustion details of the engine. Nevertheless, the present results clearly show that the engine radiation processes may be well analyzed by using the new model and that some new findings are worth noting:

(1) The most portion of radiation heat flux incident on a location in the chamber wall comes from the radiation source right near the location.

(2) The effect of surface emissivity on diesel radiation may not be negligible, in particular, when the surface temperature is high, as in new uncooled diesel engines.

(3) The diesel radiation heat transfer is highly dependent on the soot concentration and weakly sensitive to the gaseous species concentrations.

(4) The pressure effect on the radiation is almost negligible in diesel combustion.

(5) The surface temperature of the chamber wall is not a sensitive parameter on the diesel radiation heat transfer, but it will not be negligible where the local temperature is exceedingly high.

(6) The flame temperature or the fuel/air ratio variation produces very high impact on the radiation process, more than any other parameter studied.

ACKNOWLEDGEMENT

The present study has been supported by the U.S. Army Research Office, Contract No. DAAG29-83-K-0042 (Scientific Program Officer, Dr. David M. Mann).

NOMENCLATURE

a	species distribution constant
A	constants in adiabatic flame temperature equation
b	species distribution constant
B	radiosity of surface
c	speed of light
f	species distribution with respect to injection nozzle
f_0	species distribution constant
f_v	soot volume fraction
h	Planck's constant
I	radiation intensity or number of carbon atoms in a fuel

k	Boltzmann constant
p	pressure
q	radiation heat flux
r	optical path
R	radius of cylinder
s	species distribution with respect to detector
T	temperature
x,y,z	components in cylindrical coordinate
r,θ,ζ	components in spherical coordinate
ε	surface emissivity
κ	volume absorptance
λ	wavelength
ξ	fuel volume fraction of stoichiometric
σ	extinction coefficient
σ	Stefan-Boltzman constant

Subscripts

a	adiabatic
b	blackbody
d	detector
g	gas
i	index number
op	optical path
r	reference
s	soot
t	total
λ	spectral

REFERENCES

1. Ahn, S.K., Matsui, Y., Kamimoto, T. and Matusuoka, S., "Measurement of Flame Temperature Distribution in a D.I. Diesel Engine by Means of Image Analysis of Nega-Color Photographs," SAE Paper-810183, 1981.

2. Aoyagi, Y., Kamimoto, T., Matsui, Y. and Matsuoka, S., "A Gas Sampling Study on the Formation Processes of Soot and NO in a D.I. Diesel Engine," SAE Paper-800254, 1980.

3. Rhee, K.T., Myers, P.S. and Uyehara, O.A., "Time- and Space-resolved Species Determination in Diesel Combustion Using Continuous Flow Gas Sampling," SAE Paper-780226, 1978.

4. Chang, S.L. and Rhee, K.T., "An Analytical and Numerical Modeling of Radiation Heat Transfer in Combustor Having Jet Flames," 4th International Conference on Applied Numerical Modeling, December 27-29, 1984, Taiwan.

5. Chang, S.L. and Rhee, K.T., "Computation of Radiation Heat Transfer in Diesel Combustion," SAE Paper-831332, 1983.

6. Chapman, M., Friedman, M.C. and Aghan, A., "A Time-Dependent Spatial Model for Radiant Heat Transfer in Diesel Engines," SAE Paper-831725, 1983.

7. Menguc, M.P., Viscanta, R. and Ferguson, C.R., "Multidimensional Modeling of Radiative Heat Transfer in Diesel Engines," SAE Paper-850503, 1985.

8. Chang, S.L. and Rhee, K.T., "Coordinate Transformation Method for Radiation Heat Transfer Prediction in Soot Laden Combustion Products," to be published.

9. Dalzell, W.H. and Sarofim, A.F., "Optical Constants of Soot and their Application to Heat Flux Calculation," Trans. of ASME, Vol. 9, p. 100, 1969.

10. Edwards, D.K. and Balakrishnan, A., "Thermal Radiation by Combustion Gases," International Journal of Heat Mass Transfer, Vol. 16, p. 25, 1973.

11. Chang, S.L. and Rhee, K.T., "A Solution of Radiation Heat Transfer Equation in Combustors with Plumes Consisted of Radiatively Participating Species Distribution," being prepared.

12. Rhee, K.T. and Chang, S.L., "Empirical Equations for Adiabatic Flame Temperatures for Some Fuel-Air Combustion Systems," Combustion Science and Technology, Vol. 44, 75, 1985.

END

DTIC

7-86